Organically Modified Sol-Gel Derived Siloxane Networks: Mesoporous, Hybrid Aerogels Through Ambient Pressure Drying

THESIS SUBMITTED TO

COCHIN UNIVERSITY OF SCIENCE AND TECHNOLOGY
IN PARTIAL FULFILMENT OF THE REQUIREMENTS
FOR THE DEGREE OF

DOCTOR OF PHILOSOPHY
IN CHEMISTRY

UNDER THE FACULTY OF SCIENCE

BY

Shajesh P.

Under the Supervision of
Dr. K.G.K. Warrier

Materials and Minerals Division

NATIONAL INSTITUTE FOR INTERDISCIPLINARY SCIENCE AND TECHNOLOGY
(Formerly Regional Research Laboratory)
Council of Scientific and Industrial Research
Thiruvananthapuram, Kerala, India – 695 019

May 2009

Declaration

I hereby declare that the work embodied in the thesis entitled "**Organically Modified Sol-Gel Derived Siloxane Networks: Mesoporous, Hybrid Aerogels Through Ambient Pressure Drying**" is the result of the investigations carried out by me, at the Materials and Minerals Division, National Institute for Interdisciplinary Science and Technology (formerly Regional Research Laboratory), CSIR, Thiruvananthapuram, under the supervision of Dr. K.G.K. Warrier and the same has not been submitted elsewhere for any other degree

Shajesh P.

Thiruvananthapuram

May 2009

राष्ट्रीय अंतर्विषयी विज्ञान तथा प्रौद्योगिकी संस्थान
National Institute for Interdisciplinary Science and Technology
(पहले क्षेत्रीय अनुसंधान प्रयोगशाला) (formerly Regional Research Laboratory)
An ISO 9001 Certified Organisation
वैज्ञानिक एंव प्रौद्योगिकी अनुसंधान प्रयोगशाला
Council of Scientific and Industrial Research

Dr. K. G. K. Warrier Ph.D., F.IICer
Deputy Director
Head, Materials & Minerals Division
Ceramic Technology

इन्डस्ट्रियल इस्टेट डाक घर, तिरुवनन्तपुरम ६९५०१९, भारत
Industrial Estate P.O., Thiruvananthapuram - 695 019, INDIA
Phone : +91- 471- 2490674, 2515280 (O)Fax : +91- 471- 2491712
E-mail:warrier@niist.res.in Website : www.nist.res.in, http//kgkwarrier.tripod.com

Certificate

This is to certify that the work embodied in the thesis entitled "**Organically Modified Sol-Gel Derived Siloxane Networks: Mesoporous, Hybrid Aerogels Through Ambient Pressure Drying**" has been carried out by **Mr. Shajesh P.** under my supervision at Materials and Minerals Division, National Institute for Interdisciplinary Science and Technology (formerly Regional Research Laboratory), CSIR, Thiruvananthapuram, in partial fulfilment of the requirements for the award of the Degree of Doctor of Philosophy in Chemistry, under the Faculty of Science, Cochin University of Science and Technology, Thiruvananthapuram and the same has not been submitted elsewhere for any other degree.

K.G.K. Warrier

Thiruvananthapuram
May 2009

Acknowledgements

Words fall short in expressing my immense gratitude to Dr. K.G.K. Warrier, my research supervisor (Scientist G, NIIST, Thiruvananthapuram), for his constant encouragement, intellectual support and constructive criticism during the course of my doctoral studies. Without his compassion this thesis would not have materialized.

I am thankful to Dr. B.C. Pai, present Director and former Directors of NIIST for providing the facilities to carry out this research work.

I would like to acknowledge the contributions of Mr. Abhilash, Ms. Anu and Mr. Nicholas Smutek to some of the data presented in this thesis.

My sincere thanks are due, to Dr. S. Ananthakumar and Dr. S.K. Ghosh for their constant encouragement and advice. I extend my sincere thanks to Mr. P Krishna Pillai for helping me with the instruments and his warm companionship. I would also like to thank Mr. P. Mukundan for most of the characterization presented in this thesis and also to his valuable advice. The help from Mr. P. Perumal is also acknowledged. I wish to thank Dr. S. Shukla for motivating me with his enthusiastic nature and queries.

I am indebted to Mr. Anas S. for his invaluable contributions to the successful and timely completion of the thesis.

The help from Mr. Sanoj M.A. and Mr. Sumesh G. are specially acknowledged. I also thank Mr. Ajesh K. Zachariah for the AFM studies. I thankfully acknowledge the contributions of SEM, TEM and XRD groups to this work.

I specially thank Ms. Athira N. Raj for the help she extended during the compilation of this thesis. I extend my thanks to Ms. Sumaletha N. and Mr. Sanoop P.K. for their support. I wish to thank my other group members Jaimy K.B., Mirash A.J., Divish K., Smitha V.S., Manjumol K.A. and Sreeremya T.S. for sacrificing their time for the completion of this thesis.

I express my deep sense of gratitude to Mrs. Smitha who has guided me during the initial stages of this work and also for ardently supporting me throughout the period of this work.

Mr. Sankar Sasidharan and Mr. Vinod S. require special mention for the warm friendship and its comfort which has helped in molding the thesis in the final stages. I am thankful to Dr. Aravind P.R., Dr. Baiju K.V. and Mr. M. Jayasankar for their friendship and support throughout their stay at NIIST. I wish to remember Dr. C.P. Sibu, my senior for his guidance. I would like to thank Dr. Rajesh. K for the support and camaraderie he extended during the initial stages of this work. I would also like to thank Dr. P. Ramasamy, and Mr. Vinayakan for their warm friendship during my stay at NIIST.

I acknowledge the Council of Scientific and Industrial Research, New Delhi, for the Research Fellowship and Financial assistance from the DRDO.

Finally on a personal note, I am thankful to my parents, sister and nephew for bearing my untimely absence during this period. I am also thankful to Mr. G. Ajayakumar for his encouraging and loving companionship.

Shajesh P.

Preface

The ability to combine the properties of organic and inorganic materials in to a single material has helped to over look the inherent ineptness in many materials, widening the horizons of possible applications. In aerogels, the incorporation of organic luminescent dyes into the aerogel skeleton has given rise to the luminescent aerogels and use of organically modified silane precursors has resulted in flexible aerogels. The introduction of coexisting organic inorganic hybrid networks has further increased the mechanical strength of aerogels bringing down the inherent limitation associated with aerogels, their brittleness.

Added mechanical strength in aerogels presents a new path for obtaining aerogels at ambient pressure. The need to replace supercritical drying for synthesis of aerogels has been fuelled by certain limitations with respect to large scale processing. In this scenario the ambient pressure drying of co-existing organic inorganic hybrid networks for obtaining aerogels is investigated.

Initially, the effect of using an organically modified precursor in a reported ambient pressure drying technique, on the final properties of the prepared aerogels is investigated. In the next stage the development of crosslinked organic inorganic hybrid systems is detailed along with the ambient pressure drying of these systems. The variation of the properties by varying the variables in processing like precursor ratio, water ratio etc is investigated. The dielectric response of the hybrid networks has also been measured and the data are compared with those of supercritically dried counterparts. A possible application of these materials, arising from the high porosity achievable at ambient pressure, as photoactive coatings is investigated finally. Titania has been used to impart photoactivity to the hybrid network.

Acronyms

AcAc	Acetylacetone
AFM	Atomic Force Microscopy
AIBN	2,2'-Azobisisobutyronitrile
APTES	3-Aminopropyltriethoxysilane
BET	Brunauer Emmett Teller
BJH	Barrett–Joiner–Halenda
BTMSH	Bis(trimethoxysilyl)hexane
Si CP-MAS-NMR	Silicon Cross Polarisation-Magic Angle Spinning-NMR
DCCA	Drying control chemical additives
DDOA	2,3-Didecyloxyanthracene
DEO	1,2,7,8-Diepoxyoctane
DETA	Diethylenetriamine
FSD	Fourier self deconvolution
FTIR	Fourier Transform Infrared Spectroscopy
GFP	Green Fluorescent Protein
GPTMS	(3-glycidoxypropyl)trimethoxysilane
IPA	Isopropyl alcohol
IUPAC	International Union of Pure and Applied Chemistry
MCM	Mobil Crystalline Material
MTES	Methyltriethoxysilane
MTMS	Methyltrimethoxysilane
NLO	Non linear optics
NMR	Nuclear Magnetic Resonance
PAN	Poly(acrylonitrile)
PDMS	Poly(dimethoxysilane)
PEDS	Polyethoxydisiloxane)
PEO	Poly(ethylene oxide)
PF	Phenolic-Furfural
PMMA	poly(methyl methacrylate)
PVB	Poly(vinylbutyral)
PZC	Point of Zero Charge
RLCA	Reaction limited cluster aggregation
RLMC	Reaction limited Monomer cluster aggregation
RMOS	Alkyl modified trimethoxysilane
SAXS	Small Angle X-ray Diffraction
SEM	Scanning Electron Microscopy
TEM	Tunnelling Electron Microscopy
TEOS	Tetraethyl orthosilicate
TIP	Titanium isopropoxide
TMOS	Tetramethyl orthosilicate
TPMS	3-(trimethoxysilyl)propyl methacrylate
VB	Valance Band
VOC	Volatile organic compounds
VTMS	Vinyltrimethoxysilane
XRD	X-ray Diffraction

CONTENTS

Chapter 1

Introduction

During the first half of the twentieth century the concept of porosity took a hairpin turn and ceased its existence as a 'nuisance to ceramic scientists and metallurgists'. Pores became a material in itself and an object to be engineered. One of the earliest materials to base its existence on porosity is unarguably, aerogels. Ever since Kistler demonstrated the supercritical drying to remove solvent from a wet gel without shrinkage, researchers have stretched the limits of human imagination of low density solids.[1,2] In 1992 Mobil scientists engineered the first crystalline porosity or ordered porosity in silica gels.[3] This in turn developed in to an upsurge in research on porous materials and further fuelled the interest in highly porous materials. Simultaneously the concept of Metal Organic Frameworks developed to extend the nano engineering of porosity to the microporous regime.[4] The scopus database cites 7453 articles in the interval 1980-1989, 14,775 for the years 1990-1999 and 25,369 for the year 2000-2009 for the search with the word 'porous' in the title. This is a suitable reflection of the rise in the interest on porous materials during these three decades. Even though pores in the whole range from nm to μm are hot topics of research we would limit our description to the nanometre regime, since it is more applicable to the topic of this thesis.

Materials are porous if they contain cavities, channels or interstices that are deeper than they are wide.[5] The pores may be regularly arranged as in molecular sieves. However, the more common situation is an irregular pore structure, as obtained by cross-linking of polymer chains, aggregation or agglomeration of small particles or selective removal of elements of a solid (e.g. by etching or pyrolysis). The physical properties of a porous solid and its reactivity are effectively influenced by the kind, shape and size of the pores.

Applications of porous materials are limited only by imagination. A large variety of fields depend on porosity for their technological advance. Porous silicon is poised to

take centre stage in the biosensor development efforts owing to its tunable pore size and porosity.[6] Further these materials have also found application in drug delivery systems.[7] Utilization of a porous medium for combustion of liquid fuels is proving to be a promising approach for future applications. The porous medium burner for liquid fuels is more advantageous than the conventional open spray flame burner for several reasons; these include enhanced evaporation of droplet spray owing to regenerative combustion characteristics, low emission of pollutants, high combustion intensity with moderate turn-down ratio and compactness.[8] Porous polymers are the new generation polymers which are particularly investigated for applications in fuel cell membranes, as electrode materials for batteries, for gas storage and also for sorption materials/chromatography.[9,10] As the concern over global warming grows the need for renewable and clean energy sources have lead to biofuels. The conversion of biomass to biofuel requires porous materials as catalysts and improving their catalytic activity is an active area of interest.[11] Applications of inorganic porous materials in medical science have been reviewed by Wang et al. and include applications like enzyme immobilizing, enzyme simulation, biological sensors, controlled release drug carrier etc.[12] Zeolites are complex, highly porous crystals veined with tiny channels made of silicon, aluminium and oxygen and several additional elements. The very small sizes of the pore channels (~1 nm) make them very good molecular sieves and catalysts. Similar properties have been observed for mixed-valent manganese oxides and are now commonly addressed as octahedral molecular sieves (OMS).[13] One of the earliest applications of porous materials has been thermal insulations. In thermal insulation panels, the loss of heat by convection can be prevented by the presence of pores in the nanometer regime. When the pore sizes are lower than the mean free path of the gas molecules filling the pores, the gas molecule collides with the pore walls before encountering another gas molecule and the transfer of heat between the molecules is prevented. Materials scientists have nearly exhausted the list of dense materials for achieving low dielectric constants which is very much required for the next generation microelectronics. Porosity is the only alternative to achieve low dielectric constants ($k<2$).[14]

Classification of Porous Materials

Pores can be considered as cavities extending throughout a solid. Pores can be inherent, be part of the crystal structure as in zeolites or can be engineered as in MCM materials or formed during the preparation process as in sol gel derived silica gels. The pores can be classified as open and closed as applicable to material scientists. Open pores have access to the external surface of the solid where as closed pores are inaccessible. Closed pores are usually formed during processing and by uneven mass transport during thermal treatment.

A convenient classification of pores is according to their average width and is accepted by the IUPAC. Accordingly micropores have width <2 nm, mesopores have average pore width in the range 2-50 nm and above 50 nm, pores are termed as macropores. Unless chemically controlled, porous materials can have pores in the wide range mentioned. Porosity is the ratio of the volume of open pores to the total volume of the solid.

In a porous solid, the surface accessible to a guest molecule will be many times higher than that expected from the simple geometrical dimensions of the individual particles and brings in, the concept of specific surface area. It is the surface area of one gram of solid and values ranging from <<1 - >2000 can be seen in the literature. Adsorption of gases on a solid surface is a direct consequence of surface area. Valuable information regarding surface area and porosity can be obtained from the adsorption isotherm of a gas-solid system. In practice the range of suitable adsorptives are quiet narrow and nitrogen at its boiling point, 77 K is by far the most common adsorptive used to obtain information of specific surface area and porosity. The adsorption behaviour of gases on solid surfaces can be generally grouped into a few types of isotherms.

Adsorption in Porous Materials

There are mainly four types of isotherms according to the widely accepted classification of Brunauer, Deming, Deming and Teller classification.

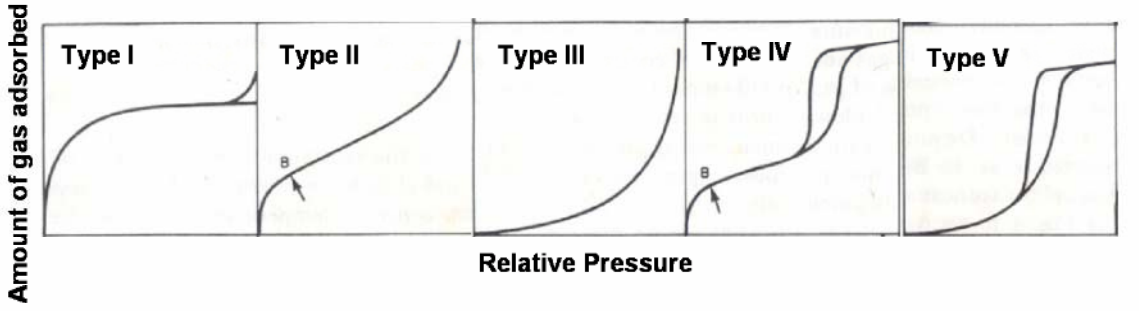

Figure 1.1.: Types of Adsorption isotherms

Type I isotherms are characteristic of microporous solids. Here the pores are no more than a few diameters in width and the potential fields from neighbouring walls overlap and the interaction between the gas and solid will be enhanced. The consequence is that the pore filling will take place at a relatively low pressure observed as the increased absorption at low relative pressure of the isotherm. The adsorption approaches a plateau and usually no hysteresis is observed. The plateau corresponds to the complete filling of the pores according to the classical view. If the isotherm us with a sharp knee and a horizontal plateau then the uptake at a point close to saturation pressure can be considered as the total pore volume.

The Type II isotherms are observed when gases are adsorbed on a non porous solid. Since there is no pores to fill it is possible evaluate the monolayer capacity of a solid from the Type II isotherm. The Brunauer Emmett Teller (BET) model is the most successful quantitative model available for the determination of surface area from a Type II adsorption isotherm. The BET model is based on the kinetic model of Langmuir and the surface of the solid is considered as an array of adsorption sites. A state of dynamic equilibrium is assumed where the rate at which molecules arriving from the gas phase and condensing on to the base sites is equal to the molecules evaporating from the occupied sites. While Langmuir adsorption assumes that adsorption occurs only on a single layer, BET model accounts for multiple layers. The assumptions used to include multiple layers are as follows. In all layers except the first layer, the heat of adsorption is equal to the molar heat of condensation (q_L). In all layers except the first the evaporation-

condensation conditions are identical. At saturation pressure of the adsorptive, it condenses to a bulk liquid on the surface of the solid, or the number of layers becomes infinite. The BET equation is given as

$$\frac{n}{n_m} = \frac{c(p/p^\circ)}{(1 - p/p^\circ)(1 + \overline{c-1}p/p^\circ)}$$

where $\frac{n}{n_m}$ is the occupied fraction of the monolayer capacity, (p/p°) is the relative pressure of the adsorptive and c is given by $c = e^{(q_1 - q_L)/RT}$ where $(q_1 - q_L)$ is the net heat of adsorption. Statistical mechanical treatments show that the parameter 'c' has significance more that that assumed by the BET model. Now 'c' also involves entropic terms as well as energetic terms. When n/n_m is plotted against (p/p°) the curve will have the shape of a Type II isotherm as long as 'c' exceed 2. The shape of the knee depends on the value of 'c' and become sharper as the value becomes greater. When 'c' is less than 2 and still positive the BET equation give rise to a curve having the general shape of a Type III isotherm. As long as 'c' exceeds 2 the BET isotherm has a point of inflection; this point is close to, but not necessarily coincident with the BET monolayer capacity. Actually the value of n/n_m at the point of inflection may deviate from unity. At the value c=9 the n/n_m has been seen to have the value 1, but for values between 9 and infinity the adsorption at the point may exceed the BET monolayer capacity by as much as 15 percent and for values of 'c' below 9 the two quantities deviates more and more widely till at c=2, the point of inflection disappears.

In practice the Type II isotherm display a rather long straight portion after the 'knee'. The point where this linear portion begins was taken by Emmett and Brunauer to indicate the completion of the monolayer capacity. The estimation of the monolayer coverage is obtained by applying the BET equation over a range of the isotherm which contains this point.

Type III and Type V isotherms are characterized by convexity towards the relative pressure axis commencing at the origin. The convexity persists through out the

length of the isotherm. These isotherms are characteristic of weakly interacting gas and solid. Type III is in fact given by non porous or macroporous solids while Type V is given by mesoporous or microporous solids. The weak interaction between the adsorbent and adsorbate cause the uptake at relatively low pressures to be small; but once the adsorption starts the adsorbed molecules will promote further adsorption and the isotherm become convex to the pressure axis. Water exhibits Type III adsorption, because the dispersion contribution to its over all interaction energy is unusually small compared to the polar contribution.

The pore size that gives rise to a Type IV isotherm is usually considered mesoporous. The characteristic feature of the Type IV isotherm is the hysteresis loop. The exact shape of the loop varies from one adsorption system to the other, but the amount adsorbed is always greater at any point on the desorption curve than on the adsorption curve.

The hysteresis loop on a Type IV isotherm can be understood based on the capillary condensation theory. According to the Kelvin equation, on thermodynamic grounds, the equilibrium vapour pressure, 'p' over a concave meniscus of liquid, must be less than the saturation vapour pressure, 'p°', at the same temperature. This implies that the vapour will condense to a liquid in the pores of a solid even when the relative pressure is less than unity. The Kelvin equation is given by

$$\ln \frac{p}{p^\circ} = \frac{-2\gamma V_L}{RT} \frac{1}{r_m}$$

Here (p / p°) is the relative pressure of vapour in equilibrium with a meniscus of radius of curvature r_m and γ and V_L are the surface tension and molar volume respectively of the liquid adsorptive. At the inception of the hysteresis loop capillary condensation commences in the finest pores. As pressure increases wider pores are filled until saturation, when the entire system is full of the condensate. If one assumes that the pores are cylindrical and the angle of contact to be zero so that the meniscus is hemispherical the mean radius of curvature r_m will be equal to the radius of the pore less the thickness of the adsorbed film on the walls. By applying the Kelvin equation it is therefore possible

to calculate the minimum radius of pores in which capillary condensation can take place from the relative pressure at the commencement of the hysteresis loop. This minimum radius varies with system but is rarely below 1 nm. The upper limit of the applicability of the Kelvin equation is ~25 nm and is set by the practical difficulty in measuring very low lowering of vapour pressure. So the mesopore range is practically defined by the applicability of the Kelvin equation.

Calculation of pore size from the Type IV isotherm uses the Kelvin equation in the region of the isotherm where the hysteresis occurs. Considering idealised geometries for the pores it can be shown that capillary condensation and evaporation occurs in a cylindrical pore closed at one end and open at the other, at the same relative pressure and there is no hysteresis. But if the cylinder is open at both ends then condensation occurs at a relative pressure different from that of evaporation and hysteresis occurs. The mean radius calculated from the desorption branch using the Kelvin equation will be equal to the core radius (radius of the pore - thickness of the adsorbed film) and twice that of the core radius if calculated from the adsorption branch. Now if a pore is considered with a body which has radius less than twice the core radius of the neck then condensation occur at the base of the pore at a relative pressure different from that required at the neck and if '$r_b/r_n < 2$' condensation will commence at the base of the pore and will fill the whole pore and neck at the relative pressure where condensation starts in the pore of radius r_b. But evaporation will commence from the hemispherical meniscus at the neck at a relative pressure required for condensation in a pore of radius r_n and will continue till the core of the body is emptied since the pressure will already be lower than the equilibrium value required for the evaporation from the body. Here the calculation of the mean radius from the adsorption branch leads to the values of the core radius of the body and the desorption branch to the values of the core radius of the neck. A new set of pores that has come to prominence in recent years is slit shaped pores. In such pores, the mechanism of pore filling and emptying are different, pore filling happens by multilayer formation and emptying by capillary evaporation. The difference in hysteresis loops can be usually associated to the pore shape. A new classification of hysteresis loops have been

recommended by the IUPAC and are designated H1, H2, H3 and H4 (figure 1.2.). H1 loops are often obtained for agglomerates or compacts of spheroidal particles of uniform size and array. Corpuscular systems tend to give H2 loops, here pore size and shapes are not well defined. H3 and H4 are obtained with adsorbents with slit shaped pores.

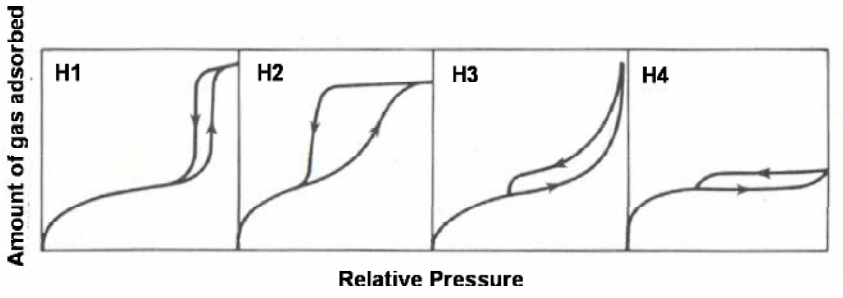

Figure 1.2.: Types of hysteresis loops

Synthesis of Porous Solids

Synthesis of porous solids requires different techniques for pores of different sizes. Pores in the nanometer regime are usually prepared using the templating method. Zeolites are typically synthesized from solutions containing the pore directing agent. Various pore arrangements can be achieved by varying the templating agent.[15-17] Mesoporous materials are easily achieved by sol gel synthesis.[18] Ordered mesoporous materials are usually prepared by templating using self assemblies of amphiphilic molecules.[3,19] Porous silicon is prepared by electrochemical dissolution. Macroporous ceramics can be made of either reticulate or foam structure.[20] Reticulate structure is made by burning out a polymeric sponge impregnated with a ceramic slurry. The foam structure is made by producing a foam from evolved gas. The polymer carrier is burnt out leaving a porous ceramic. But sol-gel method is the most versatile due to its application in preparing porous materials with pore sizes ranging from nanometres to micrometers.

Sol-Gel Synthesis

Sol-gel synthesis is the widely practiced synthesis technique for the preparation of porous materials. Many variations of the technique can be seen in the literature and

modified techniques are still prevalent in synthesis of a wide range of nano particles. Sol-gel process is a colloidal route used to synthesize ceramics with an intermediate stage of a sol or a gel state. It generally consists of the preparation of a colloidal suspension of a solid into liquid; viz (a sol) and then three dimensional structures of solid enclosing the liquid (gel). The gel on further removal of liquid results in the final material which will be in the hydroxylated state.[18,21] The starting material used in the preparation of the sol is usually inorganic metal salts or metal organic compounds such as metal alkoxides. In a typical sol-gel process the precursor is subjected to a series of hydrolysis and polymerization reactions to form a colloidal suspension or sol. The sol undergoes gelation to form a monolithic gel. With further drying and heat treatment, the gel is converted into porous or dense ceramics or glass articles. If the liquid in a wet gel is removed under supercritical conditions, a highly porous and extremely low density material called aerogel is obtained. Applying sol-gel process, it is possible to fabricate ceramic or glass materials in a wide variety of forms, ultra fine or spherical shaped, powders, thin film coatings, ceramic fibres, microporous inorganic membranes, monolithic ceramics and glasses or extremely porous aerogel materials.

Sols & Gels

A sol is a stable suspension of colloidal solid particles within a liquid. [22] Particles of a sol are small enough to remain suspended indefinitely by Brownian motion. Sols are classified as lyophobic if there is a relatively weak solvent-particle interaction and lyophilic if the interaction is relatively strong. Lyophobic sols exhibit well defined Tyndall effect. In lyophilic sols the particles are largely solvated and this lowers the differences in refractive indices of two phases. The Tyndall effect is due to the scattering of light from the surface of colloidal particles.

Sol particles are held by Van der Waals forces of attraction or dispersion energy. Van der Waals force is propotional to the polarisabilities of the atoms and inversely related to the sixth power of their separation. This Van der Waals force results from

transitory dipole-transitory dipole interactions (London forces). It is this London forces that produce long range attraction between the colloidal particles.

The attractive potential for two infinite slabs separated by distance, 'h' is given by

$$V_A = -A/12\pi h^2 \; ; \; V_A \propto -1/h^6 \text{, for atoms}$$

'A' is a material property called Hamaker's constant. Since this attractive force extends over distances of nanometers, sols are thermodynamically unstable.[23] Aggregation can be prevented by erecting necessary barriers of comparable dimensions. Electrostatic and steric stabilization are generally used to make the sols meta stable.

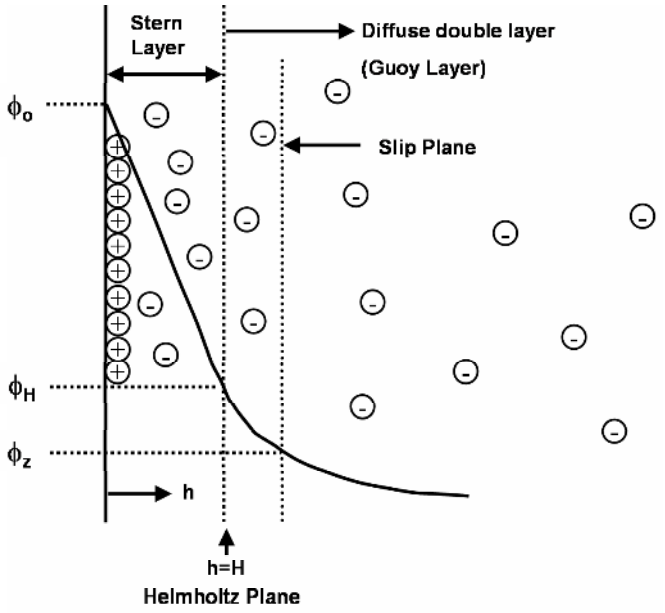

Figure 1.3.: Diffused double layer

Electrostatic stabilization is explained by DLVO theory. According to this theory the net force between particles in suspension is assumed to be the sum of the attractive Van der Waals forces and electrostatic repulsion created by charges adsorbed on particles. The repulsive barrier depends on two types of ions that make up the double layer, charge determining ions that control the charge on the surface of the particle and counter ions that are in solution in the vicinity of the particle.[18] For hydrous oxides the charge

determining ions are H^+ and OH^- which establish the charge on the particle by protonating or deprotonating the MOH bonds on the surface of the particle.

$$M\text{-}OH + H^+ \longrightarrow M\text{-}OH_2^+ \quad (1)$$

$$M\text{-}H + OH^- \longrightarrow M\text{-}O^- + H_2O \quad (2)$$

The ease with which the protons are added or removed from the oxide depends on the metal atom. The pH at which the particle is neutrally charged is called the Point of Zero Charge (PZC). At pH greater than PZC equation (2) predominates and the particle is negatively charged, whereas at pH less than PZC equation (1) gives the particle a positive charge. The magnitude of the surface potential depends on the departure of the pH from the PZC, and that potential attracts oppositely charged ions (counter ions) that may be present in the solution.

According to the standard theory, potential drops linearly through the tightly bound layer of water and counter ions, called the stern layer. Beyond the Helmholtz plane 'h = H', that is, in the Gouy layer, the counter ions diffuse freely. In this region the repulsive electrostatic potential of the double layer varies with distance from the particle, 'h', approximately according to

$$V_R \propto e^{\kappa(h-H)}, h \geq H$$

Where $1/\kappa$ is called the Debye Huckel screening length. When the screening length is large (i.e. κ is small) the repulsive potential extends far from the particle. This happens when the counterion concentration is small. When counterions are present, the potential drops more rapidly with distance. Since the repulsive force, $F_R = \frac{dV_R}{dh} \propto \kappa e^{-\kappa(h-H)}$ is propotional to the slope of the potential, the repulsive force increases with small additions of electrolyte. (i.e F_R increases with K). Large amounts of counter ions collapse the double layer. As the concentration of counter ions increases, the double layer is compressed because the same numbers of charges are required to balance the surface charge and they are now available in a smaller volume surrounding the particle. On further increase in the concentration of counter ions the double layer repulsions are

reduced to the point that net particle potential is attractive and the colloid will coagulate immediately.

When an electric field is applied to a colloid, the charged particles move towards the electrode with the opposite charge. This phenomenon is called electrophoresis. When the particle moves, it carries along the adsorbed layer and part of the cloud of counter ions, while the more distant portion of the double layer is drawn towards the opposite electrode. The slip plane or plane of shear separates the region of fluid that moves with the particle from region that flows freely. The rate of movement of particles in the field depends on the potential at the slip plane known as zeta potential. The pH at which zeta potential is zero is called the isoelectric point (IEP). The stability of the colloid correlates with zeta potential to be around 30-50 mV.

Sols can be stabilized by providing steric hindrance. An example is short chain polymers adsorbed on to the surface of particles. There are two components to this stabilization energy. As the sol particles approach one another, the adsorbed polymer loses configurational entropy. This raises the Gibb's free energy of the system, which is equivalent to the development of a repulsive force between the particles. In addition, as the polymer layers overlap the concentration of the polymer in the overlap region increases. This leads to local osmotic pressure and a repulsive force between the particles.[24]

A gel is a porous three dimensionally inter-connected solid network that expands in a stable fashion throughout the liquid medium and is only limited by the size of the container.[25] Gel results when the sol loses its fluidity. An important criterion for gel formation is that at least part of the solvent is bound. If the solid network is made up of colloidal particles, the gel is said to be colloidal (particulate). If the solid network is made up of sub colloidal chemical units the gel is called polymeric. In particulate gels, the sol gel transition is caused by physio-chemical effect and in the latter by chemical bonding.

Advantages and General Applications of Sol-Gel Approach

General advantages of sol-gel method that has made it so prominent are,

(1) Increased chemical homogeneity in multicomponent system.
(2) High surface area for the gels or powders that are obtained.
(3) High purity can be maintained because of the absence of grinding and pressing steps.
(4) A range of products in the form of fibers, powders, coatings and spheres can be prepared with relative ease, starting from simple solutions.
(5) Low temperatures for sol-gel process, saving energy and minimizing evaporation losses.
(6) Gels can be moulded in the shape of the final desired object, with dimensions enlarged to allow for shrinkage during drying and sintering.

The most prominent disadvantages of the process are the long processing times, cracking during drying and the expensive alkoxide precursors required for obtaining high purity.

Solution Chemistry of Silicon alkoxides

Sol-gel synthesis uses metal alkoxides or salts as the precursor. When the synthesis is done using metal alkoxides it is usually an aqueous based process while the use of metal alkoxides requires a non aqueous medium. In water the metal ions M^{z+} are solvated by water molecules and charge transfer occurs from the filled bonding orbital of water to the empty 'd' orbitals of the transition metal. This in turn increases the partial charge on hydrogen and the acidity of water increases. Depending on the acidity of water i.e. the magnitude of charge transfer the following equilibria is established.

$$[M(OH_2)]^{z+} + H^+ \rightleftharpoons [M\text{-}OH]^{(z-1)+} + H^+ \rightleftharpoons [M{=}O]^{(z-2)+} + 2H^+$$

This is generally defined as hydrolysis. In general, hydrolysis is facilitated by increase in charge density on the metal ion, the number of metal ions bridged by the hydroxo(OH) or oxo (-O-) ligand and the number of hydrogen contained in the ligand. [26]

The hydrolyzed precursors can undergo condensation reactions by either a nucleophilic substitution (1) or through a nucleophilic addition reaction (2).

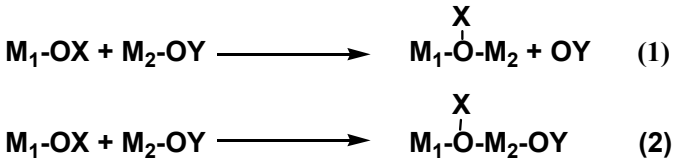

Near isoelectric point, neutral precursors are able to condense indefinitely to form metal hydroxide or oxyhydroxide products depending on δ (H_2O). When δ (H_2O) <0, hydroxide products are isolated and when δ (H_2O) >0, oxyhydroxides are formed as metal stable intermediates to fully condensed oxides. Whether precipitation or gelation occurs depends on the processing factors like pH, temperature, speed of mixing and also on condensation kinetics.

In non aqueous processing the metal alkoxides undergo the hydrolysis-condensation reactions. The most commonly used alkoxide precursor is silicon alkoxide and they are far more stable and easy to handle than transition metal alkoxides. The solution chemistry of silicon alkoxide can be summarized as follows.

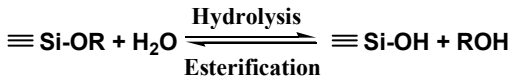

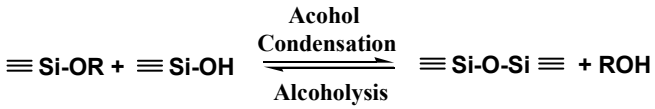

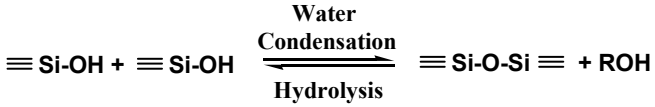

Hydrolysis occurs by the nucleophilic attack of the oxygen contained in water on the silicon atom. Hydrolysis can happen in acid or base catalyzed conditions. Under acidic conditions alkoxide group is protonated in a rapid first step. Electron density is withdrawn from silicon making it more electrophilic and thus more susceptible to attack by water. The water molecule attacks from the rear and acquires a partial positive charge. The positive charge of the protonated alkoxide is correspondingly reduced making alcohol a better leaving group. The transition state decays by displacement of alcohol, accompanied by the inversion of silicon tetrahedron. The hydrolysis rate is increased by substituents that reduce steric crowding around silicon. Electron providing substituents

that help to stabilize the developing positive charges also increase the hydrolysis rate. In base catalyzed hydrolysis, water dissociates to form hydroxyl anions. The second step involves an S_N2–Si mechanism in which OH displaces OR with inversion of the silicon tetrahedron. The mechanism is affected by both steric and inductive factors; however steric factors are more important since silicon acquires little charge in the transition state.

Polymerization to form siloxane bonds occurs by either 1) an alcohol producing condensation reaction or 2) by water producing condensation reaction. The overall condensation rate is found to be minimized at around pH 1.5 and maximised at intermediate pH. Protonated and deprotonated silanols are involved in the acid and base catalyzed condensation mechanisms at pH<2 and pH>2 respectively. Under conditions in which depolymerization is suppressed, condensation may lead to molecular networks, whereas in which depolymerization is promoted, restructuring occurs ultimately resulting in the formation of highly condensed colloidal particles.

It is generally accepted that base catalyzed condensation, occurs by an S_N2-Si mechanism involving a penta or hexa coordinated silicon intermediates or transition states as in the case of the polymerization of silicic acid. The acid catalysed condensation mechanism involves a protonated silanol species. Protonation of silanol makes the silicon more electrophilic and they are more susceptible to nucleophilic attack. The most basic silanol species contained in monomers or weakly branched are the most likely to be protonated. Therefore condensation reactions may occur preferentially between neutral species and protonated silanols situated on monomers, end groups of chains etc. Acid catalysed condensation is a slower transformation than hydrolysis. However silanols protonate more easily when it is at the end of a polymer chain. The polymers obtained are therefore linear with scarcely any branching points.

The hydrolysis and condensation reactions continue and the resultant clusters grow by condensation of polymers or aggregation of particles until the links form between the clusters to produce a single giant cluster, gel. Nuclear magnetic resonance spectroscopy, Raman and infrared spectroscopy and X- ray, neutron and light scattering are the different methods for determining the structural evolution during sol-gel transition.

[18] Sol-gel transition can also be followed by rheological characterization. In the microanalysis, the gel point is defined as the time at which the viscosity is observed to increase abruptly. The structural evolution in the silicate species in solution is explained in scales of different length. On the short length scale, the nearest neighbour of silicon may be an alkoxide group, a hydroxyl group or bridging oxygen (O-Si). On intermediate length scales, oligomeric species (dimers, trimers, tetramers etc) may be linear, branched or cyclic. On length scales large with respect to monomers and small with respect to polymers, structures may be dense with well defined solid-liquid interface, uniformly porous or tenuous network.

There are both equilibrium growth models and kinetic growth models to describe the gelation process. Flory-Stockmayer is the first among the equilibrium growth models which attempted to describe diverges in cluster and mass and average radius accompanying the gelation.[18] This model is qualitatively successful as it correctly describes the emergence of an infinite cluster at some critical extent of the reaction and provides good prediction of gel point. However it does not provide an entirely realistic picture of polymer growth.

Kinetic growth process produces objects with self-similar fractal properties. Schafer and Keefer postulated kinetic models for the growth of gel network based on SAXS data.[27-29] Two most important models are shown in figure.

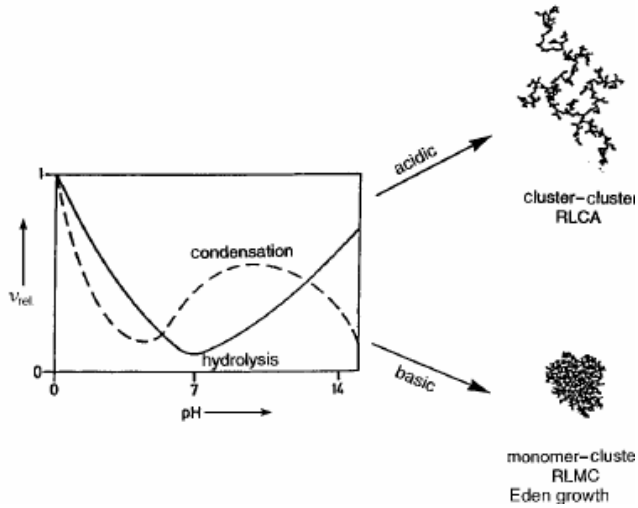

Figure 1.4.: Kinetic growth models for silica polymerization

The pH value is the decisive parameter for the relative rates of hydrolysis and condensation of tetra alkoxysilanes [Si $(OR)_4$]. Under acidic conditions (pH 2-5) hydrolysis is favoured, and condensation is the rate determining step. A great number of monomers or small oligomers with reactive Si-OH groups are simultaneously formed. Under these conditions, reactions at terminal silicon atoms are favoured for electronic reasons. This results in polymeric gels which are formed from chains with few branches; which means in other words, small clusters condense to give a polymer like network with small pores. This process is called reaction limited cluster aggregation (RLCA).[18] In contrast, hydrolysis is the rate-determining step under basic conditions. Due to different mechanism, reaction at the central silicon atoms of an oligomer unit is not favoured. The resultant network is characterized by big particles and large pores ("colloidal" gels). Hydrolysed species are immediately consumed because of the faster condensation. Condensation of clusters with each other is relatively unfavourable because it requires inversion of configuration at one of the silicon atoms involved in the reaction. There, the clusters grow mainly by condensation of monomers. This model is called reaction limited monomer cluster growth (RLMC) or Eden growth.

Aging of Gels

The composition, structure and properties of gels continue to change with time even after the gel point, in a process called aging. The subsequent drying of the gel is strongly influenced by the structure developed during aging. Particulate or polymeric gels are aged essentially to increase their strength prior to drying in order to avoid cracking and/or to alter the microstructure of the wet gels and subsequently the xerogel.

Process involved in aging are categorized as

a) Polymerization i.e. increase in connectivity of the gel network

b) Syneresis i.e. spontaneous shrinkage of the gel with the expulsion of solvent

c) Coarsening i.e. increase in pore size and reduction in surface area through dissolution and re-precipitation.

In silica gels made from hydrolysis of alkoxides, it has been shown by NMR and Raman spectroscopy that the number of bridging bonds increases long after gelation. The condensation reaction, proceeds, because of the large concentration of the silanol groups. As new bonds are formed the flexibility of the network decreases. Further hydrolysis and re-esterification can also occur.[18]

As condensation reaction proceeds, the increase in bridging bonds causes contraction of the gel network. The shrinkage of the gel and the resulting expulsion of liquid from the pores are called syneresis. The same condensation reaction that produces gelation leads to syneresis. This type of syneresis is called macrosyneresis while microsyneresis is the process of phase separation in which the polymers cluster together creating regions of free liquid and the driving force for this is the greater affinity of polymer for itself than the pore liquid. In organic polymers more syneresis produces turbidity owing to the scattering of light by separate phase. The porosity in dried organic gels is attributed to microsyneresis.

Coarsening is a process of dissolution and reprecipitation driven by difference in solubility between surfaces of different radii of curvature. The result of dissolution-reprecipitation is to reduce the net curvature of the solid phase, small particles disappear and small pores are filled in. So the interfacial area decreases and the average pore size increases. However this will not produce any shrinkage because the centres of particles do not move towards one another.

Dissolution and reprecipitation causes growth of necks between particles, increasing the strength and stiffness of the gel. Under aqueous conditions the particle growth is such that the initial aggregates restructure through dissolution-reprecipitation to form larger, more stable particles, thereby consuming the small primary particles. The mechanism by which this occurs is termed as Ostwald ripening mechanism.

The rate of coarsening is affected by factors that affect solubility such as temperature, pH, concentration and type of solvents. The amount of shrinkage that occurs during drying is dependant on the stiffness of the network.

Drying of Gels

The gel consists of a solid network enclosing a continuous liquid phase. Initially the liquid/vapour interface (meniscus) is flat. Evaporation of liquid from the pores of a gel exposes the solid phase. Since the solid/vapour interfacial energy (γ_{SV}) is larger than the solid/liquid interfacial energy (γ_{SL}), the liquid tends to squeeze out from the interior of the gel to cover the exposed solid. As the liquid stretches to cover the solid, tensile stress develops in the liquid and compressive stress is imposed on to the solid phase. The meniscus begins to develop a curvature; the pressure in the liquid at the exterior surface (Pc) is related to the radius of curvature of the meniscus (r) by,

$$P_c = \frac{2(\gamma_{SV} - \gamma_{SL})}{r}$$

Initially the gel is so compliant that the compressive stress causes viscoelastic deformation of the solid, drawing it under the surface of the liquid. The network shrinks as fast as the liquid evaporates, and the liquid/vapour meniscus remains at the exterior surface of the gel. This is known as the constant rate period.[18]

As the gel shrinks its stiffness increases, because the solid network becomes more tightly packed and the aging process occurs concurrently. As the gel stiffens, the pressure (Pc) at the surface of the liquid rises until the meniscus reaches its maximum curvature, and the capillary pressure,

$$P_R = \frac{(\gamma_{SV} - \gamma_{SL})S_p}{V_p}$$

Where Sp and Vp are the surface area and volume of the (liquid filled) pore space. When the gel is too stiff to contract under the pressure, shrinkage stops. This is known as the leather hard point. The amount of shrinkage that occurs up to that point depends on the amount of aging. After the Leather hard point the shrinkage drops abruptly. The leather hard point is also referred to as critical point of drying, as the chance of cracking of the gel is high at this point. The extend of shrinkage, collapse of gel structure and

structural changes during drying of a gel greatly depends on the initial gel structure, the aging steps involved before drying, the nature of pore fluid and the method of desiccation.

Aging helps to reduce cracking of gels. However, there are other approaches, including surfactants, drying control chemical additives, hypercritical drying and dialysis. Surfactants reduce the interfacial energy and drying control chemical additives (DCCA) like formamide and oxalic acid produce larger and uniform pores. DCCAs also improve the strength of the gel.

Supercritical drying is the method by which the shrinkage of the gel network can be avoided completely. Liquid phase cannot exist above supercritical point. The interfacial tension between a solid and a gas is very small compared to that between liquid and the solid. So, when a wet gel is subjected to temperature and pressure above the supercritical point of the pore liquid, it is converted to the gas phase and the gas can be evacuated without developing any sort of drying stress. This technique leads to the formation of aerogels where the gel network is maintained as such, even after drying.

Aerogels

The main component of this material is air which is surrounded by a very filigrane, solid network. The network is highly porous and has a density that is only three times that of air. SiO_2 aerogels have a high transparency that is close to that of glass, a thermal conductivity corresponding to that of polystyrene or polyurethane foams, or very high specific surface areas, like in charcoal. Combination of these physical properties, related to different chemical compositions, in one material define the uniqueness of aerogels. Important aspects for various applications are thus combined, for example, for heat insulation, optical applications, sensors, catalysts, or catalyst carriers. Aerogels can be defined as materials in which the typical structure of the pores and the network is largely maintained while the pore liquid of a gel is replaced by air.

The structures of aerogels are characterized by well accessible, cylindrical, branched mesopores. Aerogels are unique among mesoporous materials owing to their extremely high porosity (low density), high specific surface area, and the possibility of

making monoliths. Aerogels can also be obtained as granulates or powders. The bulk density of aerogels is in the range of 0.004 - 0.500 gcm^{-3} owing to the high porosity.

Formation of the highly porous three-dimensional network is one of the key steps in the preparation of aerogels. This can be achieved for inorganic, inorganic - organic, and purely organic systems under controlled conditions. Network formation demonstrates the influence of chemical parameters, in particular the kind of precursors and the reaction conditions, on the resulting microstructure. The microstructure influences the macroscopic properties of the resulting solid. This is of particular interest to aerogels since the network is preserved through out the drying process. To derive information on structure of aerogels one requires methods which cover the length scale from the lower nanometer (structure of the primary particles) to the micrometer range (linking of the particles).[30]

Synthesis

Sol-gel synthesis is the irreplaceable part in aerogel synthesis. A detailed discussion of the process has been presented in the previous sections. Modifications to the precursor or incorporation of foreign compounds can be added to the general sol-gel procedure.

The added role of the solvent in aerogel synthesis has to be emphasized. In general sol gel solvent act as the homogenizing agent and chelating agent; and also influences the network formation. Since gelation results in only a marginal change in volume and the drying process during the aerogel production, the volume of the aerogel body (and thus its density) is determined by the volume of the reaction solution. Therefore, the density of aerogels is simply modified by varying the precursor concentration in the starting solution.

Nearly all metal or semimetal oxides are known to form gels, and many served for the production of aerogels. Originally Kistler used water glass for his preparation of aerogels.[1] But the process was time consuming due to the need for ion exchange and subsequent solvent exchange. The use of alkoxide precursor in the synthesis of aerogel was first introduced by Teichner.[31] Tetramethoxysilane in ethanol was used as the

precursor. The pore liquid now mainly consisted of alcohol, and therefore the wet alcogels could be dried supercritically without solvent exchange. The preparation of aerogels from polymeric gels is more difficult, because diffusion processes are strongly inhibited by the smaller pores. Complete removal of the pore liquid is therefore more difficult and results in greater shrinkage upon drying.[32] For this reason SiO_2 aerogels are usually prepared by base-catalyzed reaction of tetramethoxysilane (TMOS) or tetraethoxysilane (TEOS), usually with ammonia as the catalyst. Brinker first prehydrolyzed the alkoxide with a small amount of water under acidic conditions.[33] This results in the formation of small clusters of silicic acid. In a second step a defined amount of aqueous acid or base is added. Networks formed by this two step procedure have a structure similar to that of the reaction limited cluster aggregation model; that is, they have polymeric character. The probable explanation is that the reactive clusters formed in the first step as structure-forming units are strongly responsible for the formation of the network, independent of the kind of catalyst used in the second step. The main difference caused by base or acid catalysis in the second step is the stiffness of the resulting network. The former results in a stiffening which stabilizes the gels. With this two-step procedure a more deliberate control of the microstructure and thus the particle and pore sizes of the SiO_2 gels is possible. The group of Hrubesh used the two-step sol-gel process to vary the density of aerogels within a larger range.[34] When aerogels are made by simple base-or acid-catalyzed reactions, their density is restricted to 0.030-0.300 gcm^{-3} because the alcohol formed during hydrolysis shifts the equilibrium towards species with alkoxy groups. This results in long gelation times. Tillotson and Hrubesh removed the alcohol by distillation after the first step and replaced it by an aprotic solvent (e.g. acetonitrile). Deliberate dilution, base-catalyzed hydrolysis of the remaining Si-OR groups, and condensation of the SiO_2 particles resulted in the formation of a three dimensional network and a solid with a density of only 0.004 gcm^{-3}.[34] Pajonk on the other hand synthesized oligomeric polyethoxysiloxanes of a certain size from TEOS by adding an exact amount of water and used these defined oligomers as precursors for sol-gel processing to form the three-dimensional network.[35] BASF, Hoechst, and others

developed a procedure in which a solution of aqueous sodium silicate is ion-exchanged and then hydrolyzed under acidic conditions.[35] For the production of Basogel, the aerogel product of BASF, a two step-procedure was applied. A solution of sodium silicate is mixed with sulfuric acid in the first step. Small hydrogel or aquagel droplets are formed by spraying. The metal salts are then extracted, and the water is exchanged for an organic solvent.[36] The gel droplets are then supercritically dried.

Tetramethoxysilane (TMOS) undergoes a more rapid hydrolysis than tetraethoxysilane (TEOS) and Wagh has compared the aerogels obtained from three different precursors: TEOS, TMOS and PEDS (polyethoxydisiloxane) and claimed that TMOS yields narrow and uniform pores and higher surface area than TEOS.[37-40] Aerogels have also been prepared from unusual precursors like rice hull ash.[41] Schwertfeger revisited the use of waterglass as a cheaper silica source for aerogel synthesis and Einarsrud confirmed that waterglass, produced aerogels with the highest degree of monolithicity because these gels had the highest stiffness and the largest pore size.[42,43]

The choice of alcohol as a solvent in the sol-gel process is due to the solubility of water and alkoxide in it. But it is also a by product of the reaction and can increase the rate of the esterification reaction, the backward reaction. Zhang used methylene chloride to dissolve MTES and Dai promoted ionic liquids.[44,45] Einarsrud dissolved the acid catalyst in ethylacetoacetate and added this mixture to PEDS. [42]

Aerogels of oxides other than silica

The principles for network formation of SiO_2 gels also hold for non-silicate inorganic gels and aqueous solutions of salts or molecular precursors in organic solvents can be employed for sol-gel processing. Metal alkoxides of titanium, zirconium, tin, or aluminum are much more reactive towards water than alkoxysilanes.[18] This is due to the lower electronegativity and higher Lewis acidity as well as the possibility of increasing the coordination number. The reactivity towards water is so high for many of these alkoxides that precipitates are spontaneously formed. Hence the reaction rates of metal alkoxides must be reduced to obtain gels instead of precipitates. The most common

method is the addition of a ligand like acetic acid or acetylacetone to the precursor solution.[18,46] Compared to aerogels with a silicate network, one of the most important differences of metal oxide aerogels is the possibility of forming crystalline primary particles. Alumina aerogels are one of the most extensively studied metal oxide aerogels particularly for catalytic applications. [47-50] TiO_2 and ZrO_2 aerogels are mostly prepared from alkoxide precursors.[49,51,52] TiO_2 aerogels can be prepared totally amorphous or with a network of anatase primary particles.[53,54] Similar attempts have been successful with V_2O_5 [55], Cr_2O_3 [2], Fe_2O_3 [56], MoO_2 [49], Nb_2O_5 [57]. Binary and ternary oxide aerogels of mixed oxide systems have also been reported.[58,59] Metal impregnated aerogels are another group of aerogels that has profound catalytic applications. [58-60]

Organic aerogels

Organic polymers starting from organic monomers can be supercritically dried to give a new class of monolithic aerogels. The most extensively studied of these materials are the resorcinol-formaldehyde (RF) and melamineformaldehyde (MF) aerogels. They can be prepared by polycondensation of resorcinol or melamine with formaldehyde in a slightly basic aqueous solution, often with sodium hydroxide or sodium hydrogen carbonate as the gelation catalysts.[61-63] Small clusters of approximate size 2 nm are first formed. The structure can be considered as branched polymeric species characterized by a mass fractal dimension. These clusters aggregate and form particles 4-7 nm which show a surface fractal dimension. The structure is then fixed by gelation, in a temperature range from 238 to 333 K. Finally the particle surface is smoothed out by aging.[64] Other precursors used to make organic aerogels include phenolic-furfural (PF) mixtures with poly- (dimethylsiloxane) (PDMS), 2,3-didecyloxyanthracene (DDOA) with ethanol or supercritical CO_2 as the solvent, polyacrylonitrile (PAN) or polyisocyanates.[61,65-68] The organic aerogels reported are non transparent. Bulk densities are of the order of 0.24 gcm^{-3} and a specific surface area of approximately 300 m^2g^{-1}.[69] Pyrolysis of organic aerogels, at temperatures above 500 °C, produces an electrically conductive carbon network.[62] These networks retain the high specific surface area (400-800 m^2g^{-1}), the large specific mesopore volume (>0.55 cm^3g^{-1}), and the isotherms with a hysteresis loop of their parent

organic aerogel.[70,71] These materials are called carbon aerogels and are of extreme interest in energy research for super capacitor applications.

Organic Inorganic Hybrids

The possibility of combining the properties of organic and inorganic compounds in a unique material is an old challenge that started with the beginning of the industrial era. The concept of 'hybrid organic inorganic' materials emerged only very recently, when the interest shifted to more sophisticated materials with a higher added value. The blending of organic and inorganic components and the synergism of their properties in one material is particularly useful and allows the development of materials with totally new properties. Recently, the study of organic inorganic nanocomposite networks and gels became an expanding field of investigation. These new materials promise new applications in many fields such as optics, electronics, ionics, mechanics and biology. At first glance, these materials can be considered biphasic, where the organic and inorganic phases are mixed at the nm to sub-μm scales. But the properties of these materials are not just the sum of the individual contributions; the role of the inner interfaces is predominant. The nature of the interface has been used recently to divide these materials into two distinct classes.[72] In class I, organic and inorganic compounds are embedded and only weak bonds (hydrogen, van der Waals or ionic bonds) give the cohesion to the whole structure. In class II materials, the two phases are linked together through strong chemical bonds (covalent or iono-covalent bonds). Obviously, within class II hybrid materials, organic and inorganic components can also interact via the same kind of weak bonds that define the class I hybrids.[73]

Thermal stability of organics are limited to around 250 °C, and the sol-gel process offers the most viable synthesis methodology for processing the hybrids. Hybrid materials are made by mixing organic and inorganic components. Control of the properties of the final material is achieved by controlling the chemical nature of the organic and inorganic phases, the size and morphology of these domains (nm to sub-μm scale) and the nature of the interphase interaction.

Small organic molecules entrapped in an inorganic network is the most simple representation of a hybrid material. It corresponds to the doping of sol-gel matrices by organic dyes, inorganic ions or molecules, resulting in fluorescence, photochromic or non-linear optical (NLO) properties. Organic molecules such as rhodamines, pyranines, coumarins, porphyrins, phthalocyanines and spiropyrans, as NLO dyes have been entrapped in inorganic networks such as silica, aluminosilicate or transition metal oxide based gels (ZrO_2, TiO_2).[74-76] Transparent monoliths of large size with a tunable refractive index can be obtained for optical applications by filling the pores of sol-gel derived matrices by a monomer (methylmethacrylate, butadiene and derivatives, etc.) and polymerizing it inside the pores. The properties can be tuned depending on the size and geometry of the holes, the difference in the refractive index between the two phases and the organic:inorganic ratios.[77,78] Inorganic clusters have also been prepared inside a polymer structure by starting from the polymer and metal alkoxide.[79] In extension to this method is the use of organically modified metal alkoxide precursors. Here there is no preformed network and both organic and inorganic networks are prepared from the monomers. This leads to interpenetrating organic inorganic networks which may be linked together by covalent bonds.[80,81] Organically modified silane precursors are the most extensively investigated group of alkoxides and are now available commercially with organic groups with variety of functional groups and chain lengths.

Sol-gel processing of organically modified silanes can be done sequentially. First, the inorganic network is created by the polycondensation of the silicon alkoxide, which leads to the formation of the inorganic network surrounded by organic groups. In the second step, the organic polymerization is achieved. Organic polymerization of methylmethacryl, vinyl, ally and epoxy R' groups have been extensively studied and described. The polymer brings new properties to the inorganic network like flexibility, hydrophobicity, refractive index modification, etc.[82] Organic groups which are no longer reactive have also been investigated. These network modifiers (e.g. Si-CH_3) are studied extensively for surface modification of films or particles in the fields of corrosion protection, surface treatment, membranes and chromatography.

The concept of organic inorganic hybrids in aerogels widens the spectrum of properties of aerogels without influencing the existing positive properties, such as good heat insulation, transparency, and high surface area. Most frequently encountered examples are the improved hydrophobicity and the elastic properties of SiO_2 aerogels by the incorporation of organic groups.[83,84]

Modification of aerogel network after drying imposes serious difficulties due to the need to expose the filigrane network to liquids which usually results in the shattering of the network. Gas phase reaction is an alternative but of limited use due to the ease in modifying the network prior to drying.[85-87] A more useful route is the integration of organic molecules or groups already during sol-gel processing. Embedding molecules into gels without chemical bonding is achieved by dissolving the molecules in the precursor solution. The gel matrix is formed around them and traps them. The network is then dried to obtain the modified aerogel. Doping the aerogels with fluorescent dyes has been successfully attempted for applications ranging from fluorescent probes to sensitized solar cells.[88-91] Fullerene doping has also been attempted to achieve luminescence.[92-95] Similar efforts have been reported for incorporating polypyrrole in carbon aerogels for photovoltaic applications.[96]

One of the earliest attempts in the direction of organic inorganic hybrid aerogels is the hydrophobisation of aerogel surface using alkyl modified groups. The need for hydrophobic aerogels for long term applications have led to investigations using several alkyl groups with reactive ends that can react to surface silanols. Alkyl modified silanes can be co-condensed with tetraalkoxysilanes to induce hydrophobicity in the final aerogel. Triethoxysilane, ethyltrimethoxysilane, methyltrimethoxysilane, phenyltrimethoxysilane, polyethoxydisiloxane, trifuoropropyltrimethoxysilane, hexamethyldisilazane etc. has all been used to modify the hydrophobicity of aerogels.[97-105] Rao et al. has compared the effect of six co-precursors on the hydrophobic properties of the final aerogels.[106] On the other hand Tris(hydroxymethyl)aminomethane has been incorporated in to the gel during condensation to impart hydrophobicity.[107] Surface modification with

trimethylchlorosilane is a standard procedure for the modification of aerogel surface, but involves the evolution of toxic HCl during the process.[108]

The use of methyltrimethoxysilane precursor for the preparation of aerogels has also given rise to one of the most fascinating developments in the fields, flexible aerogels. The aerogels prepared from methyltrimethoxysilane alone could endure up to ~ 80% linear compression and then spring back to more than 95% of their original size. The bulk modulus of these flexible aerogels was found to be comparable to values for conventional silica aerogels. But the Poisson's ratio was 0.12 compared to 0.2 of silica aerogels indicating that the relatively soft and continuous skeletons undergo a substantial deformation, by folding inward towards the pores.[109,110] These aerogels had contact angles as high as 160 °.[111,112]

Kim et al. attempted the preparation of aerogel-PVB composites by hot pressing in order to overcome the mechanical limitations of aerogels. Starting from a waterglass precursor and using a surface modification treatment using trimethylchlorosilane technique they prepared aerogels at ambient pressure. Aerogels were crushed and mixed with PVB. They found that a mixing technique involving wet mixing of aerogels with PVB and mixing this composite with aerogel powder prior to hot pressing gave homogeneous composites with aerogel properties.[113]

Novak investigated the development of interpenetrating organic inorganic network in sol-gel materials and their effect on mechanical properties.[114] In aerogels, their first approach involved addition of preformed polymers poly(2-vinylpyridine), poly [methylmethacrylate-co-(3-trimethoxysily)propylmethacrylate)], and silanol-terminated poly(dimethylsi1oxane) (PDMS) to the sol-gel precursor solutions. In another approach they formed the organic polymer cross-linked poly(N,N-dimethylacrylamide) in situ.[115] In both cases they found that the bonding of the organic phase to the SiO_2 structure is important and crosslinking of the organic polymer further improved the properties. Schaefer studied the structure of arylene-bridged polysilsesquioxane derived aerogels and xerogels and found domains in the nanometer range with distinct fractal character. They associate these domains with porosity rather than microphase separation of organic and

inorganic moieties. The higher the organic content, the smaller the domain size.[116] Mackenzie observed that in polydimethylsiloxane modified hybrid systems, from a macroscopic mechanical point of view, the behaviour ranges from brittle solids to rubbery elastomers according to the polymer content.[117] de la Rosa-Fox investigated these hybrid aerogels for their mechanical properties and found that the clustered elementary particles of inorganic porous silica aerogel of 1–2 nm average size are surrounded by the organic polymer forming blobs of 6–8 nm average size, which are mass fractal with dimension of 2.5. These units were clustered into larger aggregates maintained in equilibrium by the ‘‘frozen-in’’ elastic constraints between such units.[118]

Leventis added a new dimension to the organic inorganic hybrid aerogels when he started nano engineering aerogels to increase mechanical strength.[119] In order to strengthen monolithic aerogels the interparticle necks need to be widened. To accomplish this with minimum addition of new material, the contour surface of silica was used as a template for the deposition and growth of the interparticle cross-linker. Initially he chose the reaction between the surface silanol groups and a diisocyanate to introduce a polyurethane like network to reinforce the aerogel structure. The procedure involved the immersion of the hydrogel in a propylene carbonate/diisocyanate solution for the crosslinking. The gels were then dried supercritically to form the crosslinked aerogel. These composite aerogels were less hygroscopic and more robust than pure silica aerogels. There was a dramatic improvement in the strength of the new material as tested with a three point flexural bending method and took more than 100 times higher load to break a monolith with density 0.447 gcm^{-3} (~15 kg) than to break a native silica aerogel monolith (~120 g).[119] His group further extended the work to tri-isocyanates and also changed the isocyanate delivering solvent to acetone, which reduced the processing time considerably. Even though the density of the crosslinked aerogels increased compared to pure silica aerogels, large part of the porosity was retained and low dielectric constant, close to that of native aerogel was obtained. The increased shrinkage was then attributed to the compression of the inorganic network due to the organic networking. The method reinforced the aerogel structure by a factor of ~300 times.[120] The isocyanates reacted not

only with surface silanols, but also with surface adsorbed water to form amines which further reacted with isocyanate to give polyurea networks. In order to control the network formation and to convert the crosslinking network to polyurea network, the same group modified the inner lying silica surface with amine functionality. This was achieved by co-condensing amine modified silane precursor along with TEOS. This eliminated the formation of polyurethane network formed from the reaction between surface silanols and isocyanate. They also observed that the all compressive specimens failed due to lateral strain.[121] The observed properties were found to depend quadratically on the silane concentration, isocyanate concentration, water concentration, number of washings performed after gelation and temperature of synthesis.[122,123] The diisocyanate was replaced with epoxy functionalities to develop an epoxy crosslinked network. It was found that while elastic modulus follows a similar trend with density, maximum strength is attained neither at the maximum density nor at the highest concentration of amine groups, suggesting surface saturation effects. Aerogels cross-linked with the trifunctional epoxide always show improved strength compared with aerogels cross-linked with tetra or di epoxides under identical conditions.[124] On reacting the surface amine groups with p-chloromethylstyrene free-radical polymerization process could be initiated using AIBN and styrene to develop a polystyrene network. These mechanically strong aerogels had very high hydrophobicity (>120 °).[125,126]

Drying methods

Drying is the most important step in the preparation of aerogels. This is the stage where the property of an aerogel is decided against that of the xerogel. If the drying happens without the shrinkage of the gel network then aerogel results, considerable shrinkage leads to xerogels. According to earlier definition, only supercritically dried gels were called aerogels. But ambient pressure drying techniques has developed considerably in recent years and aerogel like properties have been achieved by drying at ambient pressure.

Evaporation of the liquid from a wet gel is very complex, and occurs in different stages.[18] At the first stage, the gel shrinks by the volume that was previously occupied by

the liquid followed by the liquid flowing from the interior of the gel body to its surface. If the network is compliant, as for gels derived from alkoxides, the gel deforms. Upon shrinkage, hydroxyl groups at the inner surface approach and condense with each other. As drying proceeds the network becomes increasingly stiffer and the surface tension in the liquid rises correspondingly, because the pore radii become smaller. In the second stage of the drying process the gel body is too stiff for further shrinkage and the surface tension is no longer capable of deforming the network. At this critical point the tension in the gel becomes so large that the gel cracks. During the second stage of drying, the liquid/gas interface retreats into the gel body. Nevertheless, a continuous funicular liquid film remains at the pore walls; that is, most of the liquid still evaporates from the exterior surface of the gel body. In the next stage of drying this film is ruptured. Eventually only isolated pockets contain liquid, which can leave the network only by diffusion into the gas phase. Collapse of the network can happen due to two reasons: First, the slower shrinkage of the network in the interior of the gel body results in a pressure gradient which causes cracks. Second, larger pores empty faster than smaller ones during drying; that is, the meniscus of the liquid drops faster in larger pores and the walls between pores of different sizes are therefore subjected to uneven stress and crack. [18]

Supercritical drying eliminates the capillary stress by eliminating the gas liquid interface. Practically, supercritical drying consists of heating the wet gel in a closed container, so that the pressure and temperature exceeds the critical temperature, Tc, and critical pressure, Pc, of the liquid entrapped in the pores inside the gel. Supercritical drying is performed either hot (organic solvents) or cold (CO_2) depending on Tc. Commonly used organic solvents are acetone and alcohol and the conditions required are about 250 °C and 5 - 8 MPa. Problems arise from the combination of high temperatures and high pressures as well as the flammability of these solvents. In addition to the risks connected with supercritical drying in organic fluids, rearrangement reactions in the gel network are highly probable because of the high temperatures. Organically modified aerogels are particularly sensitive to the high temperatures, and functional organic groups may be destroyed during drying.[127] An alternative to drying in organic solvents is the use

of liquid carbon dioxide.[128,129] The advantage of the process is the low critical temperature (31 °C) and moderate critical pressure (7.3 Mpa) required. Exchanging the original pore liquid for liquid CO_2 is required and is determined by the diffusion of carbon dioxide into the gel, and is therefore dependent on the dimensions of the gel body. Hence the solvent exchange process is time consuming.[33] Deliberate structural changes can be induced in SiO_2/TiO_2, ZrO_2, and Nb_2O_5 aerogels by varying the temperature above Tc during supercritical drying with CO_2, for example, the ratio between crystalline and amorphous regions.[130]

Another possibility for avoiding phase boundaries between the liquid and gas phases during drying is freeze-drying. The pore liquid is frozen and then sublimed under vacuum. Several attempts were made to use this method for producing aerogels.[131] However, aging periods have to be extended to stabilize the gel network, the solvent must be exchanged for another with a low expansion coefficient and a high pressure of sublimation, and low freezing temperatures should be achieved by addition of salts. Another disadvantage is that the network may be destroyed by crystallization of the solvent in the pores. Cryogels are therefore only obtained as powders.

Even though the low temperature supercritical drying brought down the risks involved in supercritical drying large scale application still prefers an ambient pressure process that will give aerogel properties.[35] Efforts in this direction have always been part of the growing aerogel technology. Kirkbir studied the drying of silica gels using different solvents at various pressures ranging from supercritical pressures to atmospheric pressure. Aerogels could be thus obtained at pressures much lower than the supercritical pressure depending on the solvent.[132] Techniques for ambient pressure drying mainly centre on increasing the strength and stiffness of the gel network and hydrophobisation of the gel surface.

Increasing the strength and stiffness of the gel network help the gel to cope with the stress developed during drying. Aging of the wet gel in a precursor solution mostly tetraethylorthosilicate is a general method to increase the stiffness of the gel. Haereid et al. studied the effect of aging of alkoxide derived gels in silane solution. New monomers

add to the already formed network and hydrolysis, condensation and specific precipitation of these monomers favourably increase the strength and stiffness of the alcogel.[133] In tetramethoxysilane (TMOS)-based gels, the shear modulus, G, was increased by 15 times and the corresponding shrinkage was reduced by about 30% giving xerogels with a considerably lower density compared with unaged samples. Density as low as 0.24 gcm^{-3} could be achieved by changing aging parameters such as time and temperature. Monomers precipitate on to necks between the primary particles, where the silica solubility is lowest and then in the smallest pores. The shear modulus increased by 23 times and the modulus of rupture by five times, reducing the corresponding shrinkage during drying to ~ 0.5%. They also identified that the removal of water from the pores of the gel prior to drying and the use of a low surface tension liquid as the drying solvent improved the drying technique.[134-137] They later extended the technique to water glass based aerogels. Colloidal silica based gels had an added advantage that their pore radius was larger and hence the capillary stress developed was low.[138] Fidalgo observed that the chemical control, particularly pH of the hydrolysis condensation reactions could give aerogel like properties when dried at ambient pressure.[139] Einarsrud has reviewed the aging of the wet gel in the precursor solution and subsequent silylation to improve the gel strength for drying at ambient pressure.[140,141] This formed the basis of the ambient pressure process developed by Rajesh et al. which was successfully extended to mixed oxide aerogels by Aravind.[46,142] They optimised the aging concentration, aging time and temperature to obtain high surface area aerogels.[143,144]

Hydrophobisation of the gel network prior to drying introduces a large concentration of alkyl groups on the inner surface of the gel. During ambient pressure drying the shrinkage of the gel network cannot produce irreversible pore collapse due to the elimination of condensation reactions between the silanol groups on the pore walls. Further more on close approach the bulky alkyl groups start to repel and the repulsion push back the gel network to the original shape. This spring back effect is exploited for the ambient pressure dying of aerogels. The method was demonstrated by Brinker for the preparation of aerogel films at ambient pressure. [145] Later Schwertfeger used the process

to dry water glass derived gels to obtain aerogels.[43] Rao et al. further compared the effects of precursors, alkoxide and water glass, different solvents and surface modifying agents to obtain transparent aerogel monoliths through modified ambient pressure drying. They found that the while alkoxide precursors with the modifying agent, hexamethyldisilazane and alkane solvents gave the best transparency, water glass based aerogels had the best monolithicity based on the strength and larger pore sizes.[146] Investigations on the effect of preparation conditions were also performed.[147] Recently the research team from Korea successfully demonstrated the spring back phenomenon on water glass derived silica gels on drying at ambient pressure. Ideal ratios could be identified which gave gels that could recover fully from drying shrinkage.[148]

Applications of aerogels

Applications of aerogels are limitless and almost every feature of aerogel gives rise to a potential application. The table points to the versatility of the material.

Apart from these other very interesting applications has also been reported. Some of the interesting reported commercial applications include: wastewater treatment, moulds for casting aluminium metal, aerocapacitors, and heat storage device for automobiles, cosmic dust capture, muonium atom studies, and helium phase transition studies.[36,149-156]

Aerogels were used for particle detection using the Cherenkov Effect even in the early 1980s. High energy physics studies relied on aerogels having specific refractive indexes for threshold detectors.[157] Preparation of large aerogel plates were attempted for application in Cherenkov counters. Another important early application of aerogel material was as fuel capsules for direct-drive, inertial confinement fusion experiments.[33]

The supercapacitor is a high power density, high energy density, electrochemical double layer capacitor that uses carbon aerogels as electrodes. The electrodes possess very high surface per unit volume and are electrically continuous in both the carbon and electrolyte phases.

Property	Features	Applications
Thermal conductivity	Best insulating solid Transparent High temperature Lightweight	Architectural and appliance insulation, portable coolers, transport vehicles, pipes, cryogenic, skylights Spae vehicles and probes, casting molds
Density / porosity	Lightest synthetic solid Homogenous High surface area Multiple composition	Catalysts, sorbers, sensors, fuel storage, ion exchange Targets for ICF, X-ray lasers
Optical	Low refractive index solid Transparent Multiple composition	Cherenkov detectors, lightweight optics, lightguides, special effect optics
Acoustic	Lowest sound speed	Impedance matchers for transducers, range finders, speakers
Mechanical	Elastic lightweight	Energy absorber, hypervelocity particle trap
Electrical	Lowest dielectric constant High dielectric strength High surface area	Dielectrics for ICs, spacers for vacuum electrodes, vacuum display spacers, capacitors

Table 1.1. Property and corresponding possible application of aerogels

Aerogel materials exhibit the lowest thermal conductivities of any of the solid or porous materials. This key property of the material leads to many applications including insulation for architectural purposes, piping, heat and cold storage appliances and devices, automotive exhaust pipes, transport vehicles and vessels.[158]

Catalytic applications of aerogels are obvious. Almost all catalytic oxides can be prepared in the form of aerogels. Compounded by these facts there are numerous reactions that can be thought of which can be catalyzed by aerogels. Some are nitroxidation of hydrocarbons to nitriles (NiO/Al_2O_3 with SiO_2 and MgO, PbO/ZrO_2), hydrogenation of nitrobenzene to aniline and of toluene to methylcyclohexane (Ni/SiO_2, Pd/Al_2O_3), hydrogenation and hydrogenolysis after hydrogen spillover activation (ZrO_2,

SiO_2, MgO, Al_2O_3), isomerizations (Nb_2O_5, Nb_2O_5/SiO_2), Fischer- Tropsch syntheses (Fe_2O_3/Al_2O_3, Fe_2O_3/SiO_2), polymerization of ethene or propene ($TiCl_4/Al_2O_3$), deNOx reactions ($Fe_2O_3/Cr_2O_3/Al_2O_3$, Pt/C), catalysis for combustion of car exhaust (Pd/Al_2O_3 , Pt/Al_2O_3 , $Pd/Al_2O_3/SiO_2$), and fluorinations (Cr_2O_3).[35,159-161]

Aerogels can be sintered at low temperatures and can therefore be processed to extremely pure and totally homogeneous glasses.[162-165] Partially sintered aerogels can be used for the storage, thickening, or transport of liquids, like rocket fuels.[166]

SiO_2 aerogels are suitable as ecologically sound insecticides against pests in grain and seeds or on the ground, such as mites, ticks, cockroaches, or silver fish.[167-170]

SiO_2 aerogels are currently one of the standard media for collecting cosmic dust, and they are fixed outside a spacecraft.[149] Silica aerogels were also engaged in the PATHFINDER MARS mission to insulate the Sojourner Mars Rover, which had an inside temperature of 21 °C, even when the outside temperature of Mars dropped to -67 °C at night. The space exploration applications of aerogels have been well reviewed by Jones.[171]

Power et al. described a solid biosensor prepared and tested under the form of an aerosol of aerogel containing Escherischia coli and the green fluorescent protein (GFP). When a virus, like the bacteriophage T7 polymerase promoter also in the form of an aerosol, contacts the bacteria, green fluorescence is emitted. Silica aerogels offer the advantage to immobilise the sensor part of the detector, which can then give an easily detectable and even quantified response to a biological organism existing as an aerosol in the environment.[172]

In the search of new biomaterials for clinical applications that require low density bioactive monoliths with high pore volume, like small bone prosthesis, organic-inorganic hybrid aerogels have been tested for their bioactivity.[173]

Silica aerogels has also been investigated for nuclear waste confinement. Since aerogels can be easily converted to glass, the approach will give waste, immobilised in glass matrix at pretty low temperatures.[174]

A novel concept of using aerogels as an architectural model for the creation of functional 3-D linked quantum dots has been reported. According to this methodology metal chalcogenide nanoparticles are assembled into nanostructures by controlled oxidative removal of surface thiolate ligands, followed by supercritical drying to retain the structure of the wet gel. The technique represents an effective way to organize metal chalcogenide nanoparticles into 3D architectures without the presence of intervening ligands that can potentially limit the electron transport properties and thermal stability.[175]

The research and application of photoactive molecules confined or covalently bound in an inorganic network has been increased over the last few years, since they excite much interest in the fluorescent sensors fields. Fluorescent benzazole dyes have been covalently bound to the aerogel silica matrix with an eye on potential applications like UV-light polymer stabilizers, solid-state laser dyes, fluorescent probes for labelling proteins and scintillation detectors.[176]

Solid state dye lasers are new application prospect investigated for aerogels. Open porous network of the aerogel was saturated with laser dyes dissolved in appropriate organic monomers, and polymerized inside the silica structure. Highly photostable laser emission with good lasing efficiency was observed.[177]

Aerogels present a vivid landscape of potential applications and the recent advances in the field have proved that the possibilities are really endless.

Definition of the Present Problem

As observed in the introduction aerogels present a seemingly endless possibility of applications in a vivid landscape of areas and are limited only by the brittleness and the supercritical drying required for the preparation. As pointed out, the need to explore ambient pressure drying for aerogel like materials is inevitable for the wide scale and commercial applications for these materials. Even though many attempts are made for using ambient pressure drying techniques with varying degree of success, there is need for further investigation to incorporate new developments in the fields. For example, organically modified aerogels have escorted the aerogel technology to the new functional materials era, but the attempts to incorporate these advances in to the ambient pressure drying techniques is largely missing from the state of the art in aerogel technology.

Leventis has demonstrated the advantage of developing organic networks coexisting with the inorganic network in preparing mechanically strong aerogels.[119-125,178,179] Simultaneously Warrier's group had optimised the conditions for an ambient pressure drying technique for the synthesis of high surface area silica aerogels.[46,142-144] This thesis envisages combining the concept of organic inorganic hybrid networks and ambient pressure drying for aerogel like hybrid networks. The organic functionalisation and ambient pressure process for its preparation is expected to double the potential impact of these materials in the field.

Optimisation of the ambient pressure process for organic inorganic hybrid aerogels is primarily required. Chemical control of the sol-gel reactions by varying the parameters like precursor ratio, water for hydrolysis ratio and the effect of an organic crosslinker also needs to be addressed. More over, the actual performance of the network needs to be compared with that of supercritically dried aerogels. Demonstration of a potential application is also necessary.

So the effect of organically modified precursors on the properties of ambient pressure dried aerogels will be investigated first. Crosslinking of the organic groups will be attempted next. This requires the identification of a polymerisable organic group which will be compatible with sol-gel processing. 3-glycidoxyrpopyl group is an epoxy

group which can link by the polymerization of the epoxy group. The epoxy polymerization is far more facile than other reported cross linking mechanisms. The presence of an added organic crosslinker will also be considered. This will help to increase the organic network density independent of the inorganic network. The cross linked systems will be characterized for the dielectric response to identify the ideal composition to achieve exact aerogel properties. Finally from an application perspective photoactive aerogel coatings for possible application as cleaning of noxious gases will be undertaken. Titania is an eco friendly and widely accepted photocatalyst prevalent in development of self cleaning surfaces. Titania supported on the aerogel represents a symbiotic hybrid material where the titania will act as the degrading agent and the porous nature of the aerogel support will ensure the presence of large volume of the contaminant on the titania surface. The applicability of these surfaces will be finally checked.

Summing up in brief the work under taken in this thesis can be divided as follows.

1) Studying the effect of an organically modified precursors on the ambient pressure process for aerogels.
2) Developing a synthesis methodology for the preparation of crosslinked organic inorganic networked gel structure and the ambient pressure drying of these networks.
3) Measurement of dielectric properties of these ambient pressure dried networks.
4) Potential application of these networks as support for photoactive surfaces in the form of films on glass substrates

References

1. Kistler, S. S., *Nature*, 127 (1931) 741.

2. Kearby, K.; Kistler, S. S.; Swann, S., *Industrial and Engineering Chemistry*, 30 (1938) 1082.

3. Kresge, C. T.; Leonowicz, M. E.; Roth, W. J.; Vartuli, J. C.; Beck, J. S., *Nature*, 359 (1992) 710.

4. Yaghi, O. M.; Li, G.; Li, H., *Nature*, 378 (1995) 703.

5. Rouquerol, J.; Avnir, D.; Fairbridge, C. W.; Everett, D. H.; Haynes, J. H.; Pernicone, N.; Ramsay, J. D. F.; Sing, K. S. W.; Unger, F. K., *Pure and Applied Chemistry*, 66 (1994) 1739.

6. Jane, A.; Dronov, R.; Hodges, A.; Voelcker, N. H., *Trends in Biotechnology*, 27 (2009) 230.

7. Anglin, E. J.; Cheng, L.; Freeman, W. R.; Sailor, M. J., *Advanced Drug Delivery Reviews*, 60 (2008) 1266.

8. Mujeebu, M. A.; Abdullah, M. Z.; Bakar, M. Z. A.; Mohamad, A. A.; Abdullah, M. K., *Progress in Energy and Combustion Science*, 35 (2009) 216.

9. Thomas, A.; Kuhn, P.; Weber, J.; Titirici, M.-M.; Antonietti, M., *Macromolecular Rapid Communications*, 30 (2009) 221.

10. Potter, O. G.; Hilder, E. F., *Journal of Separation Science*, 31 (2008) 1881.

11. Stöcker, M., *Angewandte Chemie International Edition*, 47 (2008) 9200.

12. Wang, H.-J.; Zhang, K.-Y.; Liu, Y.-Q., *Journal of Clinical Rehabilitative Tissue Engineering Research*, 12 (2008) 8189.

13. Suib, S. L., *Accounts of Chemical Research*, 41 (2008) 479.

14. Hatton, B. D.; Landskron, K.; Hunks, W. J.; Bennett, M. R.; Shukaris, D.; Perovic, D. D.; Ozin, G. A., *Materials Today*, 9 (2006) 22.

15. Wilson, S. T.; Lok, B. M.; Messina, C. A.; Cannan, T. R.; Flanigen, E. M., *Journal of the American Chemical Society*, 104 (1982) 1146.

16. van Santen, R. A., 444 (2006) 46.

17. O'Brien, M. G.; Beale, A. M.; Catlow, C. R. A.; Weckhuysen, B. M., *Journal of the American Chemical Society*, 128 (2006) 11744.

18. Brinker, C. J.; Scherer, G. W. *Sol-Gel Science:The physics and Chemistry of sol-gel processing*, ed. Academic Press: London, 1990.

19. Tanev, P. T.; Pinnavaia, T. J., *Science*, 267 (1995) 865.

20. Saggio-Woyansky, J.; Scott, C.; Minnear, W., *American Ceramic Society Bulletin*, 11 (1992) 1674.

21. Pierre, A. C. *Introduction to Sol-Gel Processing*, ed. Kluwer Academic publishers: The Netherlands, 1998.

22. Hiemenz, P. C. *Principles of Colloidal and Surface Chemistry*, ed. Marcel Dekker: New York, 1997.

23. Narula, C. K. *Ceramic Precursor Technology and its Application*, ed. Marcel Dekker: New York, 1995.

24. Turner, C. W., *American Ceramic Society Bulletin*, 70 (1487) 1487.

25. Roizin, Y. O.; Gevelyuk, S. A.; Prokopovich, L. P.; Savin, D. P.; Rysiakiewicz-Pasek, E.; Marczuk, K., *Journal of Porous Materials*, 4 (1997) 151.

26. Livage, J.; Henry, M.; Sanchez, C., *Progress in Solid State Chemistry*, 18 (1988) 259.

27. Schaefer, D. W.; Keefer, K. D., *Physical Review Letters*, 53 (1984) 1383.

28. Schaefer, D. W.; Martin, J. E.; Wiltzius, P.; Cannell, D. S., *Physical Review Letters*, 52 (1984) 2371.

29. Martin, J. E.; Schaefer, D. W., *Physical Review Letters*, 53 (1984) 2457.

30. Smith, D. M.; Hua, D.-W.; Earl, W. L., *MRS Bulletin*, 19 (1994) 44.

31. Nicolaon, G. A.; Teichner, S. J., *Bulletin de la Societe Chimique de France*, (1968) 1900.

32. Heinrich, T.; Klett, U.; Fricke, J., *Journal of Porous Materials*, 1 (1995) 7.

33. Brinker, C. J.; Ward, K. J.; Keefer, K. D.; Holupka, E.; Bray, P. J.; Pearson, R. K., Springer Proceedings in Physics, (1985), Wurzburg, Springer-Verlag, Berlin, 6, 57.

34. Tillotson, T. M.; Hrubesh, L. W., *Journal of Non-Crystalline Solids*, 145 (1992) 44.

35. Hüsing, N.; Schubert, U., *Angewandte Chemie - International Edition*, 37 (1998) 22.

36. Herrmann, G.; Iden, R.; Mielke, M.; Teich, F.; Ziegler, B., *Journal of Non-Crystalline Solids*, 186 (1995) 380.

37. Nakanishi, K.; Minakuchi, H.; Soga, N.; Tanaka, N., *Journal of Sol Gel Science and Technology*, 13, (1998) 163.

38. Minakuchi, H.; Nakanishi, K.; Soga, N.; Ishizuka, N.; Tanaka, N., *Analytical Chemistry*, 68 (1996.) 3498.

39. Ishizuka, N.; Minakuchi, H.; Nakanishi, K.; Soga, N.; Hosoya, K.; Tanaka, N., *Journal of Chromatography A*, 797 (1998) 133.

40. Wagh, P. B.; Begag, R.; Pajonk, G. M.; Rao, A. V.; Haranath, D., *Materials Chemistry and Physics*, 57 (1999) 214.

41. Tang, Q.; Wang, T., *Journal of Supercritical Fluids*, 35 (2005) 91.

42. Einarsrud, M.-A.; Nilsen, E.; Rigacci, A.; Pajonk, G. M.; Buathier, S.; Valette, D.; Durant, M.; Chevalier, B.; Nitz, P.; Ehrburger-Dolle, F., *Journal of Non-Crystalline Solids*, 285 (2001.) 1.

43. Schwertfeger, F.; Frank, D.; Schmidt, M., *Journal of Non-Crystalline Solids*, 225 (1998) 24.

44. Zhang, X.; Huang, S., *Journal of Chromatography A*, 939 (2001) 13.

45. Dai, S.; Ju, Y. H.; Gao, H. J.; Lin, J. S.; Pennycook, S. J.; Barnes, C. E., *Chemical Communications*, 2 (2000) 243.

46. Aravind, P. R., *Mixed Oxide Silica Aerogels Synthesized Through Non Supercritical Route for Functional Applications*, PhD. Thesis, (2008), Faculty of Science, Cochin University of Science and Technology.

47. Suh, D. J.; Park, T.-J.; Kim, J.-H.; Kim, K.-L., *Chemistry of Materials*, 9 (1997) 1903.

48. Mizushima, Y.; Hori, M., *Journal of Non-Crystalline Solids*, 167 (1994) 1.

49. Teichner, S. J.; Nicolaon, G. A.; Vicarini, M. A.; Gardes, G. E. E., *Advances in Colloid and Interface Science*, 5 (1976) 245.

50. Mizushima, Y.; Hori, M., *Journal of Non-Crystalline Solids*, 170 (1994) 215.

51. Schneider, M.; Baiker, A., *Catalysis Today*, 35 (1997) 339.

52. Schneider, M.; Baiker, A., *Journal of Materials Chemistry*, 2 (1992) 587.

53. Zhu, Z.; Tsung, Y.; Tomkiewicz, M., *Journal of Physical Chemistry*, 99 (1995) 15945.

54. Zhu, Z.; Lin, M.; Dagan, G.; Tomkiewicz, M., *Journal of Physical Chemistry*, 99 (1995) 15950.

55. Sudoh, K.; Hiroshima, H., *Journal of Non-Crystalline Solids*, 147/148 (1992) 386.

56. Foster, H. D.; Keyes, D. B., *Industrial and Engineering Chemistry*, 29 (1937) 1254.

57. Maurer, S. M.; Ko, E. I., *Journal of Catalysis*, 135 (1992) 125.

58. Pajonk, G. M., *Applied Catalysis*, 72 (1991) 217.

59. Schneider, M.; Baiker, A., *Catalysis Review Science and Engineering*, 37 (1995) 515.

60. Taghavi, M. B.; Pajonk, G. M.; Teichner, S. J., *Journal of Colloid and Interface Science*, 71 (1979) 451.

61. Pekala, R. W., *Journal of Materials Science*, 24 (1989) 3221.

62. Tamon, H.; Ishizaka, H. J., *Journal of Colloid and Interface Science*, 223 (2000) 305.

63. Pekala, R. W.; Alviso, C. T.; Kong, F. M.; Hulsey, S. S., *Journal of Non-Crystalline Solids*, 145 (1992) 90.

64. Tamon, H.; Ishizaka, E., *Journal of Colloid and Interface Science*, 206 (1998) 577.

65. Lee, K. N.; Lee, H. J.; Kim, J. H., *Journal of Supercritical Fluids*, 17 (2000) 73.

66. Placin, F.; Desvergne, J. P.; Cansell, F., *Journal of Materials Chemistry*, 10 (2000) 2147.

67. Gouerec, P.; Miousse, D.; Tran-Van, F.; Dao, L. H., *Journal of New Materials for Electrochemical Systems*, 2 (1999) 221.

68. Biesmans, G.; Randall, D.; Francais, E.; Perrut, M., *Journal of Non-Crystalline Solids*, 225 (1998) 36.

69. Biesmans, G.; Mertens, A.; Duffours, L.; Woignier, T.; Phalippou, J., *Journal of Non-Crystalline Solids*, 225 (1998) 64.

70. Zhang, S. Q.; Wang, J.; Shen, J.; Deng, Z. S.; Lai, Z. Q.; Zhou, B.; Attia, S. M.; Chen, L. Y., *Nanostructured Materials*, 11 (1999) 375.

71. Tamon, H.; Ishizaka, H.; Yamamoto, T.; Suzuki, T., *Carbon*, 37 (1999) 2049.

72. Sanchez, C.; Ribot, F., *New Journal of Chemistry*, 18 (1994) 1007.

73. Judeinstein, P.; Sanchez, C., *Journal of Materials Chemistry*, 6 (1996) 511.

74. Sol-Gel Optics-Proceedings of the SPIE, (1990), San Diego, CA, USA, 1328, 1.

75. Sol-Gel Optics II-Proceedings of the SPIE, (1992), San Diego, CA, USA, 1758, 1.

76. Sol-Gel Optics III, Proceedings of the SPIE, (1994), San Diego, CA, USA, 2288, 1.

77. Reisfeld, R.; Brusilovsky, D.; Eyal, M.; Miron, E.; Burshtein, Z.; Ivri, J., *Chemical Physics Letters*, 160 (1989) 43.

78. Pope, E. J. A.; Asami, A.; Mackenzie, J. D., *Journal of Materials Research*, 4 (1989) 1018.

79. Morikawa, A.; Iyoku, Y.; Kakimoto, M.; Imai, Y., *Journal of Materials Chemistry*, 2 (1992) 679.

80. Novak, B. M.; Davies, C., *Macromolecules*, 24 (1991) 5481.

81. Ellesworth, M. W.; Novak, B. M., *Chemistry of Materials*, 5 (1993) 839.

82. Luneau, I. G.; Mosset, A.; Galy, J.; Schmidt, H., *Journal of Materials Science*, 89 (1990) 3739.

83. Schwertfeger, F.; Glaubitt, W.; Schubert, U., *Journal of Non-Crystalline Solids*, 145 (1992) 85.

84. Venkateswara Rao, A.; Bhagat, S. D.; Hirashima, H.; Pajonk, G. M., *Journal of Colloid and Interface Science*, 300 (2006) 279.

85. Song, X.-Y.; Cao, W.; Ayers, M. R.; Hunt, A. J., *Journal of Materials Research*, 10 (1995) 1995.

86. Hunt, A. J.; Ayers, M. R.; Cao, W., *Journal of Non-Crystalline Solids*, 185 (1995) 227.

87. Schwertfeger, F.; Schubert, U., *Chemistry of Materials*, 7 (1995) 1909.

88. Wu, X.; Wu, D.; Fu, R., *Journal of Hazardous Materials*, 147 (2007) 1028.

89. Pietron, J. J.; Stux, A. M.; Compton, R. S.; Rolison, D. R., *Solar Energy Materials and Solar Cells*, 91 (2007) 1066.

90. Rodembusch, F. S.; Campo, L. F.; Rigacci, A.; Stefani, V., *Macromolecular Symposia*, 229 (2005) 188.

91. Costela, A.; García Moreno, I.; Gómez, C.; García, O.; Sastre, R.; Roig, A.; Molins, E., *Journal of Physical Chemistry B*, 109 (2005) 4475.

92. Shen, J.; Wang, J.; Zhou, B.; Deng, Z.; Weng, Z.; Zhu, L.; Zhao, L.; Li, Y., *Journal of Non-Crystalline Solids*, 225 (1998) 315.

93. Shen, J.; Zhu, L.; Wang, J.; Wu, X.; Yufen, L., *Wuji Cailiao Xuebao/Journal of Inorganic Materials*, 11 (1996) 374.

94. Zhu, L.; Li, Y.; Wang, J.; Shen, J., *Journal of Applied Physics*, 77 (1995) 2801.

95. Zhu, L.; Li, Y.; Wang, J.; Shen, J., *Chemical Physics Letters*, 239 (1995) 393.

96. Kim, P.-H.; Kwon, J.-D.; Kim, J. S., *Synthetic Metals*, 142 (2004) 153.

97. Pauthe, M.; Despetis, F.; Phalippou, J., *Journal of Non-Crystalline Solids*, 155 (1993) 110.

98. Liu, C.; Komarneni, S., Materials Research Society Symposium - Proceedings, (1995), 371, 217.

99. Venkateswara Rao, A.; Haranath, D., *Microporous and Mesoporous Materials*, 30 (1999) 267.

100. Muller, C. A.; Deck, R.; Mallat, T.; Baiker, A., *Topics in Catalysis*, 11-12 (2000) 369.

101. Deng, Z.-S.; Wei, J.-D.; Wu, A.-M.; Bao, Y.-P.; Wang, J.; Shen, J.; Zhou, B.; Chen, L.-V., *Wuji Cailiao Xuebao/Journal of Inorganic Materials*, 15 (2000) 384.

102. Reynolds, J. G.; Coronado, P. R.; Hrubesh, L. W., *Journal of Non-Crystalline Solids*, 292 (2001) 127.

103. El Rassy, H.; Buisson, P.; Bouali, B.; Perrard, A.; Pierre, A. C., *Langmuir*, 19 (2003) 358.

104. Chen, Y.-M.; Xie, K.; Zhao, D.-F.; Xiao, J.-Y., *Gongneng Cailiao/Journal of Functional Materials*, 36 (2005) 903.

105. Chen, Y.; Zhao, D.; Xie, K.; Xiao, J., *Kuei Suan Jen Hsueh Pao/ Journal of the Chinese Ceramic Society*, 33 (2005) 727.

106. Rao, A. V.; Kalesh, R. R., *Science and Technology of Advanced Materials*, 4 (2003) 509.

107. Rao, A. V.; Wagh, P. B., *Materials Chemistry and Physics*, 53 (1998) 13.

108. Jung, S.-B.; Park, H.-H., *Thin Solid Films*, 420-421 (2002) 503.

109. Kanamori, K.; Aizawa, M.; Nakanishi, K.; Hanada, T., *Journal of Sol Gel Science and Technology*, 48 (2008) 172.

110. Kanamori, K.; Aizawa, M.; Nakanishi, K.; Hanada, T., *Advanced Materials*, 19 (2007) 1589.

111. Rao, A. V.; Bhagat, S. D.; Hirashima, H.; Pajonk, G. M., *Journal of Colloid and Interface Science*, 300 (2006) 279.

112. Hegde, N. D.; Rao, A. V., *Journal of Materials Science*, 42 (2007) 6965.

113. Kim, G. S.; Hyun, S. H., *Journal of Materials Science*, 38 (2003) 1961.

114. Novak., B. M., *Advanced Materials*, 5 (1993) 422.

115. Novak, B. M.; Auerbach, D.; Verrier, C., *Chemistry of Materials*, 6 (1994) 282.

116. Schaefer, D. W.; Beaucage, G.; Loy, D. A.; Shea, K. J.; Lin, J. S., *Chemistry of Materials*, 16 (2004) 1402.

117. Mackenzie, J. D.; Huang, Q.; Iwamoto, T., *Journal of Sol Gel Science and Technology*, 7 (1996) 151.

118. de la Rosa-Fox, N.; Morales-Florez, V.; Toledo-Fernandez, J. A.; Pinero, M.; Esquivias, L.; Keiderling, U., *Journal of Sol-Gel Science and Technology*, 45 (2008) 245.

119. Leventis, N.; Sotiriou-Leventis, C.; Zhang, G.; Rawashdeh, A.-M. M., *Nano Letters*, 2 (2002) 957.

120. Zhang, G.; Dass, A.; Rawashdeh, A.-M. M.; Thomas, J.; Counsil, J. A.; Sotiriou-Leventis, C.; Fabrizio, E. F.; Ilhan, F.; Vassilaras, P.; Scheiman, D. A.; McCorkle, L.; Palczer, A.; Johnston, J. C.; Meador, M. A.; Leventis, N., *Journal of Non-Crystalline Solids*, 350 (2004) 152.

121. Katti, A.; Shimpi, N.; Roy, S.; Lu, H.; Fabrizio, E. F.; Dass, A.; Capadona, L. A.; Leventis, N., *Chemistry of Materials*, 18 (2006) 285.

122. Capadona, L. A.; Meador, M. A. B.; Alunni, A.; Fabrizio, E. F.; Vassilaras, P.; Leventis, N., *Polymer*, 47 (2006) 5754.

123. Meador, M. A. B.; Capadona, L. A.; McCorkle, L.; Papadopoulos, D. S.; Leventis, N., *Chemistry of Materials*, 19 (2007) 2247.

124. Meador, M. A. B.; Fabrizio, E. F.; Ilhan, F.; Dass, A.; Zhang, G.; Vassilaras, P.; Johnston, J. C.; Leventis, N., *Chemistry of Materials*, 17 (2005) 1085.

125. Ilhan, U. F.; Fabrizio, E. F.; McCorkle, L.; Scheiman, D. A.; Dass, A.; Palczer, A.; Meador, M. B.; Johnston, J. C.; Leventis, N., *Journal of Materials Chemistry*, 16 (2006) 3046.

126. Nguyen, B. N.; Meador, M. A. B.; Tousley, M. E.; Shonkwiler, B.; McCorkle, L.; Scheiman, D. A.; Palczer, A., *Applied Materials and Interfaces*, 1 (2009) 621.

127. *Journal of Non-Crystalline Solids (Proceedings of the 4th International Symposium on Aerogels)*, 186 (1995).

128. Tewari, P. H.; Hunt, A. J.; Lofftus, K. D., *Materials Letters*, 3 (1985) 363.

129. van Bommel, M. J.; de Haan, A. B., *Journal of Materials Science*, 29 (1994) 943.

130. Brodsky, C. J.; Ko, E. I., *Journal of Non-Crystalline Solids*, 186 (1995) 88.

131. Dorcheh, A. S.; Abbasi, M. H., *Journal of Materials Processing Technology*, 199 (2008) 10.

132. Kirkbir, F.; Murata, H.; Meyers, D.; Chaudhuri, S. R., *Journal of Non-Crystalline Solids*, 225 (1998) 14.

133. Einarsrud, M.-A.; Haereid, S., *Journal of Sol Gel Science and Technology*, 2 (1994) 903.

134. Einarsrud, M.-A.; Nilsen, E.; Rigacci, A.; Pajonk, G. M.; Buathier, S.; Valette, D.; Durant, M.; Chevalier, B.; Nitz, P.; Ehrburger-Dolle, F., *Journal of Non-Crystalline Solids*, 285 (2001) 1.

135. Haereid, S.; Dahle, M.; Lima, S.; Einarsrud, M.-A., *Journal of Non-Crystalline Solids*, 186 (1995) 96.

136. Haereid, S.; Einarsrud, M.-A.; Scherer, G. W., *Journal of Sol-Gel Science and Technology*, 3 (1994) 199.

137. Haereid, S.; Nilsen, E.; Einarsrud, M.-A., *Journal of Non-Crystalline Solids*, 204 (1996) 228.

138. Einarsrud, M.-A.; Nilsen, E., *Journal of Non-Crystalline Solids*, 226 (1998) 122.

139. Fidalgo, A.; Rosa, M. E.; Ilharco, L. M., *Chemistry of Materials*, 15 (2003) 2186.

140. Haereid, S.; Nilsen, E.; Einarsrud, M.-A., *Journal of Porous Materials*, 2 (1996) 315.

141. Einarsrud, M.-A., *Journal of Non-Crystalline Solids*, 225 (1998) 1.

142. Kumar, S. R., *High Surface Area Porous Sol Gel Silica and Mixed Oxide Aerogels Through Sub Critical Drying*, PhD. Thesis, (2002), Department of Chemistry, University of Kerala.

143. Smitha, S.; Shajesh, P.; Aravind, P. R.; Kumar, S. R.; Pillai, P. K.; Warrier, K. G. K., *Microporous and Mesoporous Materials*, 91 (2006) 286.

144. Smitha, S.; Shajesh, P.; Kumar, S. R.; Krishna Pillai, P.; Warrier, K. G. K., *Journal of Porous Materials*, 14 (2007) 1.

145. Prakash, S. S.; Brinker, C. J.; Hurd, A. J.; Rao, S. M., *Nature*, 374 (1995) 439.

146. Rao, A. V.; Nilsen, E.; Einarsrud, M.-A., *Journal of Non-Crystalline Solids*, 296 (2001) 165.

147. Rao, A. P.; Pajonk, G. M.; Rao, A. V., *Journal of Materials Science*, 40 (2005) 3481.

148. Hwang, S.-W.; Jung, H.-H.; Hyun, S.-H.; Ahn, Y.-S., *Journal of Sol-Gel Science and Technology*, 41 (2007) 139.

149. Tsou, P., *Journal of Non-Crystalline Solids*, 186 (1995) 415.

150. Ahmed, M. S.; Attia, Y. A., *Journal of Non-Crystalline Solids*, 186 (1995) 402.

151. Alkemper, J.; Buchholz, T.; Murakami, K.; Ratke, L., *Journal of Non-Crystalline Solids*, 186 (1995) 395.

152. Li, J.; Wang, X.; Huang, Q.; Gamboa, S.; Sebastian, P. J., *Journal of Power Sources*, 158 (2006) 784.

153. Ng, E., *Elektron*, 22 (2005) 48.

154. Meng, Q.-H.; Liu, L.; Song, H.-H.; Ling, L.-C., *Gongneng Cailiao/Journal of Functional Materials*, 35 (2004) 457.

155. Schwarz, W.; Ebert, V.; Geerds, H.; Jungmann, K.; Kirches, S.; Koppe, S.; Maas, F.; Mundinger, H.-J.; zu Putlitz, G.; Rosenkranz, J.; Schäfer, W.; Schiff, G.; Zhang, Z.; Boshier, M. G.; Hughes, V. W., *Journal of Non-Crystalline Solids*, 145 (1992) 244.

156. Ma, J.; Kim, S. B.; Hrubesh, L. W.; Chan, M. H. W., *Journal of Low Temperature Physics*, 93 (1993) 945.

157. Hrubesh, L. W., *Journal of Non-Crystalline Solids*, 225 (1998) 335.

158. Fricke, J.; Lu, X.; Wang, P.; Buttner, D.; Heinemann, U., *International Journal of Heat and Mass Transfer*, 35 (1992) 2305.

159. Pajonk, G. M.; Manzalji, T., *Catalysis Letters*, 21 (1993) 361.

160. Armor, J. N.; Carlson, E. J.; Zambri, P. M., *Applied Catalysis*, 19 (1985) 339.

161. Maurer, S. M.; Ng, D.; Ko, E. I., *Catalysis Today*, 16 (1993) 319.

162. Woignier, T.; Phalippou, J.; Prassas, M., *Journal of Materials Science*, 25 (1990) 3118.

163. Mulder, C. A. M.; van Lierop, J. G.; Frens, G., *Journal of Non-Crystalline Solids*, 82 (1986) 92.

164. Papanikolau, E.; Meerman, W. C. P. M.; Aerts, R.; van Roy, T. L.; van Lierop, J. G.; Meeuwsen, T. P. M., *Journal of Non-Crystalline Solids*, 100 (1988) 247.

165. Rahaman, M. N.; de Jonghe, L. C.; Shinde, S. L.; Tewari, P. H., *Journal of the American Ceramic Society*, 71 (1988) C388.

166. Gesser, H. D.; Goswami, P. C., *Chemical Reviews*, 89 (1989) 765.

167. Ebeling, W.; Reierson, D. A.; Pence, R. J.; Viray, M. S., *Pesticide Biochemistry and Physiology*, 5 (1975) 81.

168. White, N. D. G.; Loschiavo, S. R., *Journal of Economic Entomology*, 82 (1989) 960.

169. Loschiavo, S. R., *Journal of Economic Entomology*, 81 (1988) 1231.

170. Loschiavo, S. R., *Journal of Economic Entomology*, 81 (1988) 1237.

171. Jones, S. M., *Journal of Sol Gel Science and Technology*, 40 (2006) 351.

172. Power, M.; Hosticka, B.; Black, E.; Daitch, C.; Norris, P., *Journal of Non-Crystalline Solids*, 285 (2001) 303.

173. Salinas, A. J.; Vallet-Regi, M.; Toledo-Fernandez, J. A.; Mendoza-Serna, R.; Pinero, M.; Esquivias, L.; Ramirez-Castellanos, J.; Gonzalez-Calbet, J. M., *Chemistry of Materials*, 21 (2009) 41.

174. Reynes, J.; Woignier, T.; Phalippou, J., *Journal of Non-Crystalline Solids*, 285 (2001) 323.

175. Yu, H.; Brock, S. L., *ACS Nano*, 2 (2008) 1563.

176. Rodembusch, F. S.; Campo, L. F.; Stefani, V.; Rigacci, A., *Journal of Materials Chemistry*, 15 (2005) 1537.

177. Costela, A.; Garcia Moreno, I.; Gomez, C.; Garcia, O.; Sastre, R.; Roig, A.; Molins, E., *Journal of Physical Chemistry B*, 109 (2005) 4475.

178. Bertino, M. F.; Hund, J. F.; Zhang, G.; Sotiriou-Leventis, C.; Tokuhiro, A. T.; Leventis, N., *Journal of Sol-Gel Science and Technology*, 30 (2004) 43.

179. Leventis, N.; Palczer, A.; McCorkle, L.; Zhang, G.; Sotiriou-Leventis, C., *Journal of Sol-Gel Science and Technology*, 35 (2005) 99.

Chapter 2

Effect of Organically Modified Precursors on an Ambient Pressure Drying Technique for Aerogels

For several potential technical applications such as chromatography, sensors, or immobilization of enzymes or metal complexes, solids with reactive sites at their inner surface, not just porous inorganic materials, are required. A controlled processing of inorganic precursors in the presence of functionalizing agents is necessary to achieve both a tailored microstructure and porosity and a deliberate positioning of the reactive sites. The sol-gel process is an obvious choice to the preparation of organically modified inorganic materials with a tailored microstructure.

Aerogel materials are an excellent choice to correlate the chemistry during sol-gel processing with the structural characteristic of the gel network.[1] Use of organically modified precursors is not new to sol-gel chemistry. Organically modified precursors are regularly used in sol-gel processes to decrease the hydrolysis rates of transition metal ions and to induce hydrophobicity.[2,3] In silica systems organic modifications have been routinely attempted to increase the hydrophobicity of the aerogel network. Standard procedure uses reactive alkylsilanes, which reacts with the surface silanol groups.[4] This treatment is done on preformed gels. Alternately co-condensation of alkyl modified silanes has also been attempted.[5,6] But co-condensation brings in the intricacies of sol-gel chemistry of different precursors. Sol-gel chemistry of trialkoxysilanes is in no way straight forward and they usually form cyclic and cage like closed species that hinder the homogeneous gelling of the starting solution.[7]

Considerable efforts have been made for the studies related to rates of hydrolysis-condensation reactions of trialkoxysilane precursors. The slow gelation of tetraethylorthosilicate and tetramethylorthosilicate in basic conditions proceed with the formation of cage-like silsesquioxane structures or siloxane rings.[8] The cages or rings interconnect into a three-dimensional network structure very slowly. When one of the alkoxy groups are replaced by a methyl group, cages are formed but their solubility is

limited.[7,9] When the concentration of cages or rings is large enough, they will crystallize or precipitate from the solution. When bis(trimethoxysilyl)ethane is used instead of methyltrimethoxysilane, the siloxane cages or rings initially formed are easily connected to each other because of the pre-existing ethylene bridges. As in basic conditions, transparent homogeneous gels are formed in acidic conditions in samples prepared from bis(trimethoxysilyl)ethane and bis(trimethoxysilylpropyl)amine. In contrast, the samples prepared from methyltrimethoxysilane and bis(trimethoxysilyl)hexane were inhomogeneous.[10] Brennan achieved the preparation of monolithic gels from methyltrimethoxysilane with a variety of porosities using a two step method where the hydrolysis is done below the isoelectric point of silica and condensation above it using acid and base catalysts.[11] de Buyl studied the hydrolysis and condensation kinetics of 3-glycidoxypropyltrimethoxysilane (GPTMS) and concluded that hydrolysis of GPTMS to its silanetriol equivalent in a 2%aqueous solution is a fast reaction i.e., completed within about 2 h at 26 °C and condensation into oligomer species and epoxy ring opening take place at slower rate, i.e., completed within about 2 months at 26 °C.[12] Kiefer investigated the kinetics of hydrolysis and condensation of the GPTMS-aminopropyltriethoxysilane system and observed the existence of a penta-coordinated silicon centre as a transition state during hydrolysis.[13] According to Hook, the electronic and steric effects of substituents on the ethoxysilanes used to prepare sol-gels can be used to predict the relative rates of reaction of these compounds. However, these rate trends can change with reaction conditions, particularly if low levels of acid are used. The effects of a particular substituent on the hydrolysis and condensation processes are not necessarily the same; hence, overall polymerisation data must be considered in order to achieve the appropriate reaction procedure required to prepare homogeneous gels. Of the diethoxysilanes, the methylphenyl compound condenses at the slowest rate as expected due to the bulk of the aromatic substituent. The similarity of the methylvinyl-and dimethylsilane results reinforces the fact that a second substituent does not exert the same level of influence as the first.[14] From the studies of Matejka it was found that the structure evolution in the sol-gel polymerization of organotrialkoxysilanes $RSi(OR')_3$ is dependent on the type of the

substituent R. Evolution of the silsesquioxane structure is controlled by the competition between intermolecular polycondensation and cyclization. Increasing the size of R results in slowing down the polymerization, the intermolecular reaction is sterically hindered, and the cyclization is advanced. Because of cyclization competing with the intermolecular condensation, the trialkoxysilanes with long substituents do not form high-molecular-weight polymers and do not gel even at high concentrations. The octamer cages proved in isolated fractions as well as larger incompletely condensed polyhedral clusters are the main reaction products. The silsesquioxane with long substituents are stable because of a high fraction of intramolecularly fully condensed species and steric restrictions to intermolecular condensation. The cage buildup is also preferred at high temperatures and in dilute systems. Because of incompatibility of the silsesquioxane framework and pendant organic chains, microphase separation takes place and self-organization into micelles occurs. In contradiction, trialkoxysilanes with small substituents undergo faster condensation and intermolecular branching because of lower steric hindrance. As a result, the growth of a high-molecular-weight poly silsesquioxane with dangling organic groups is preferred and the system finally gels. A low extent of cyclization and small fraction of polyhedrons were found, no micelles created, and regular arrangement absent.[15,16] While basic and neutral catalysis with dibutyltindilaurate lead to pronounced cyclization and self-organization, the acid catalyst produces less polyhedral structures and no regular arrangement.[15] In neutral conditions the hydrolysis of vinyltrialkoxysilanes in acetonitrile is an extremely slow process. However, in the presence of even very small amounts either of acid or base the rate constants increased dramatically up to four orders of magnitude. It was found that in the conditions of acidic hydrolysis the steric effect of an alkoxy group did not have serious influence. Also, both acid and base dramatically increased the rates of intermolecular condensation.[17] The sol-gel synthesis of hybrid methacrylate-silica materials using methacryloxypropyltrimethoxysilane as precursor, has been analyzed by Babonneau.[18] Under the experimental conditions (H_2O/REOS=3; pH=2), hydrolysis of methoxy groups was fast. However, 5% of unreacted alkoxy groups were still present in the sol after 14

days aging. Condensation reactions lead mainly to cyclic or short linear species with the number of cross-linking points never exceeding 20% of the Si units preventing the formation of a gel.[18] Feuillade suggested that for methacryloxypropyltrimethoxysilane system, when thermodynamically controlled (long aging times) formation of cyclic species is favored. On the contrary, in a kinetically controlled system, linear structures are mainly created.[19]

Organically modified precursors, in the context of aerogels have assumed significance in recent years due to the increased attention paid to extending their functional properties. Rodembusch created fluorescent aerogels by covalently linking fluorescent dyes to the aerogel matrix and drying them supercritically. Similarly the open pore structure of aerogels have been filled with laser dyes for solid state dye laser applications.[20]

Supercritically dried inorganic-organic hybrid silica aerogels modified with alkyl and aryl groups starting from $R'Si(OR)_3/Si(OR)_4$ mixtures (R'= alkyl, aryl) have been synthesized by Husing.[21,22] The gels were prepared under basic conditions by adding a calculated amount of 0.01N aqueous NH_4OH, corresponding to the amount of water necessary to hydrolyze all Si-OMe groups. Karl-Fischer-titration showed that the base catalyzed hydrolysis and condensation of $R'Si(OR)_3$ was much slower than that of tetramethylorthosilicate. Therefore, it can be assumed that in the first stage of the reaction SiO_2 particles are formed to which the organically substituted groups condense in the later stage.[23]

On the other hand use of organically functionalised silane precursor, methyltrimethoxysilane has led to the development of flexible aerogels.[24] Leventis used the concept of organic inorganic networks to obtain flexible and mechanically strong aerogels.[25,26] The added mechanical strength would mean that these aerogels could be dried at ambient pressure.[27,28] The organic inorganic hybrid concept presents an interesting prospect for achieving ambient pressure dried aerogels.[29,30]

Warrier and co workers had reported on an ambient pressure drying technique for the synthesis of silica aerogels involving solvent washing and aging.[31,32] This was

successfully extended to mixed oxide gels.[33] So in this chapter we attempt to extend this ambient pressure method to organic inorganic hybrid systems. The effect of the organically modified precursor in the process is studied. The variation of pore structure and porosity with varying organic content and type is followed.

Experimental

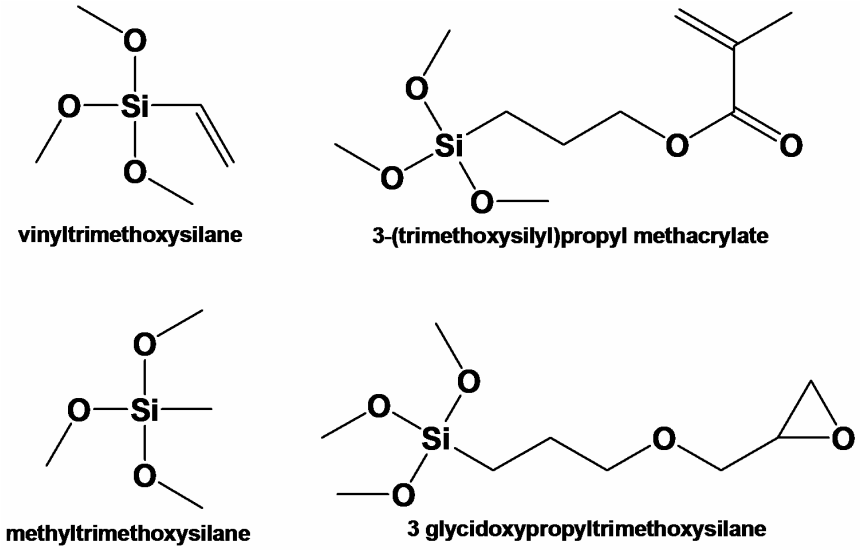

Scheme 2.1.: Alkyl modified silanes used in this study

3-glycidoxypropyltrimethoxysilane (GPTMS), methyltrimethoxysilane (MTMS), vinyltrimethoxysilane (VTMS), 3-(trimethoxysilyl)propyl methacrylate (TPMS) and tetraethylorthosilane (TEOS) were procured from Aldrich (Steinheim, Germany) and used as obtained. Isopropyl alcohol and hydrochloric acid were obtained from S.D. Fine chemicals (Mumbai, India). Doubly distilled water was used for the preparation. In a typical preparation weighed amounts of GPTMS and TEOS were mixed with weighed quantity of isopropanol by stirring on a magnetic stirrer. To this solution weighed amount of 10^{-3}N HCl was added. For other alkoxy silanes the silane solutions were hydrolysed separately and mixed after three hours. The initial water content is the amount of the acid taken for the preparation of the gel. The solution was stirred for 3 hours and poured in to polypropylene vials. The vials were kept at 50 °C for gelation. The gelation times

reported are the time at which the flow stops in the vials when tilted. Gels were prepared with varying RMOS(modified silane)/TEOS molar ratio. Molar ratio was varied as 0.05, 0.1, 0.2, 0.3 and 0.5. In the case of GPTMS initial water content was also varied. The initial water/Si molar ratio was varied as 4, 8, 12 and 16. Gels are designated as xP, where x is the RMOS/TEOS molar ratio. The isopropanol/Si molar ratio was kept constant at 4.

The alcogels were aged in water solutions for a period of 24 hours followed by solvent exchange with isopropanol. The GPTMS gels were aged in water alone, but these gels were all obtained cracked. The cracking of the network was traced back to the density mismatch between the pore liquid (alcohol-water) and aging solution (water). So the gels from other modified precursors were aged in 50% alcohol solution. In order to exchange the solvent, the gels were immersed in isopropanol and the solution replaced with fresh alcohol, 5 times in 24 hours. The solvent exchanged gels were then aged in a solution of 80% TEOS in isopropanol for a period of 48 hours. The silane aged gels were washed with n-hexane following the same procedure used for solvent exchange. In all the steps the soaking solutions had volume twice as that of the gels immersed in them. The gels were then kept for drying in sealed containers at 70 °C. The container seals were perforated with pins after a day for the solvent to escape slowly. The dried gels were used for further characterization.

Thermal analysis of the gels were performed on a thermogravimetric analyzer (Shimadzu TG 50, Kyoto, Japan) and a differential thermal analyzer (Shimadzu DTA 50, Kyoto, Japan) in air at a heating rate of 5 °C min^{-1}. A Fourier transform infrared spectroscope (Magna 560, Nicolet, Madison, Wisconsin) was used for recording the FTIR spectra of the samples. The spectra were acquired using the KBr pellet method in the range 400 – 4,000 cm^{-1}. Nitrogen adsorption data were obtained using a BET surface area analyzer (Gemini 2360, Micromeritics, Norcross, USA) at 77 K. All analysis were conducted after degassing the sample at 200 °C for 2 hours unless specified. The pore size distributions were calculated using the Barrett–Joiner–Halenda (BJH) method from

the isotherm. All calcinations were performed at a heating rate of 1 °C min^{-1} and soaked at the respective temperature for 2 hours.

Results and Discussion

The gelation time observed for samples prepared with varying GPTMS content and varying water content is provided in table 2.1.

GPTMS/TEOS molar ratio	Gelation time (h)			
	Initial water content (water/Si molar ratio)			
	4	8	12	16
0.05	25.30	4.5	9.30	12.20
0.1	41	5.45	14.45	10.20
0.3	62.3	18	39.15	71.45

Table 2.1.: Gelation times observed for GPTMS gels prepared with varying water content and precursor ratio

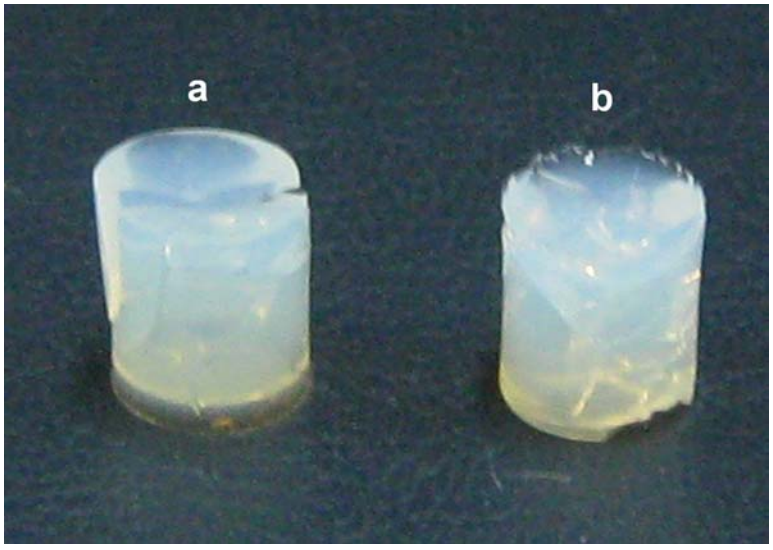

Figure 2.1.: Photographs of dried gels prepared with a molar ratio water/Si = 8 and GPTMS/ TEOS molar ratio(a) 0.3 and (b) 0.1

The gelation time increases with the GPTMS content. The amount of water used for the hydrolysis also affect the gelation time and there seems to be an optimal amount of water ratio for which the gelation times are low, above and below which gelation time increases. Only the gels prepared at the optimum water ratio was further processed. All the gels cracked after drying. Photograph of dried gels are provided as figure 2.1.

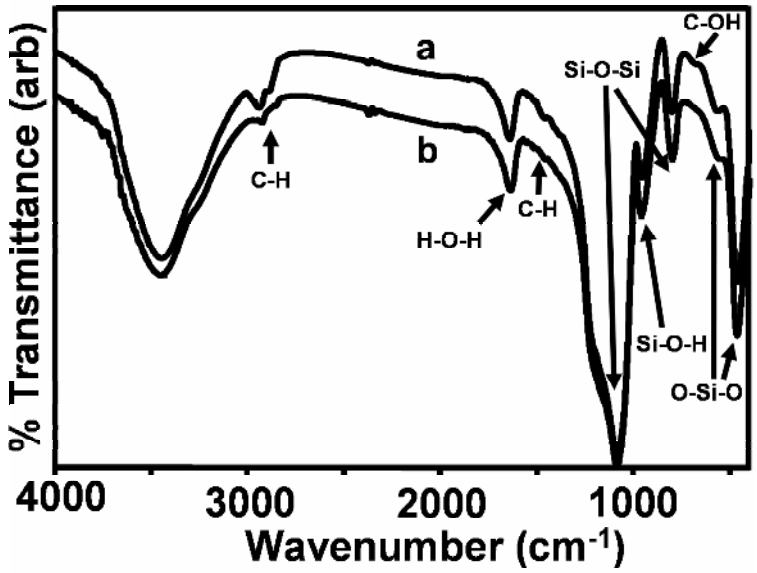

Figure 2.2.: FTIR spectra of gels prepared by using water/Si ratio 8 and GPTMS/TEOS molar ratio (a) 0.5 (b) 0.3 dried at 70 °C

The FTIR spectra of all the GPTMS gels were similar and two are provided in figure 2.2. The peaks were assigned based on available literature.[34-36] The broad absorption between 3100 and 3700 cm^{-1} is due to the OH stretching vibrations. The stretching of alkyl hydrogens are visible around 2930 cm^{-1} and the corresponding bending vibrations can be seen around 1490 cm^{-1}. The absorption around 1639 cm^{-1} is due to the bending vibrations of water adsorbed on the silica surface. The Si–O–Si asymmetric stretching vibrations appear as a strong and broad absorption around 1090 cm^{-1}. The ether linkages in the glycidoxy group also absorb in the same region and will be overlapped by the strong Si–O–Si absorption. The Si–OH asymmetric stretching vibrations can be seen at 950 cm^{-1}. The peak around 800 $cm^{-1}$is due to the symmetric Si–O–Si stretching

vibrations. The peak at 565 and 460 $cm^{-1}$is attributed to the O–Si–O vibrations. The out of plane bending vibrations of C–OH groups can be seen as a weak peak at 698 cm^{-1}.

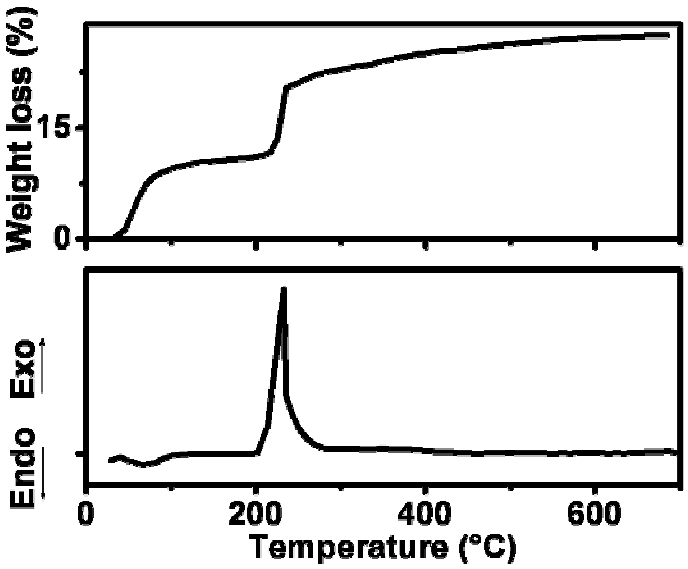

Figure 2.3.: Thermal analysis of the gel dried at 70 °C. Molar ratio GPTMS/TEOS = 0.3, water/Si = 8

Thermal analysis of the 0.3P8W gel is provided as figure 2.3. All the prepared gels followed the same pattern. The exothermic peak centred on 230 °C corresponds to the decomposition of the organic part on the silica network. The small endothermic peak observed below 100 °C is due to the removal of water from the gel. The corresponding weight loss can be seen in the TG curve provided in the same figure. The thermogravimetric curve shows a two step weight loss where the first step is due to the removal of adsorbed water. While a total weight loss of ~27% was observed, the weight loss due to removal of water accounts for ~10%. The weight loss becomes constant above 600 °C. Dehydroxylation of surface silanol groups are expected around 600 °C. Assuming that only SiO_2 is present above 600 °C and that the decomposition of the glycidoxypropyl groups occur with the cleavage of the Si–C bond and knowing the molar ratio of the precursor, the percentage weight loss due to the decomposition of the glycidoxypropyl group can be calculated.

Initial weight of the gel =100 g

Final weight of the gel = 100-$(\%WL)_{600}$ g

$$(\%WL)_{expected} = (\frac{100 - (\%WL)_{600}}{M_{SiO_2}}) \times \frac{P}{(P+1)} \times M_R$$

Where WL is the weight loss and subscript the temperature, P is the molar ratio GPTMS/TEOS used and M_R is the molecular weight of the alkyl chain. In the case of the 0.3P gel prepared at water ratio 8, the weight loss calculated is around 14%. This is close to the observed weight loss for the second step which indicates that the composition of the gel is well maintained through the preparation. The FTIR spectrum of the same gel after calcination at 600 °C was taken and is compared with that obtained for the 70 °C dried gel in figure 2.4.

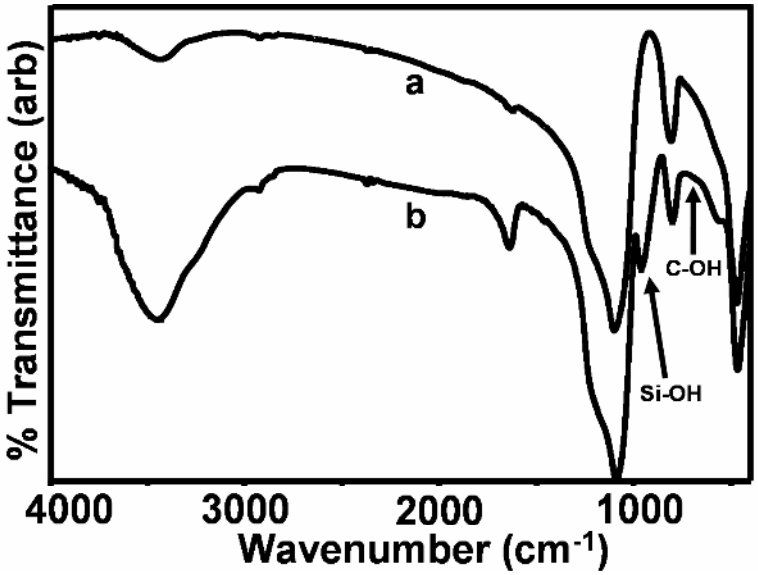

Figure 2.4.: FTIR Spectra of the gel (Molar ratio GPTMS/TEOS = 0.3, water/Si = 8) (a) dried at 600 °C, (b) dried at 70 °C

Upon calcination at 600 °C peaks corresponding to the alkyl hydrogen stretching and bending disappear along with the Si-OH stretching at 950 cm^{-1}. The C-OH absorptions at 698 cm^{-1} is also removed providing substantial support to the above

discussion. The peaks corresponding to the adsorbed water is also reduced after the calcination.

The BET surface area analysis of the gels was conducted to understand the nature of porosity and surface characteristics of the samples. The isotherms obtained for the gels calcined at 250 °C are provided in Figure 2.5. The isotherms have the characteristic hysteresis loop of type IV nature. The gels are all mesoporous.

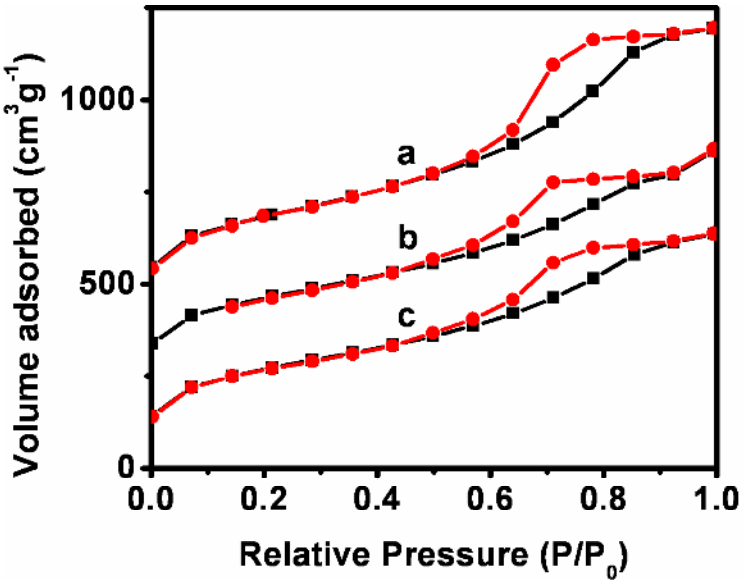

Figure 2.5.: Adsorption isotherms of the gels prepared with a molar ratio water/Si = 8 and GPTMS/TEOS (a) 0.5, (b) 0.1, (c) 0.05. The y axis has been offset by 200 units to separate the isotherms

The increase in gelation times with increasing trialkoxy precursor has been observed by many researchers and is attributed to the poor networking ability of the $RSiO_{1.5}$ network.[7,37] The rate of hydrolysis of the trialkoxy precursor will be less than the tetraalkoxy precursor due to the steric and inductive effects of the alkyl substituent. The slower rate of hydrolysis of the trialkoxy precursor ensures that a larger proportion of these molecules are present towards the outer surface of the initially formed clusters as condensation proceeds. The increasing presence of unhydrolysable glycidoxygroup towards the surface decreases the condensation sites retarding condensation. Husing

studied the effect of different alkyl substituted alkoxides in the formation of the gel structure when used as a co-precursor with tetraethoxysilane.[22] For these studies a base catalysed hydrolysis using ammonium hydroxide was followed by supercritical drying of the gels. Increasing gelation times were observed with the increase in concentration of the alkyl substituted precursor but all compositions were prepared at a water ratio of 1 (OR/H_2O). Here we could observe a decrease in gelation time irrespective of the GPTMS content when the water ratio was increased to 8 (H_2O/Si). When the water ratio was further raised the gelation time increased. The molar ratio indicates the availability of two molecules of water for each alkoxy group when the precursor is tetraalkoxysilane and 2.6 for the trialkoxysilane precursor. The acid catalysed hydrolysis of TEOS is first order with respect to the concentration of water.[2] Hence the rate of hydrolysis reaction of the alkoxide precursor can be considered to increase with the increasing water content. But as the water content increases, alkoxide to alcohol ratio remaining constant, the concentration of the precursor decreases in solution proving detrimental to the condensation reaction rates. The increasing gelation times with increasing water content for the TEOS system is reported.[2] Kretschmer studied the hydrolysis condensation reactions of GPTMS in a 2 wt% GPTMS aqueous solution (molar ratio ~0.002) at pH 5.4 and found that the molar ratio of condensed species with more than one Si–O–Si linkages approached 50% only after 10 days.[38] In the present study the presence of the catalyst and the higher temperature used for gelation can increase the reaction rates but it is not enough to stifle the influence of the decreasing concentration.

The BET surface area of the gels dried at 70 °C and degassed for 3 hours at 150 °C is provided in Table 2.2. The low surface area values are a clear indication of the presence of alkyl groups on the internal surface of the gels. These groups hinder the adsorption of nitrogen resulting in a decrease in surface area. The decreasing trend in surface area is essentially due to the increase in alkyl groups. The decomposition of organic groups occur around 240 °C according to the thermal analysis. In order to analyze the surface characteristics after partial removal of the organic groups the samples were calcined at 250 °C for 3 h and then BET analysis was performed. The BET surface

area values showed almost a two fold increase with the partial removal of the organic groups.

GPTMS/TEOS (molar ratio)	Dried at 70° C	Calcined at 250 ° C		
	Surface Area (m^2g^{-1})	Surface Area (m^2g^{-1})	Total Pore Volume (m^3g^{-1})	Average Pore Radius (nm)
0.05	432	901	0.98	4.3
0.1	434	903	1.02	4.5
0.3	364	934	0.96	4.1
0.5	324	984	1.23	4.9

Table 2.2.: Surface area analysis of GPTMS gels prepared at a water ratio of 8, dried at 70 °C and calcined at 250 °C

This would mean that the entire network skeleton is made up of the TEOS derived silica particles and the GPTMS molecules condense on to the networked structure. Schubert arrived at similar conclusions for the base catalysed system and we find that similar mechanism acts in the acid catalysed hydrolysis condensation where the network will be more polymeric.[2] The trend for the surface area values is reversed and the gel with the higher organic content has the larger surface area as expected. There is an increase in pore volume with increasing GPTMS content indicating the effect of GPTMS in the drying stages. The presence of the glycidoxy group on the surface of the pores prevents the condensation of the Si–OH bonds which lead to pore collapse during drying. This effective removal of pore collapse results in the increase in pore volume. The close values of the average pore radius shows that the pore structure of the gels are similar and that GPTMS has no real influence in the formation of the pore structure. Rather the effect is restricted to the drying stages. The pore size distribution curves obtained for the gels are provided as figure 2.6. and show that similar pore size distribution is present in all the gels.

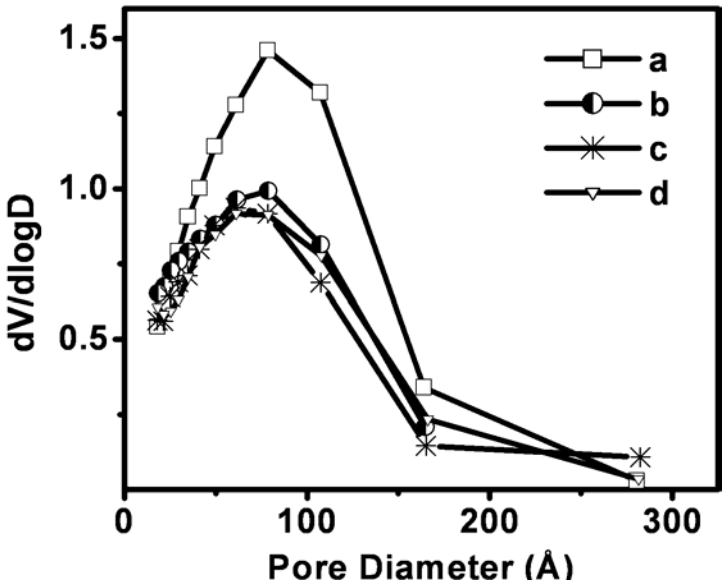

Figure 2.6.: Pore size distribution of the gels prepared with a molar ratios, water/Si = 8 and GPTMS/TEOS (a) 0.5, (b) 0.3, (c) 0.1, (d) 0.05

So the use of GPTMS as a co-precursor assists the drying at ambient pressure by preventing the condensation of silanols during drying. The gel network is largely dictated by the condensation reactions of TEOS and the influence of GPTMS is observed during the drying stages. The nature of the pores is not affected by the presence of GPTMS but the total pore volume increases with the increasing presence of GPTMS. The use of GPTMS is seen to further enhance the ambient pressure drying. Effect of the nature of the precursor chain on the ambient pressure drying technique remains to be investigated. So we decided to investigate the effect of other precursors, chosen mainly due to their chain length, methyltrimethoxysilane, vinyltrimethoxysilane and 3-(trimethoxysilyl)propyl methacrylate on the ambient pressure drying. By themselves, the selected alkyl chains are not expected to influence the sol-gel reactions leading to the network formation. So their influence is expected in the drying stages and the effect of the chain length can be observed.

Based on the observations from the use of glycidoxy precursor we modified the aging solution used in the first step for the preparation of other hybrids. For the GPTMS gels we had used water for the aging and hair line cracks could be observed on most gels

by the end of the aging step. Upon drying most of the gels cracked and monoliths were difficult to prepare even after repeated attempts. For aging, the gel rods are transferred to a beaker containing water. Initially the gels remain afloat and gradually sink. This is due to the mismatch in the densities of the pore liquid and water. The pore liquid mainly consists of isopropyl alcohol and a small amount of water formed from the condensation of the silanol species. The low density of this alcohol solution results in the floating of the gel. The consequence is that evaporation of the pore liquid takes place from the exposed surface of the gel and this will lead to development of stress on this surface which in turn leads to cracks. So the need is to minimize the exposed surface and also the time that gel will remain afloat. So we changed the aging solution to a 50% alcohol solution. Only compositions with the optimal water content (Water/Si) of 8 were prepared. In an attempt to decrease the gelation times the solutions of the precursor silanes were hydrolysed separately and then mixed. The surface area measurements were performed after calcination and degassing at 200 °C for 4 h.

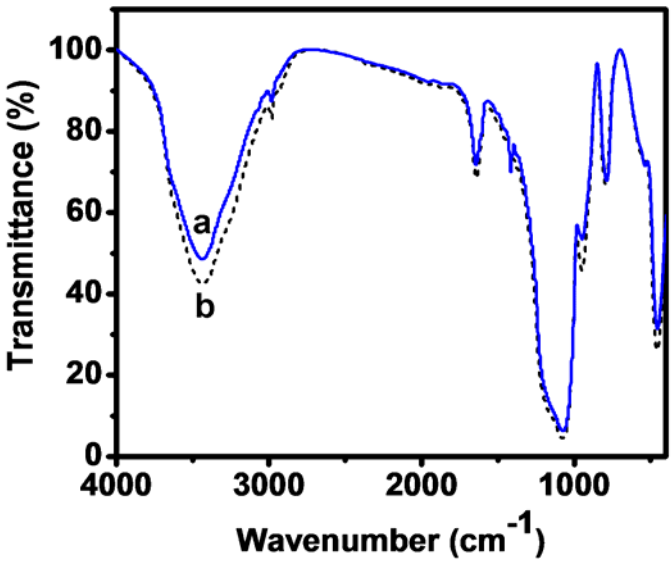

Figure 2.7.: FTIR Spectra of VTMS gels prepared at a VTMS/TEOS (a) 0.2, (b) 0.1

The FTIR spectra obtained for the gels prepared using VTMS precursor at different molar ratios is given in figure 2.7. The peak observed at 2980 cm^{-1} is due to the stretching vibrations of the alkyl group. But the vinyl hydrogens usually have stretching

frequency above 3000 cm^{-1}. This peak is rather weak in our spectra and can be seen when the regions is viewed closely, figure 2.8. The broad absorption centered around 3450 cm^{-1} is due to adsorbed water and surface silanol groups. The C=C stretching vibration of the vinyl group appears in the 1640-1660 cm^{-1} region. Unfortunately the bending vibrations of adsorbed water appear in the same region (1640 cm^{-1}). The double bond stretch of the vinyl group is rather sharp and the distinct nature of the band observed here compared to the band due to adsorbed water in the GPTMS hybrid can be taken as the indication of the presence of the vinyl stretch. The peak at 1420 cm^{-1} is due to the bending vibrations of the vinyl hydrogen. These bending vibrations are distinct due to their sharp nature and is finger print for the vinyl group. Alkyl hydrogen bending will be weak and diffuse as was observed in the case of GPTMS hybrid. The intense broad band centered around 1090 cm^{-1} is due to Si-O-Si stretching vibrations and the sharp peak at 950 cm^{-1} is due to the Si-OH groups.

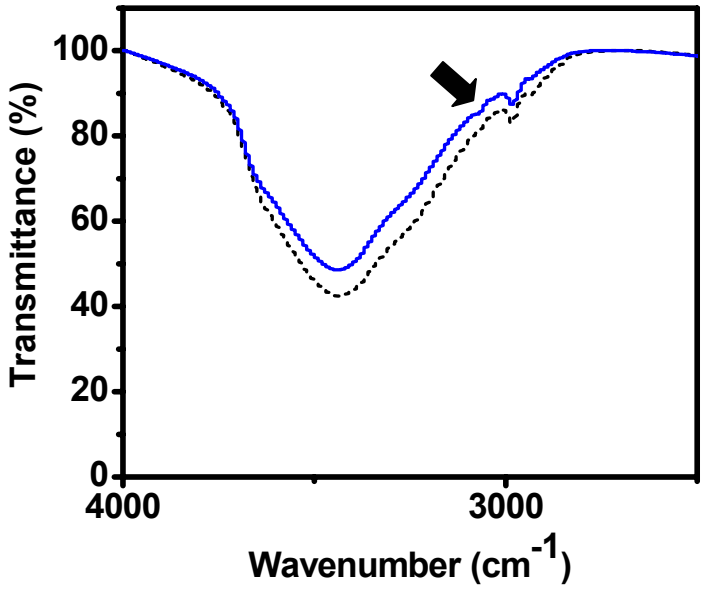

Figure 2.8.: FTIR Spectra in the region 4000-2500 cm^{-1} of VTMS gels prepared at a VTMS/TEOS (a) 0.1, (b) 0.2

The Si-O-Si groups stretch symmetrically in the 800 cm^{-1} region and the peak is observed at 790 cm^{-1}. If we look at the band intensities it is clear that the hydroxyl

stretching decreases as the concentration of the organic precursor increases. As observed from the GPTMS series the substituted silanes condense on to the surface of the already formed siloxane network at a later stage of the condensation process. Then the progressive inclusion of the vinyl species will result in a decrease in the concentration of surface silanol groups, since they will condense with the vinyl modified silane species. The increase in the organic groups will also decrease the amount of water adsorbed on to the surface of the gels. The decrease in band intensity of the Si-OH asymmetric stretch at 950 cm^{-1} with increasing organic precursor ratio also corroborates this. The peaks below 500 cm^{-1} is due to O-Si-O vibrations.

FTIR spectra of MTMS gels prepared at molar ratios of 0.05 and 0.1 are provided as figure 2.9. The C-H stretching vibrations are present at 2980 cm^{-1} and 2930 cm^{-1} corresponding to the asymmetric stretch and symmetric stretch respectively.

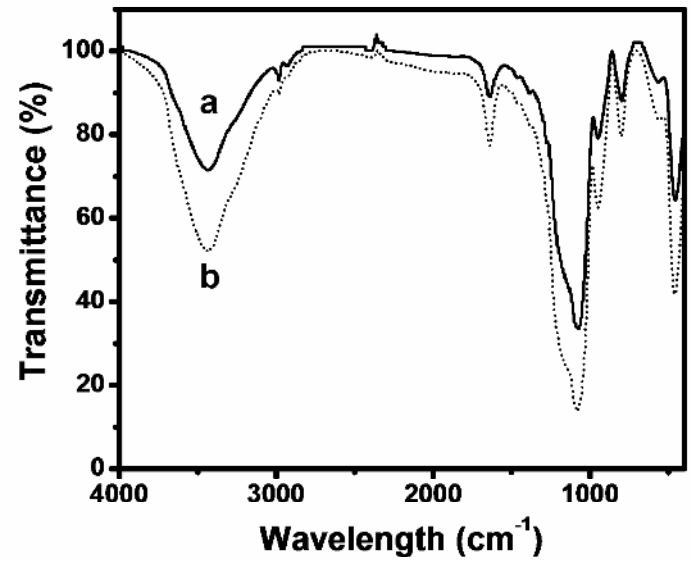

Figure 2.9.: FTIR Spectra of MTMS gels prepared at a MTMS/TEOS (a) 0.1, (b) 0.05

The bending modes of the methyl group absorbs at 1380 cm^{-1} and 1470 cm^{-1}. The lower absorption is due to the symmetric bend and the higher one due to asymmetric bending. The absorption due to the bending vibrations is weak and diffuse as discussed earlier. Absorption due to hydroxyl stretch is present as the broad peak at 3440 cm^{-1}. The

absorption due to adsorbed water is also present at 1640 cm^{-1}. The absorptions due to SiO_2 network is similar to that observed in the case of VTMS gels. Here also the absorptions due to silanol stretch decreases with progressive increase in the concentration of MTMS.

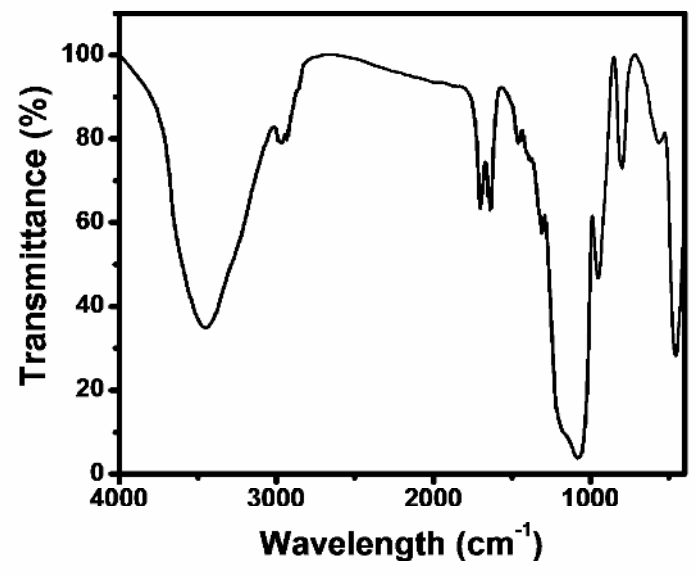

Figure 2.10.: FTIR Spectra of TPMS gels prepared at a TPMS/TEOS of 0.1

The FTIR spectra of a gel prepared in the molar ratio 0.1 using TPMS is given as figure 2.10. The absorptions due to silica network and hydroxyl absorptions are observed in the same regions as the other gels. The alkyl chains on the methacrylate precursor contain methylene and methyl groups. So the C-H stretching bands from these groups can be observed. There is the symmetric stretch from the methylene group, which is observed at 2860 cm^{-1}. This is very weak. On the other hand, the methyl asymmetric and symmetric stretch is observed along with the methylene asymmetric vibrations in the 2900 cm^{-1} to 3000 cm^{-1}. The sharp band at 1700 cm^{-1} is due to the presence of the carbonyl group on the methacrylate. The free carbonyl absorption value is 1715 cm^{-1} and is observed in the silane precursor. So the shift in absorption towards the lower wavelength must be due to the participation of the carbonyl group of methacrylate in hydrogen bonding. Hydrogen bonding can decrease the electron density in the C=O bond

leading to a slight increase in length of the bond. This will cause the bond to vibrate at a lower frequency. This can have definite implications on the surface properties. Hydrogen bonding can happen with both surface silanols and adsorbed water. If the methacrylate groups are hydrogen bonded with the surface groups then the chains would prefer a confirmation which will allow the chain to remain parallel to the surface i.e. the effective surface covered by a methacrylate chain will be much larger than the effective area required to anchor the Si-O_3 group. This is represented as scheme 2.2.

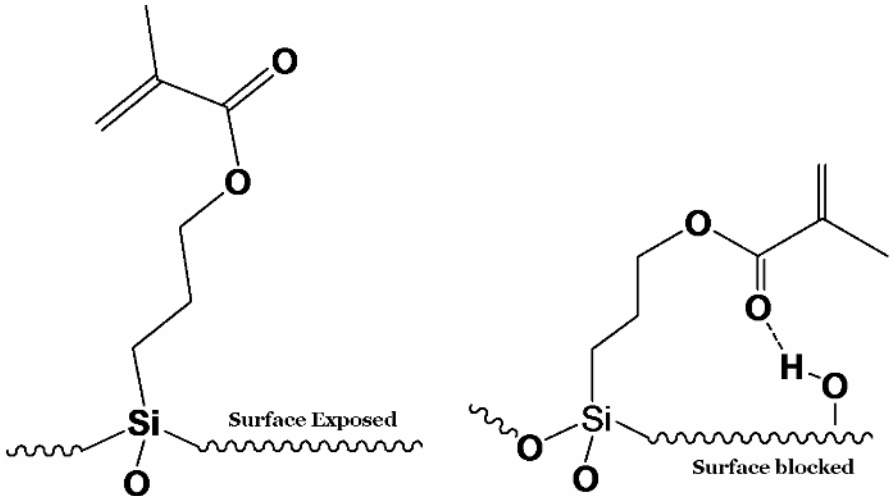

Scheme 2.2.: Schematic representation of hydrogen bonded and nonbonded confirmations of methacrylate chain and its effect on the accessible surface

The band present at 1640 cm^{-1} is due to the C=C in the methacrylate group. As already mentioned the absorptions due to adsorbed water also absorbs here. The absorptions at 1460 cm^{-1} and 1390 cm^{-1} corresponds to the bending vibrations of the C-H bonds. The methacrylate group contain both methyl and methylene groups and so the absorptions are rather broad and accommodate the absorptions due to all these groups. The absorption due to the vinyl hydrogen is not observed as in the case of VTMS modified gels. But the peaks due to bending vibrations of C-H bonds are rather broad and may contain the vibrations from the vinyl hydrogen. FTIR studies, hence suggest that there is an effective incorporation of the modified silane into the gel network.

The differential thermal analysis curve for the VTMS gels is provided as figure 2.11. There is an endothermic peak close to below 100 °C and is due to the removal of volatilities. The removal of any solvent remaining or water adsorbed happen in this region. The exothermic peak due to the decomposition of organic groups in the gel network happens around 350 °C. So the organic functionality will be available only up to this temperature. The decomposition of the organic group occurs in a single step.

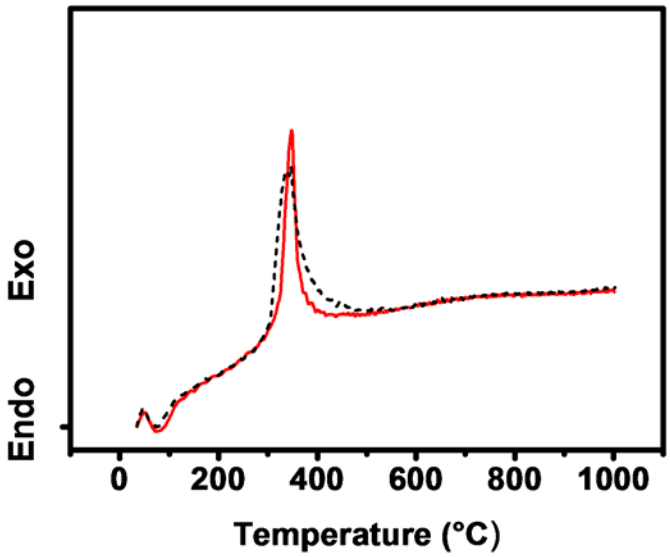

Figure 2.11.: DTA curve of VTMS gels prepared at a VTMS/TEOS molar ratio of 0.1 (continuous line) and 0.2 (broken line)

The thermal decomposition of MTMS gels occurs in the broad region 240 °C to 680 °C (figure 2.11a.). There are two distinct peaks in the region, one around 324 °C and the other around 540 °C. It is rather unusual for such decomposition step in methyl modified silane because the Si bonded methyl group is one of the most thermally stable groups. Methyl modified silane surfaces have been reported to lose their organic functionality above 500 °C.[39,40] But similar decomposition patterns have been observed by researchers studying the decomposition of sol gel glasses prepared with MTMS. The decompositions were followed with mass spectrometry and the decompositions below

400 °C was found to occur due to the decomposition of a series of by products like C_2H_5Cl formed during sol gel reactions.[41] It is rather unlikely that any such species can remain in our gels due to the long process of washing and aging. But the effect of any impurity will appear much magnified due to the lower molecular weight of the methyl group.

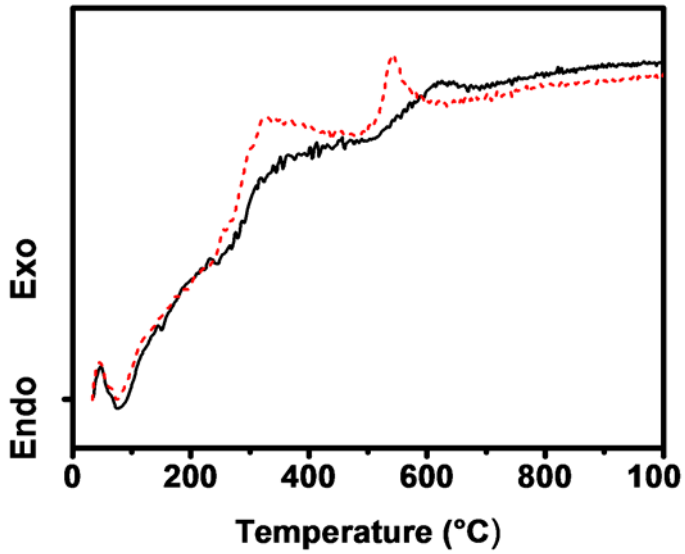

Figure 2.11a.: DTA curve of MTMS gels prepared at a MTMS/TEOS molar ratio of 0.05 (continuous line) and 0.1 (broken line)

The DTA curves of TPMS modified gels are provided as figure 2.12. The curves indicate that the thermal stability of the gels is up to 350 °C. Again the thermal decomposition occurs in a single step.

From the thermal decomposition curves it can be seen that the methyl modified gels are the most stable, thermally. All the curves have endotherm below 100 °C indicating the presence of solvent. The shaper nature of the endotherm indicates that the removed entitles contain water. The drying solvent is hexane, and has a low vapour pressure. So the endothermic peak corresponding to its removal would have been very weak or even absent.

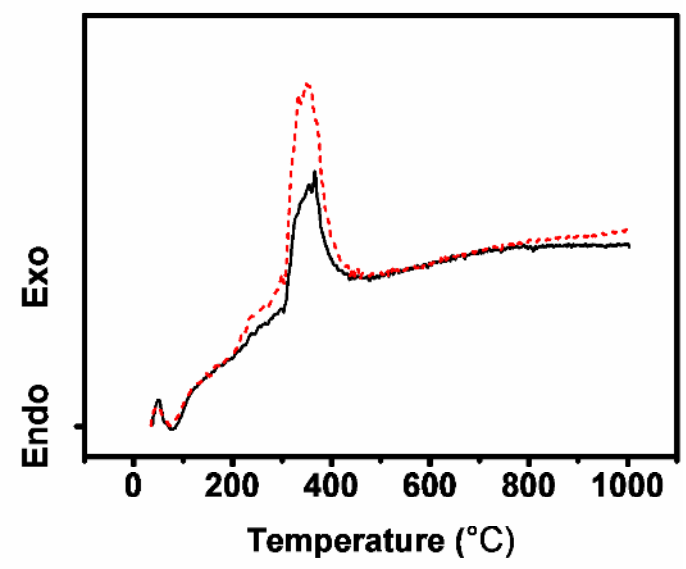

Figure 2.12.: DTA curve of TPMS gels prepared at a TPMS/TEOS molar ratio of 0.05 (continuous line) and 0.1 (broken line)

REOS/TEOS (molar ratio)	Density (cm^3g^{-1})		
	VTMS	MTMS	TPMS
0.05	0.724	0.704	0.754
0.1	0.733	0.655	0.798
0.2	0.669	-	-
0.3	0.647	0.637	0.817
0.5	0.602	-	-

Table 2.3.: Density obtained for various gels

The density of various gels obtained are presented as table 2.3. The values fall in the higher range observed for aerogels.[42] For the VTMS and MTMS gels the density decreases with increasing organic content. Meanwhile for the TPMS gels the density increases. The variation in density with the varying organic content is very small for the TPMS modified gels. Two different factors need to be considered while interpreting this

trend. One is that there is an increase in weight for the same volume of the gel when the organic content increases. Where as this increase in weight is 27 $gmol^{-1}$ for vinyl and 15 $gmol^{-1}$ for methyl, it is 127 $gmol^{-1}$ for methacrylate. So a four times increase in volume is required for the TPMS gels than the VTMS gels to obtain the same density as the VTMS gel. So unless there is a drastic change in drying shrinkage the densities of TPMS gels will be higher even when the drying shrinkage is same for all the samples. Surface Area analysis of the samples is required to understand the effect since the pore volume data will suffice the densities observed.

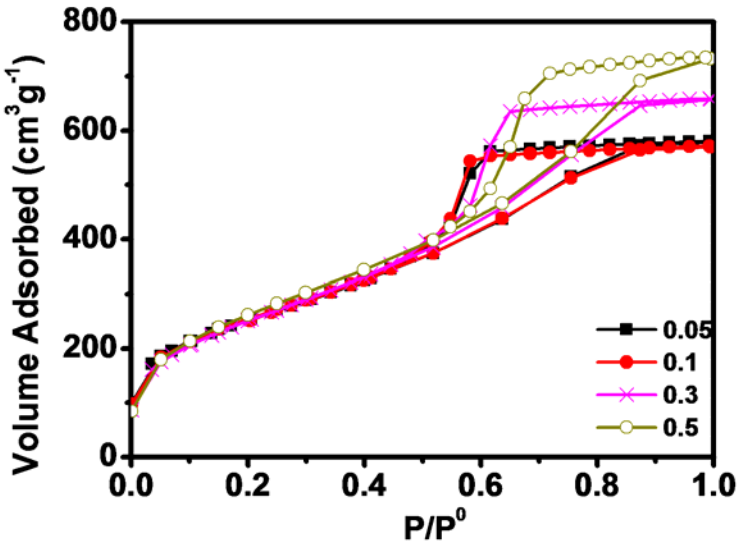

Figure 2.13.: Adsorption isotherms of VTMS gels prepared with varying (VTMS/TEOS) ratio as provided in the legend.

The N_2 adsorption isotherms of VTMS modified gels are provided as figure 2.13. The isotherms have the typical hysteresis loop observed for mesoporous materials. It can be seen that there is an increase in adsorption with increasing organic content. Microporosity is manifested as a sharp increase in adsorption below P/P° <0.1. In these gels there is a slight indication of microporosity, but the micropore volume is very small. The typical nature of the hysteresis loop indicates that the shape of the pores is bottle necked. If bottle necked pores are present, the pore size distribution obtained from the

adsorption and desorption legs of the adsorption isotherm will be different. The desorption leg of the isotherm will give a narrow distribution than that obtained from the adsorption curve.[43] This has been detailed in the introductory chapter.

VTMS/TEOS (molar ratio)	Surface Area (m^2g^{-1})	C Parameter	Total Pore Volume (cm^3g^{-1})	Average Pore Radius (nm)
0.05	904	122	0.89578	1.8
0.1	909	107	0.88190	1.9
0.2	912	99	0.91221	2.0
0.3	916	71	1.01723	2.2
0.5	962	63	1.13331	2.3

Table 2.4.: BET analysis along with total pore volume of VTMS modified gels

The BET analysis of the VTMS modified samples are provided as table 2.4. The specific surface area of the samples can be seen as increasing with the increasing concentration of the organic precursor. On the other hand the interaction parameter C which is the net heat of adsorption can be seen as decreasing with the organic content. The C parameter can be considered as a scale for the nature of the surface.[22] The lower the value of C the lower will be its hydrophilic nature. Typical silica surfaces, highly hydrophilic have a value of C around 120. So the progressive incorporation of the organic precursor with the increasing ratio is evident from the trend in the C value.

The total pore volume increases with the increasing organic content and this is in accordance with the observed trend in density. The vinyl inclusion decreases the density and hence the total pore volume. Pore collapse during drying is reduced. The average pore radii are similar for all gels and there is no significant variation observed.

The pore size distribution curves obtained by the BJH treatment on the adsorption leg of the isotherm is provided as figure 2.14. The pore size distribution curves are similar for all the gels and the distribution spans between 1-8 nm. As the organic content increases it can be seen that the volume of pores with higher pore radii increases. This is

a direct consequence of the reduction in pore collapse. It has been generally seen that the pores with higher pore sizes are more prone to collapse due to drying stress.[2,31,32] This is attributed to the fact that the larger pores are formed between larger particles, secondary particles which are weakly linked compared to the smaller primary particles.

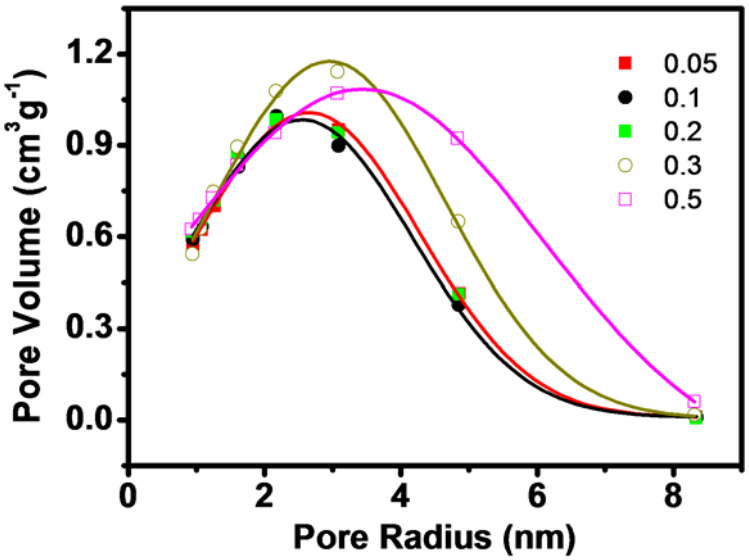

Figure 2.14.: Adsorption pore size distribution curves obtained for VTMS gels

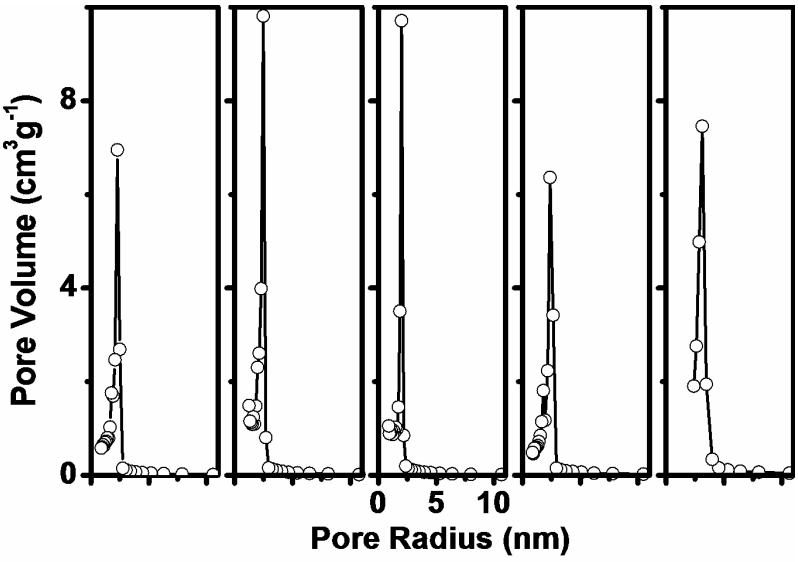

Figure 2.15.: Desorption pore size distribution curves obtained for VTMS gels. Molar ratio (VTMS/TEOS) from left 0.05, 0.1, 0.2, 0.3 and 0.5. Scale of X axis is same for all.

The pore size distribution obtained from the desorption curve of the isotherm is shown in figure 2.15. The discussed bottle neck effect of the pore shapes can be seen. The pore size distributions are narrow and are a reflection of the size of the necks of the pores. All distributions fall in the same region. The distribution of the 0.5 molar ratio gel has the widest distribution. The qualitative conclusions from the adsorption pore size distribution can also be obtained from the adsorption pore size distribution. We believe that the smaller necks are formed during the aging steps when the dissolution re-precipitation of silane species occur preferentially at the neck regions due to the negative curvature between the necks.[44] Here the pore surface is preferentially filled with non hydrolysable alkyl groups and the silane precipitation is concentrated on smaller areas, free of alkyl groups which lead to smaller necks.

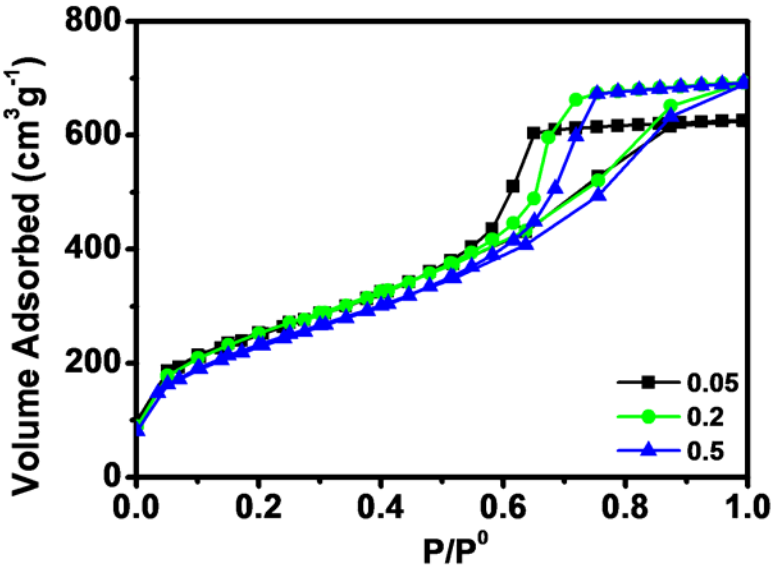

Figure 2.16.: Adsorption isotherms of MTMS gels prepared with varying (MTMS/TEOS) ratio as provided in the legend.

The adsorption isotherm of the MTMS gels are shown in figure 2.16. All isotherms show the typical type IV nature indicating mesoporous materials. The similar nature of the isotherms indicates the similar type of pore structure of the gels. Total amount of Nitrogen adsorbed increases with the amount of modified silane in the gel. As

observed in the case of the VTMS modified gels the pore shapes indicate a bottle neck structure.

MTMS/TEOS (molar ratio)	Surface Area (m^2g^{-1})	C Parameter	Total Pore Volume (cm^3g^{-1})	Average Pore Radius (nm)
0.05	912	123	0.96653	2.1
0.1	902	104	0.99234	2.2
0.2	904	85	1.00771	2.2
0.3	895	88	1.00453	2.2
0.5	846	77	1.06723	2.5

Table 2.5.: BET analysis along with total pore volume of MTMS modified gels

The BET analysis of the MTMS gels gives a reverse trend for surface area from that observed in VTMS gels. The surface area decreases with the increase in organic content. This would mean that the contributions from larger pores to the total pore volume are higher for the methyl modified gels.

The C parameter can be seen to follow the same trend as observed in the case of VTMS gels. Larger organic content increases the hydrophobic nature of the gel surface. The pore volume can be seen to increase with the organic content and demonstrates the effect of the organic modification on the drying process. The larger organic content increases the stability of the pores towards the drying stress. The average pore radii have similar values as that observed for the VTMS modified gels. On the other hand the effect of increasing concentration of vinyl group is gradual; where as the effect of methyl concentration is sudden. The total pore volume observed for the different molar ratio hybrids of methyl modified gels are in the range 0.96 to 1.06, while that observed for vinyl is in the range 0.89-1.13. This spread in the pore volume may be related to the nature of methyl and vinyl chains. The methyl groups are small and cover the surface well so the saturation effect is reached faster. On the other hand the vinyl groups are planar and extend perpendicular to the surface. The pore size distributions obtained from

the adsorption curves, figure 2.17. extends from 1 to 8 nm. The larger pore volumes are observed for the 0.5 molar ratio hybrid. Similarly the distribution of larger pores is larger in this set of hybrids.

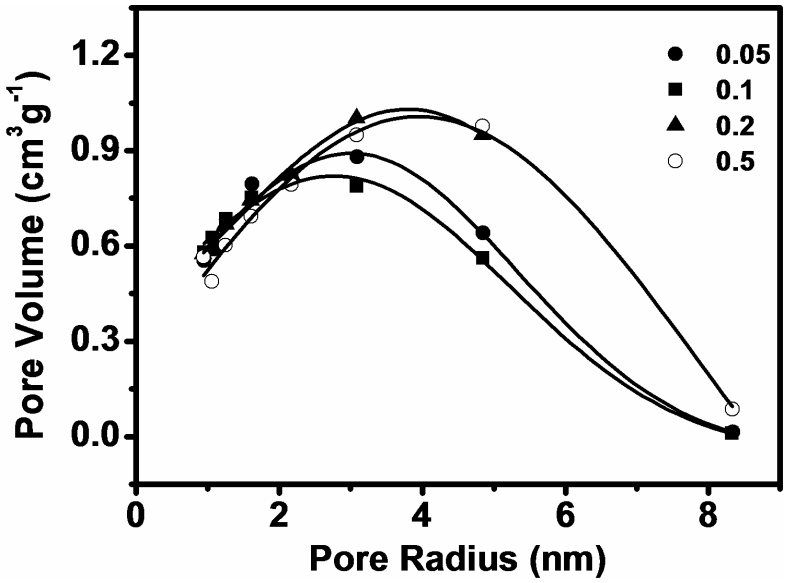

Figure 2.17.: Adsorption pore size distribution curves obtained for MTMS gels

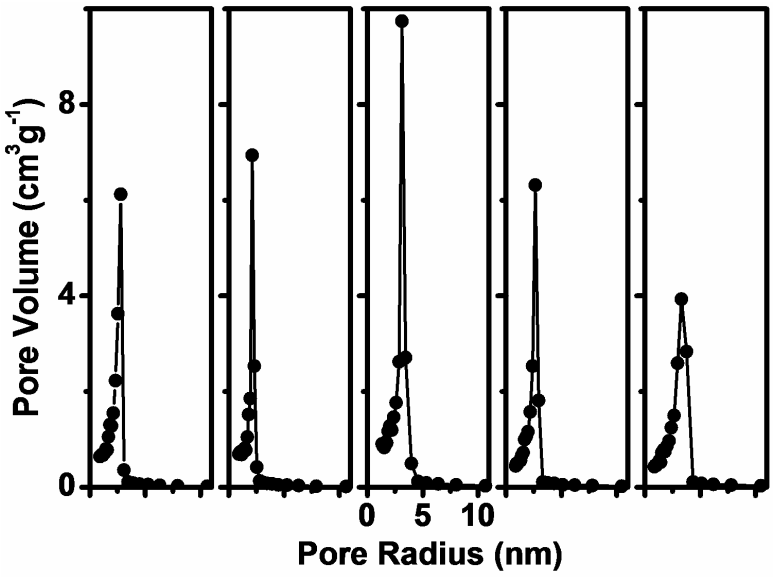

Figure 2.18.: Desorption pore size distribution curves obtained for MTMS gels. Molar ratio (MTMS/TEOS) from left 0.05, 0.1, 0.2, 0.3 and 0.5

The pore size distribution from the desorption leg of the isotherm of the MTMS gels calculated using the BJH method is given as figure 2.18. The distributions are narrower as expected.

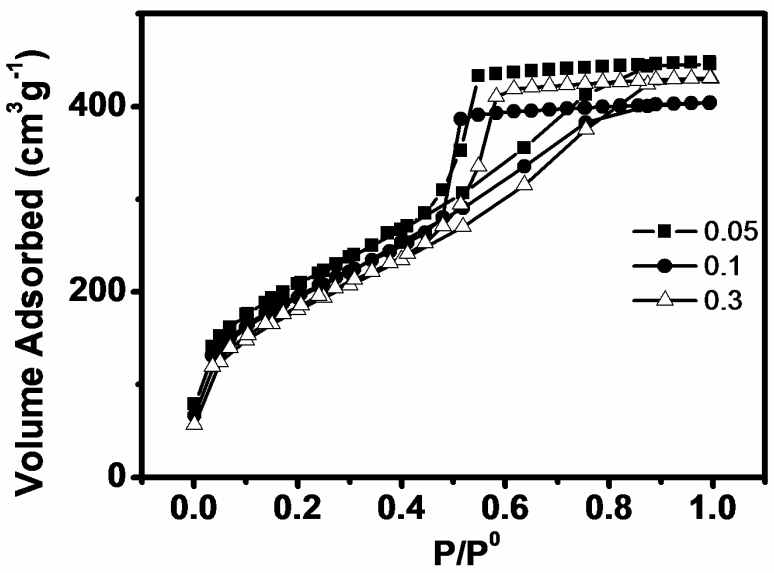

Figure 2.19.: Adsorption isotherms of TPMS gels prepared with varying (TPMS/TEOS) ratio as provided in the legend.

The adsorption isotherm obtained for the TPMS modified gels are provided as figure 2.19. The adsorption isotherms are similar to those obtained for the other gels.

TPMS/TEOS (molar ratio)	Surface Area (m^2g^{-1})	C Parameter	Total Pore Volume (cm^3g^{-1})	Average Pore Radius (nm)
0.05	744	118	0.68977	1.9
0.1	696	95	0.62532	1.8
0.2	617	79	0.5314	1.7
0.3	658	69	0.66523	2.0

Table 2.6.: BET analysis along with total pore volume of TPMS modified gels

The BET analysis of the TPMS gels are provided in table 2.6. The BET surface area values are rather close and the expected trends are not observed. The values are much lower than that observed for the MTMS or VTMS gels. The pore volume is also very low. Only the C parameter follows a trend and is in accordance with the increasing organic content. So the increase in density with increase in methacrylate content happens with a decrease in pore volume and hence a shrinkage of the network. Surface area values are also much lower than that observed for other gels. Shrinkage effects have been reported for modifications for alkyl silanes due to their poor networking ability. But we had observed a reverse trend in the case of GPTMS modified gels.

The hydrolysis condensation reactions of alkyl modified silanes have been followed by NMR techniques by various authors and the most significant conclusions of these studies are that hydrolysis reactions of substituted silanes are not rate determining.[7,14] Hydrolysis reactions proceed fast in trialkoxysilane solutions at acidic conditions. But condensation reaction rates are considerably reduced due to the steric and inductive effects of the alkyl substituents. The trialkoxysilanes prefer to form cyclic structures against long chains and they have been found to be very stable due to the steric hindrance offered to such structures by the alkyl chains.[7,15] This behaviour is particularly increased with the increase in chain length of the alkyl group. Feuillade has observed the formation of cyclic structures in methacryloxypropyltrimethoxysilane solutions catalyzed by acids.[19] In our systems where the alkoxysilanes are separately hydrolysed cyclisation is most probable. But the cyclisation in methacrylate sol must have been much more and the cyclic condensation of these chains may not have helped the integration of these groups into the gel network effectively. These organic moieties which are loosely bound to the gel network may be the reason for its inability to prevent the shrinkage of the network. In the case of GPTMS gels the hydrolysis and condensation reactions of the modified silane happens in the presence of the tetraalkoxysilane. Hydrolysis rates of tetraalkoxysilane are much faster than that of trialkoxysilanes. So the hydrolysis condensation reactions of the tetraalkoxy species would have proceeded to some extent by the time, monomers (hydrolyzed species) from trialkoxy moieties appear. The faster

condensation of tetraalkoxysilanes would mean that condensed clusters will be available in the solution once the trialkoxysilane monomers are formed. The condensation mechanism in conditions above the isoelectric point of silica prefer the condensation of monomers to preformed clusters rather than monomer to monomers.[2] This would mean that the GPTMS monomers would preferentially condense on to the clusters rather than undergoing self condensation.

The adsorption pore size distribution observed for the TPMS gels is provided as figure 2.20. The distributions are rather narrow, but there is a slight indication of pore stability for the higher percentage hybrid (0.3) which has higher distribution of pores in the larger size range.

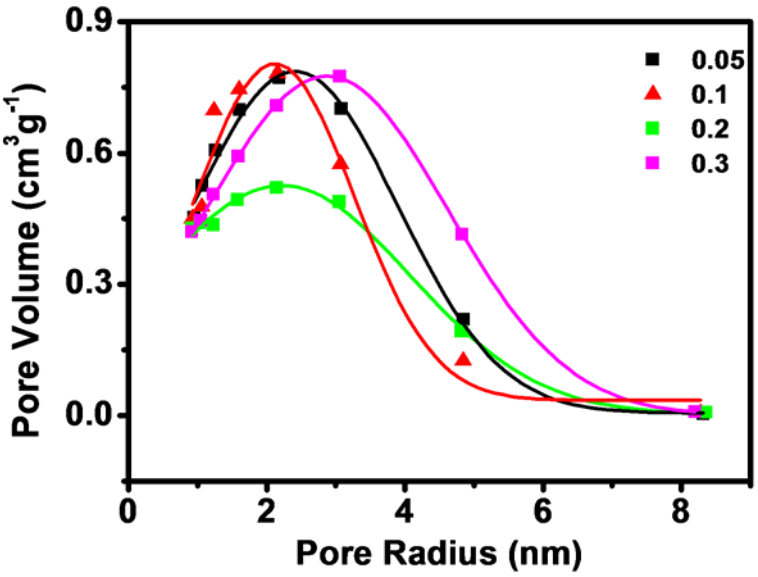

Figure 2.20.: Adsorption pore size distribution curves obtained for TPMS gels

The desorption pore size distribution curves for the TPMS gels are given in figure 2.21. Here also the distributions obtained are narrower than that obtained from the adsorption curve. But the distributions are a bit broad for the 0.3 ratio hybrid.

The photographs of the gels obtained are given in figure 2.22. The blue scattering observed for aerogels can be seen in the prepared gels figure 2.23.

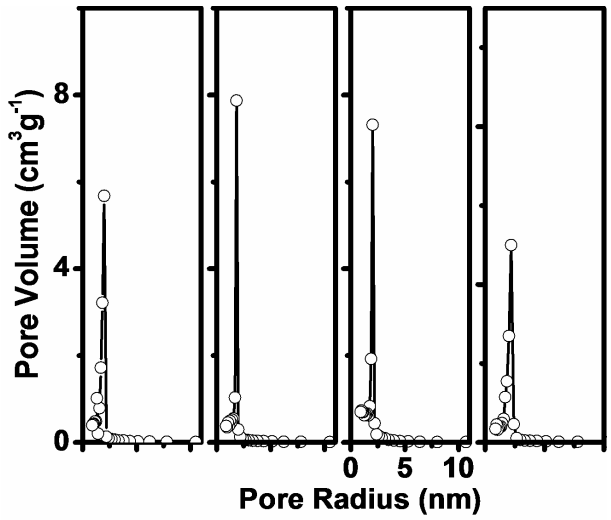

Figure 2.21.: Desorption pore size distribution curves obtained for TPMS gels. Molar ratio (TPMS/TEOS) from left 0.05, 0.1, 0.2 and 0.3

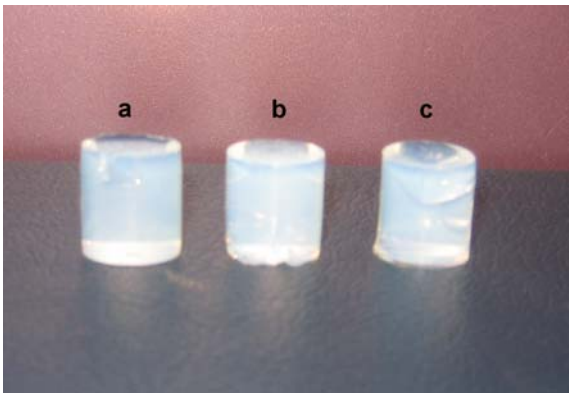

Figure 2.22.: Photographs of (a) VTMS (b) MTMS (c)TPMS gels prepared at a molar ratio 0.3

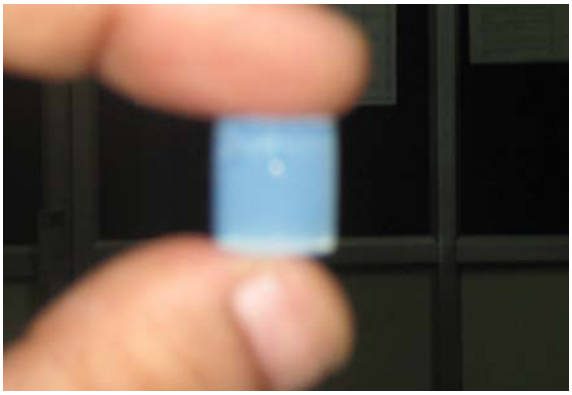

Figure 2.23.: Blue Scattering in prepared aerogels

Conclusion

In conclusion, the modifications of the ambient pressure process for aerogels using an organically modified silane precursor has been found to be highly advantageous with respect to the various properties. The presence of the organic chains during the drying stages stabilizes the pore structure and shrinkage is reduced. The stabilization of the pore structure happens through the prevention of condensation of the surface silanols by the organic groups. Increasing the organic precursor ratio increases the stabilization and significant changes are observed at high concentrations of the hybrid. Unfortunately higher organic precursor content combinations are marred by long gelation times. Optimal water content (water/alkoxide molar ratio = 8) has been identified for the mixed precursor system where the effects of increasing hydrolysis rates and lowering concentration of the precursors are balanced. Organic groups were found to occupy positions along the pore walls, mainly due to the difference in rate of sol-gel reactions of the tetraalkoxy and trialkoxy precursors. The effect of chain length on the drying technique seems to suggest that at low concentrations of the organic content, the maximum stabilization is observed when the organic group is small and thus covers the surface well. However, at higher concentrations longer alkyl chains have more prominent effect. These results will be helpful in areas where functional porous materials are required. The organic functionality can be further modified for properties like luminescence and the requirements of the alkyl chain to maximize porosity are available from this study. For the use as aerogel replacements, the technique needs to be refined and the concept of crosslinking the organic groups will be a better prospect. This will be treated in the next chapter.

References

1. Hüsing, N.; Schubert, U., *Angewandte Chemie - International Edition*, 37 (1998) 22.

2. Brinker, C. J.; Scherer, G. W. *Sol-Gel Science:The physics and Chemistry of sol-gel processing*, ed. Academic Press: London, 1990.

3. Pauthe, M.; Despetis, F.; Phalippou, J., *Journal of Non-Crystalline Solids*, 155 (1993) 110.

4. Shewale, P. M.; Rao, A. V.; Rao, A. P., *Applied Surface Science*, 254 (2008) 6902.

5. Schwertfeger, F.; Glaubitt, W.; Schubert, U., *Journal of Non-Crystalline Solids*, 145 (1992) 85.

6. Martin, L.; Osso, J. O.; Ricart, S.; Roig, A.; Garcia, O.; Sastre, R., *Journal of Materials Chemistry*, 18 (2008) 207.

7. Loy, D. A.; Baugher, B. M.; Baugher, C. R.; Schneider, D. A.; Rahimian, K., *Chemistry of Materials*, 12 (2000) 3624.

8. Ng, L. V.; Thompson, P.; Sanchez, J.; Macosko, C. W.; McCormick, A. V., *Macromolecules*, 28 (1995) 6471.

9. Zhang, Z.; Tanigami, Y.; Terai, R.; Wakabayashi, H., *Journal of Non-Crystalline Solids*, 189 (1995) 212.

10. Tan, B.; Rankin, S. E., *Journal of Non-Crystalline Solids*, 352 (2006) 5453.

11. Dong, H.; Brook, M. A.; Brennan, J. D., *Chemistry of Materials*, 17 (2005) 2807.

12. de Buyl, F.; Kretschmer, A., *Journal of Adhesion*, 84 (2008) 125.

13. Riegel, B.; Kiefer, W.; Hofacker, S.; Schottner, G., *Journal of Sol-Gel Science and Technology*, 13 (1999) 385.

14. Hook, R. J., *Journal of Non-Crystalline Solids*, 195 (1996) 1.

15. Matejka, L.; Dukh, O.; Hlavata´, D.; Meissner, B.; Brus, J., *Macromolecules*, 34 (2001) 6904.

16. Ukrainczyk, L.; Bellman, R. A.; Anderson, A. B., *The Journal of Physical Chemistry B*, 101 (1997) 531.

17. Dubitsky, Y.; Zaopo, A.; Zannoni, G.; Zetta, L., *Materials Chemistry and Physics*, 64 (2000) 45.

18. Delattre, L.; Dupuy, C.; Babonneau, F., *Journal of Sol-Gel Science and Technology*, 2 (1994) 185.

19. Feuillade, M.; Croutxe´-Barghorn, C.; C.Carre´, *Progress in Solid State Chemistry*, 34 (2006) 87.

20. Costela, A.; García Moreno, I.; Gómez, C.; García, O.; Sastre, R.; Roig, A.; Molins, E., *Journal of Physical Chemistry B*, 109 (2005) 4475.

21. Husing, N.; Schubert, U., *Journal of Sol Gel Science and Technology*, 8 (1997) 807.

22. Husing, N.; Schubert, U.; Misof, K.; Fratzl, P., *Chemistry of Materials*, 10 (1998) 3024.

23. Riegel, B.; Plitterdorf, S.; Kiefer, W.; Husing, N.; Schubert, U., *Journal of Molecular Structure*, 410-411 (1997) 157.

24. Rao, A. V.; Bhagat, S. D.; Hirashima, H.; Pajonk, G. M., *Journal of Colloid and Interface Science*, 300 (2006) 279.

25. Capadona, L. A.; Meador, M. A. B.; Alunni, A.; Fabrizio, E. F.; Vassilaras, P.; Leventis, N., *Polymer*, 47 (2006) 5754.

26. Leventis, N.; Sotiriou-Leventis, C.; Zhang, G.; Rawashdeh, A.-M. M., *Nano Letters*, 2 (2002) 957.

27. Kanamori, K.; Aizawa, M.; Nakanishi, K.; Hanada, T., *Advanced Materials*, 19 (2007) 1589–1593.

28. Leventis, N.; Palczer, A.; McCorkle, L.; Zhang, G.; Sotiriou-Leventis, C., *Journal of Sol-Gel Science and Technology*, 35 (2005) 99–105.

29. Haereid, S.; Nilsen, E.; Einarsrud, M.-A., *Journal of Porous Materials*, 2 (1996) 315.

30. Prakash, S. S.; Brinker, C. J.; Hurd, A. J.; Rao, S. M., *Nature*, 374 (1995) 439.

31. Smitha, S.; Shajesh, P.; Aravind, P. R.; Kumar, S. R.; Pillai, P. K.; Warrier, K. G. K., *Microporous and Mesoporous Materials*, 91 (2006) 286.

32. Smitha, S.; Shajesh, P.; Kumar, S. R.; Krishna Pillai, P.; Warrier, K. G. K., *Journal of Porous Materials*, 14 (2007) 1.

33. Aravind, P. R., *Mixed Oxide Silica Aerogels Synthesized Through Non Supercritical Route for Functional Applications*, PhD. Thesis, (2008), Faculty of Science, Cochin University of Science and Technology.

34. Jabbour, J.; Calas, S.; Gatti, S., *Journal of Non-Crystalline Solids*, 354 (2008) 651.

35. Rassy, H. E.; Pierre, A. C., *Journal of Non-Crystalline Solids*, 351 (2005) 1603.

36. Yoda, S.; Ohshima, S., *Journal of Non-Crystalline Solids*, 248 (1999) 224.

37. Loy, D. A.; Mather, B.; Straumanis, A. R.; Baugher, C.; Schneider, D. A.; Sanchez, A.; Shea, K. J., *Chemistry of Materials*, 16 (2004) 2041.

38. Buyl, F.; Kretschmer, A., *Journal of Adhesion*, 84 (2008) 125.

39. Rao, A. V.; Kulkarni, M. M.; Amalnerkar, D. P.; Seth, T., *Journal of Non-Crystalline Solids*, 330 (2003) 187.

40. Kang, S. K.; Choi, S. Y., *Journal of Materials Science*, 35 (2000) 4971.

41. Nocun, M.; Gajerski, R.; Siwulski, S., *Optica Applicata*, 35 (2005).

42. Pierre, A. C.; Pajonk, G. M., *Chemical Reviews*, 102 (2002) 4243.

43. Gregg, S. J.; Sing, K. S. W. *Adsorption, Surface Area and Porosity*, ed. 2nd; Academic Press: San Diego, 1995.

44. Haereid, S.; Dahle, M.; Lima, S.; Einarsrud, M.-A., *Journal of Non-Crystalline Solids*, 186 (1995) 96.

Chapter 3

Crosslinked Organic Inorganic Hybrid Networks Dried at Ambient Pressure

Ambient pressure drying techniques for the preparation of aerogel like highly porous networks has evolved into a process, competent enough to replace supercritical drying in recent years. Aging of the wet gel in a precursor solution leads to stiffening of the gel network, reducing shrinkage during drying.[1-3] Modifying the gel surface with alkyl groups prevents condensation of silanol groups during drying and results in a spring back effect of the network, reversing the shrinkage during drying.[4,5] Gels prepared from methyltrimethoxysilane can be dried at ambient pressure owing to this spring back effect.[6-8] Coexisting organic inorganic hybrid networks have received considerable attention in recent years due to the increased mechanical strength observed in such systems.[9]

Leventis prepared a polyurethane reinforced silica network by reacting the surface silanol groups of the wet gel with a diisocyanate.[10,11] The properties of the final gel depend on their density, which in turn depended on the concentration of diisocyanate in the bath. Relative to native silica, composite aerogels shrink by up to 10-12% and they become up to ~3 times more dense and the shrinking was associated with cross-linking. A new material was seen introduced conformally to the secondary particles, but individual particles and the necklace-like structure remained. The mesoporosity reduced, as secondary particles appeared fused. It took more than 100 times higher load to break a monolith with density 0.447 gcm^{-3} than to break a native silica aerogel monolith. Wider interparticle necks formed from the accumulation of isocyanate increased the stiffness of the gels as well.[10] By replacing the silanol species with an amine bearing alkyl group the isocyanate could be used to create a polyurea network.[12,13] Since amines react with isocyanate faster than hydroxyls, crosslinking could be achieved at room temperature. The polymer conformally coats the surface of the skeletal nanoparticles, leaving the mesoporous voids open. The skeletal framework of APTES-modified aerogels also

allowed incorporation of larger number of particles than observed with typical native silica aerogels. The cross-linked samples had porosity in the order of 65%. The thermal diffusivity of a polyurea cross-linked APTES-modified aerogel was in the range of that of glass wool. The specific compressive stress at ultimate failure of these aerogels were in the same order of magnitude as poly(methyl methacrylate) (PMMA)20 and Kevlar-49 epoxy.[12] The amine can also react with diepoxy bearing organic compound to give a cross linked organic inorganic network.[14] The diisocyanate crosslinking reinforces the underlying silica network by almost 300 times and enables drying at ambient pressure to obtain aerogel properties.[15] These crosslinked aerogels were sensitive to the surface tension of the solvent and when submerged in low molecular weight, low surface tension hydrocarbons (e.g., pentane, hexane) suffer the least shrinkage, and a crosslinked aerogel soaked in pentane and subsequently re-dried at ambient pressure, retained the microstructure practically identical to that of another crosslinked monolith dried supercritically. Density, surface area, average pore diameter and rupture strength (by a three-point flexural bending test) of the of crosslinked aerogels dried at ambient pressure were identical to that dried supercritically. The dimensional stabilization gained by crosslinking was seen to depend on the amount of the crosslinker. Aerogels with density below 0.3 g cm^{-3} could not be dried at ambient pressure suggesting a threshold above which the total bond energy added per unit volume by crosslinking is greater than the energy that would be released by the collapse of the underlying plain silica framework. They were able to dry cross-linked hydrogels under ambient pressure with dimensions larger than what could be achieved by supercritical drying owing to the limitation in autoclave space.[15] Nguyen recently experimented with the idea of unifying the concepts of flexible aerogels obtined by alkyl modification and conformal polymer coating obtained by crosslinking.[6,10,16] Bis(trimethoxysilyl)hexane was used to induce flexiblity and vinyl silane was used to create polymerisable group on the inorganic network. Styrene was polymerised with the vinyl group using AIBN initiator. It was found that incorporation of the hexyl links from BTMSH improved elastic recovery after

compression to 25% strain in the resulting monoliths. The inclusion of BTMSH also lead to more hydrophobic aerogels.[16]

3-Glycidoxypropyltrimethoxysilane (GPTMS) is an important organically modified precursor that can crosslink through the polymerization of the epoxy group. Even though initial use for GPTMS was for enhancing moisture stability of glass-fiber-reinforced plastics, it also provides similar benefits in numerous applications where a metal oxide–adhesive interface needs improvement.[17] Organic-inorganic polymer membranes were prepared by reacting 3-glycidoxypropyltrimethoxysilane with diamines containing polyether segments, followed by hydrolysis and condensation with acid catalysis for gas separation.[18] Organic-inorganic hybrids derived from GPTMS have been as host materials for lithium salts for application as solid electrolytes.[19] It has also been used to prepare optical waveguides by including zirconia and titania.[20-22] Incorporation of fullerenes, infrared dyes and push pull chromophores has extended their use to optical limiting, and optical amplification applications.[23-25] To improve energy conversion efficiency and to avoid CO poisoning of catalysts, polymer electrolyte-type fuel cells which can operate in the medium temperature range (100–200 °C) are strongly desired. Proton conductive inorganic–organic hybrid films with high proton conductivity, even at temperatures higher than 100 °C and at low humidity have been prepared from GPTMS for this purpose.[26,27]

Epoxy groups of GPTMS react to form polyethylene oxide (PEO) chains via photo or thermal induced polymerization or via basic or acid catalysis.[28-30] Many of the compounds used as initiators of organic polymerization often act, at the same time, as catalysts of the siloxane polymerization. 1-methylimidazole and (γ-aminopropyl)triethoxysilane are examples of basic catalysts.[19,31] These compounds act at the same time as catalysts of the siloxane polymerization. Lewis acids, such as titanium, zirconium, or aluminum alkoxides, are also efficient initiators of organic polymerization.[21,32,33] These alkoxides, cohydrolyzed, with GPTMS will be incorporated into the silicon-based inorganic network. BF_3 etherate has also been used in the synthesis of GPTMS-derived hybrid materials that can act as a host for fullerene derivatives to

fabricate an optical limiting device.[34,35] BF_3 can also promote the inorganic polymerization to a larger extent compared to other metal alkoxides.[35] An important point in the synthesis of this class of hybrids is related to the effect on the PEO chain lengths of the simultaneous organic and inorganic polymerization. For example, larger amounts of BF_3 enhance the inorganic network crosslinking and give oligo(ethylene oxide) derivatives. Boron has been found to remain in the matrix as a network former of the inorganic side.[36] If the silica network is formed much faster than the organic polymer, the organic chains cannot find enough space to grow and their length is greatly reduced.[36] Diethylenetriamine is a very fast and reactive epoxy-ring opening reagent and most of the organic network is completed at room temperature. Since the amines are basic, they also catalyse the condensation of silanol groups to form the silica network. Davis et al developed epoxy-based inorganic–organic hybrid polymers, for use as a matrix in coatings, starting from 3-glycidoxypropyltrimethoxysilane by a sol–gel process. Diethylenetriamine was used to open the epoxy rings and form the organic network and the results indicated that the formation of the two networks did not occur independently and the rate or extent of organic cross-linking had a direct effect on the extent of the inorganic network formation, and vice-versa.[37]

These studies had shown that sol-gel hydrolysis, condensation reactions of glycidoxypropyltrimethoxysilane can proceed without causing the epoxy ring opening.[37] This gives considerable leverage in the preparation of porous hybrids. Surprisingly there is little information available on the use of this precursor in the preparation of cross linked porous systems. Husing had earlier used it as a co-precursor to obtain organically modified aerogels through supercritical drying.[38]

Extending the findings from the first chapter here we have investigated the preparation of porous hybrid networks from 3-glycidoxypropyltrimethoxysilane and tetraethoxysilane precursors and their drying at ambient pressure. The ambient pressure drying technique presented in the first chapter is utilized for the drying of the hybrid networks. Considering the facts that glycidoxypropyltrimethoxysilane is frequently reported for the preparation of dense organic inorganic hybrids and as binders in coatings

and also considering the fact that hydrolysis-condensation reactions of alkyl substituted alkoxides preferentially give cyclic structures, increasing gelation times and inducing phase separation in mixed alkoxide systems, the right balance of precursor ratio and control of hydrolysis-condensation reactions are required to obtain highly porous organic inorganic hybrid systems. Hence the effect of water molar ratio used for hydrolysis of the alkoxide groups and the effect of varying the molar ratio between the organically modified precursor and the inorganic precursor is investigated. Further the the nature of the organic network is also varied by adding a crosslinker diepoxyoctane. The crosslinker provides a way to develop an organic network which has less anchorage to the inorganic network. Here the network should be flexible and the influence of increasing the extent of this network is also investigated. The nature of the organic networks formed at various organic content is also investigated using Fourier Transform Infrared Spectroscopy.

Experimental

3-glycidoxypropyltrimethoxysilane (GPTMS), tetraethylorthosilicate (TEOS) 1,2,7,8 diepoxyoctane (DEO) and diethylenetriamine (DETA) were procured from Aldrich (Steinheim, Germany) and used as obtained. Isopropyl alcohol and hydrochloric acid were obtained from S.D. Fine chemicals (Mumbai, India). Water used for the preparation was doubly distilled. In a typical preparation, weighed amounts of GPTMS and TEOS were mixed with weighed quantity of isopropanol by stirring on a magnetic stirrer. To this solution weighed amount of 10^{-3} N HCl was added. The initial water content is the amount of the acid taken for the preparation of the gel. The solution was stirred for 3 hours. Weighed amount of DETA was then added to this solution under stirring. In samples prepared with a crosslinking agent DEO was added prior to DETA. After stirring for 5 minutes the solutions were transferred to polypropylene vials. The vials were kept at 50 °C for gelation. Gelation occurred within 30 minutes for all samples. DETA catalyzes the organic networking through a nucleophilic attack on the epoxy ring. The GPTMS/DETA molar ratio was fixed at 3 for all preparations. In crosslinked samples DEO/GPTMS molar ratio was varied. Gels were prepared with

varying precursor (TEOS/GPTMS) molar ratio and initial water content. Samples with precursor molar ratio of 3, 2, 1 and 0.5 were prepared. Initial water content was varied according to H_2O/OR molar ratio of 0.5, 1 and 2. Samples with crosslinker were prepared with crosslinker ratio (DEO/GPTMS) 0.25, 0.5, 1 and 1.5. Samples with crosslinker were prepared only for the precursor ratio 2 and water ratio 0.5. So a sample with crosslinker of 1 contained an organic network equivalent to the sample with precursor ratio 1 without any crosslinker, but an inorganic network equivalent to the precursor ratio 2, i.e. the organic network is increased independent of the inorganic network.

A mole of alkoxy group requires 0.5 mole water for complete hydrolysis and condensation according to the stoichiometry of the equation.

$$Si(RO)_4 + 2H_2O \longrightarrow SiO_2 + 4ROH$$

In practice complete hydrolysis may require more water and an H_2O/OR molar ratio of 1 represent the availability of a water molecule for each Si-OR bond. Use of excess water for hydrolysis is represented by the molar ratio of 2. Gels are designated as xPyWzCwd, where 'x' is the precursor molar ratio and 'y' is the H_2O/OR molar ratio, 'z' is the DEO/GPTMS molar ratio and 'd' is the fixed density for the rest of the text. Only for samples prepared with a fixed density is the notation d included in the designation. The isopropanol/Si molar ratio was either kept constant at 4 or evaluated to fix the final density of the gel.

The theoretical densities of the gels are calculated by assuming that the gel network is formed from SiO_2, $RSiO_{1.5}$, DEO (if crosslinker present) chains and DETA becomes part of the network.[38] So the dried gel consists of only SiO_2, $RSiO_{1.5}$, DEO and DETA. So the weight of the dried gel network will be

$$W_{gel} = n_{TEOS} \times M_{SiO_2} + n_{GPTMS} \times M_{RSiO_{1.5}} + n_{DEO} \times M_{DEO} + n_{DETA} \times M_{DETA}$$

The volume of the gel will be the total volume of all the components used, assuming that there will be no change in volume after drying.

$$V_{gel} = V_{TEOS} + V_{GPTMS} + V_{DEO} + V_{DETA} + V_{Alcohol} + V_{Water}$$

and the calculated density of the gel will be $\rho_{gel} = W_{gel} / V_{gel}$

So if the density of the final gel needs to be fixed keeping all other variables like precursor ratio, water ratio, crosslinker ratio etc constant, the alcohol volume needs to be changed. Volume of alcohol is calculated as

$$V_{alcohol} = \frac{W_{Gel}}{\rho_{Gel}} - (V_{TEOS} + V_{GPTMS} + V_{DEO} + V_{DETA} + V_{Water})$$

The density were fixed for a set of samples with precursor ratio 2 and water ratio 0.5 prepared without the crosslinker. The densities were fixed as 0.16, 0.2 and 0.25. All samples with crosslinker were prepared by fixing the density at 0.187. This is the density calculated for the gel prepared with (TEOS/GPTMS) ratio of 2 and a water ratio of 0.5. The density of crosslinked samples was fixed at this value so that the effect of increasing the organic network independent of inorganic network can be followed.

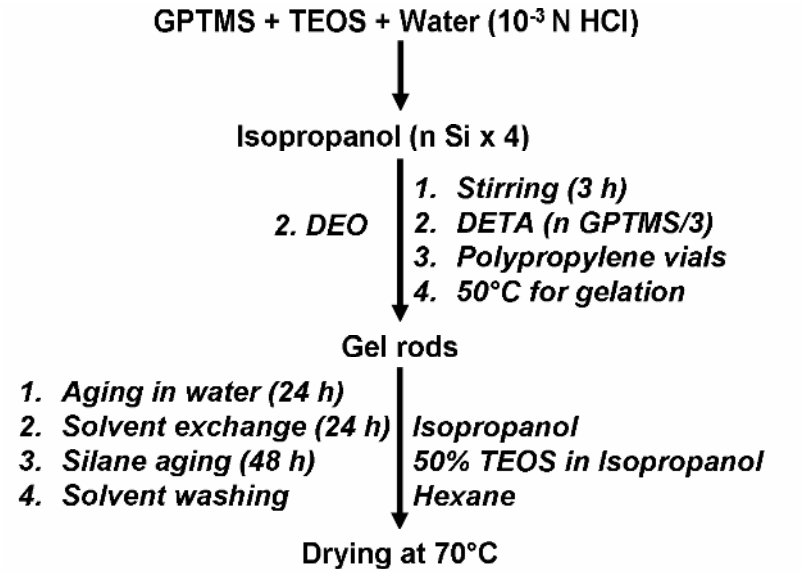

Scheme 3.1. Synthesis scheme for the crosslinked hybrids

The alcogels were aged in water for a period of 24 hours followed by solvent exchange with isopropanol. In order to exchange the solvent, the gels were immersed in isopropanol and the solution replaced with fresh alcohol, 5 times in 24 hours. The solvent exchanged gels were then aged in a solution of 50% TEOS in isopropanol for a period of 48 hours. The silane aged gels were washed with n-hexane following the same procedure

used for solvent exchange. In all the steps the soaking solutions had volume twice as that of the gels immersed in them. The gels were then kept for drying in sealed containers at 70 °C. The container seals were perforated with pins after a day for the solvent to escape slowly. The dried gels were used for further characterization. The procedure is presented as scheme 3.1.

The bulk density of the dried gels was calculated from the measured dimensions and weight. Thermal analysis of the gels were performed on a Thermogravimetric analyzer (Shimadzu TG 50, Kyoto, Japan) and a Differential thermal analyzer (Shimadzu DTA 50, Kyoto, Japan) in air at a heating rate of 5 °Cmin^{-1}. A Fourier Transform Infrared Spectroscope (Magna 560, Nicolet, Madison, Wisconsin) was used for recording the FTIR spectra of the sample. The spectra were acquired using the KBr pellet method in the range 4000-400 cm^{-1}. The samples were stored in an oven maintained at 70 °C and care was taken to avoid excessive exposure to atmosphere prior to measurement. The precautions prevent interference of humidity in the measurements. The Fourier Self Deconvolution Trace analysis was carried out using the Omnic software provided by the manufacturer on the spectra obtained for the crosslinked samples. For Fourier trace analysis the samples were degassed in flowing Nitrogen at 150 °C for 4 hours prior to taking FTIR. Nitrogen adsorption data were obtained using a BET surface area analyzer (Gemini 2375, Micromeritics, Norcross, U.S.A) at 77 K. All analysis were conducted after degassing the sample at 150 °C for 6 hours. The pore size distributions were calculated using the Barrett Joiner-Halenda (BJH) method from the desorption curve of the isotherm. The calculations were performed by the software StarDriver V2.03 supplied by the manufacturer. The BJH average pore radius was calculated using the equation (2V/A), where V is the BJH desorption total pore volume and A is the specific surface area. Skeletal density measurements were performed on a He pycnometer (Accupyc, Micromeritics, Norcross, U.S.A). The samples were heated at 100 °C for 24 hours prior to measurements. TEM observations were made on a FEI high-resolution transmission electron microscope (Technai 30 G2 S-TWIN, Eindhoven, Netherlands). Dielectric measurements were done on pellets prepared by polishing dried gel rods. Silver paste was

used for preparing the electrodes and copper leads for contact. The measurements were made on a HP impedance analyzer HP 4192 A. Temperature dependence of dielectric property was studied by heating the samples to the respected temperature and measuring the dielectric constant.

Results and Discussion

The success of the drying technique is evident from figure 3.1. The figure shows a sample with low shrinkage along with the wet gel. Figure 3.2. includes most of the samples prepared along with the pellets used for dielectric measurements.

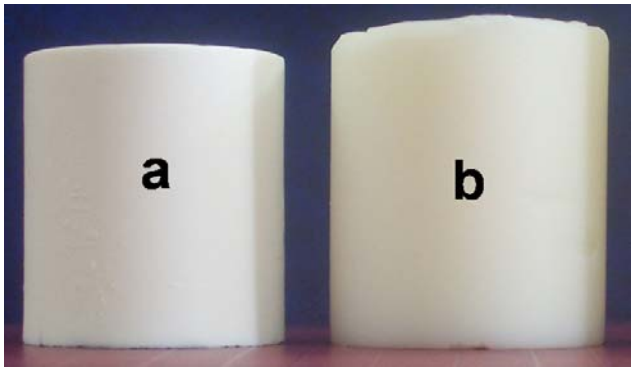

Figure 3.1.:Photograph of (a)dry (b)wet gel prepared at a precursor ratio 2 and water ratio 0.5

The characterization of the samples prepared without the crosslinker will be discussed first. The structural characteristics of the hybrids were investigated using FTIR spectroscopy. The FTIR peaks were assigned based on available literature. The FTIR spectra of the samples with varying precursor ratio, without any crosslinker, in the region 4000 cm^{-1} to 3500 cm^{-1} are provided as figure 3.3.

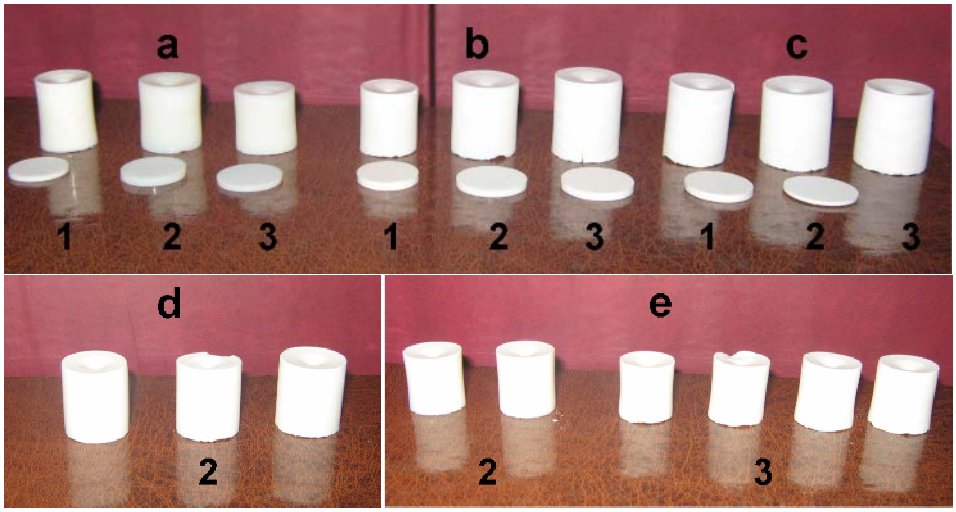

Figure 3.2.: Photographs of dried gels with precursor ratio (a) 1 (b) 2 (c) 3 (d) 2 (e) 2. Numbers represents the water ratios used (1) 2 (2) 1 (3) 0.5. In (e) crosslinker ratio increases as 0.25, 0.5, 1 and 1.5 from right to left. (d) is prepared by fixing the target density and it increases as 0.16, 0.2 and 0.25 from left to right.

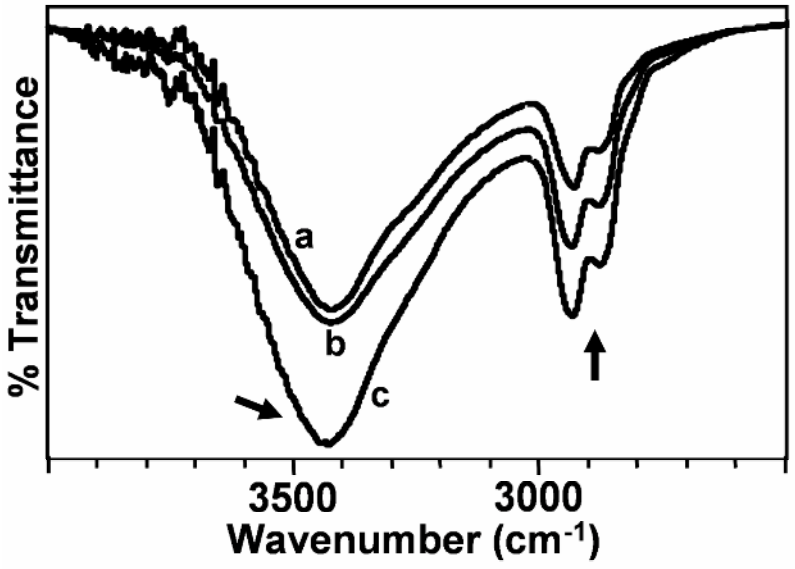

Figure 3.3.: FTIR spectra of samples prepared with a precursor ratio of (a) 2 (b) 1 and (c) 0.5 and water ratio of 0.5 in the region 4000 cm^{-1} to 3500 cm^{-1}

The broad absorption centred on 3400 cm^{-1} is due to the OH groups in the sample.[39] The strong absorption around 2900 cm^{-1} is due to the alkyl hydrogen, which are

part of the organic network, stretching vibrations.[40,41] The increase in intensity of the C-H stretch is proportional to the GPTMS content in the sample. But the intensity of the hydroxyl absorption for the samples with TEOS/GPTMS molar ratio 2 and 1 are comparable, while there is a much higher absorption when the ratio decreases to 0.5.

The absorption of the samples in the IR region 1800 cm^{-1} to 400 cm^{-1} is given in figure 3.4. The absorption at 1650 cm^{-1} is due to the bending vibrations of adsorbed water.[41] The peak around 1460 cm^{-1} is the bending vibrations of the CH bonds of the alkyl groups in the organic network. The Si-O-Si asymmetric stretching vibration absorbs intensely around 1100 cm^{-1} and can be seen as a strong and broad band in this region.[39,41-44] The small shoulder to this peak at 950 cm^{-1} is due to the asymmetric stretching vibrations of Si-OH groups.[39,41,42,44,45] It can be seen that when the molar ratio of GPTMS in the sample increases, the Si-O-Si stretching vibrations split indicating the presence of hybrid structures.[45]

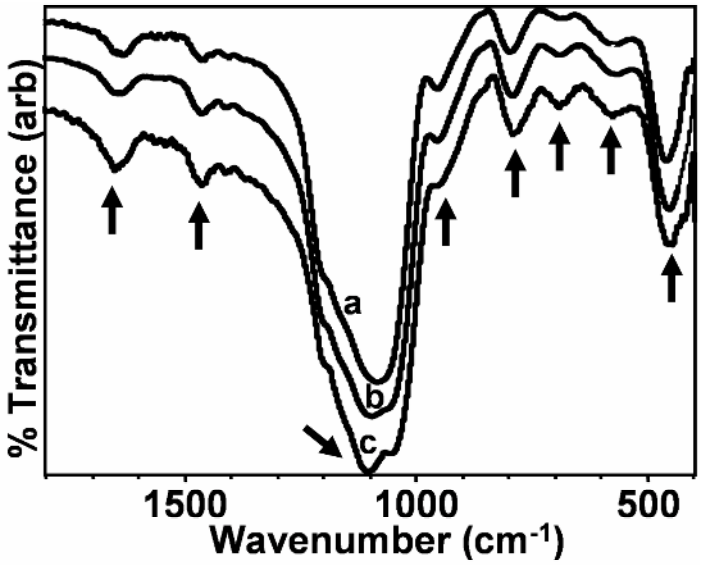

Figure 3.4.: FTIR spectra of samples prepared with a precursor ratio of (a) 2 (b) 1 and (c) 0.5 and water ratio of 0.5 in the region 1800 cm^{-1} to 400 cm^{-1}

The asymmetric C-O-C stretching vibration of the ether linkage in the organic network also absorbs in this region, 1150-1085 cm^{-1}.[40] The absorption due to the Si-OH bond

stretching weakens as the molar ratio of GPTMS increases in the sample. The symmetric Si-O-Si stretching vibrations are visible at 785 cm^{-1}.[41,42,44,45] The O-Si-O stretching vibrations can be observed at 575 cm^{-1} and 455 cm^{-1}.[41,42,44,45] The out of plane bending of the C-O-H group is observed at 687 cm^{-1}.[46] It can be seen that this peak shows a significant increase in intensity when the precursor molar ratio is 0.5. The epoxy ring breathing vibrations appear as sharp absorptions at 1250 cm^{-1} and asymmetric ring stretch around 850 cm^{-1} region.[40] The absence of these bands in the hybrid confirms the complete opening of the epoxy rings. Figure 3.5. presents the FTIR spectra of samples prepared at a precursor ratio of 0.5 and water ratios of 0.5 and 2. There is no significant change in the spectra when the water ratio used for hydrolysis is varied.

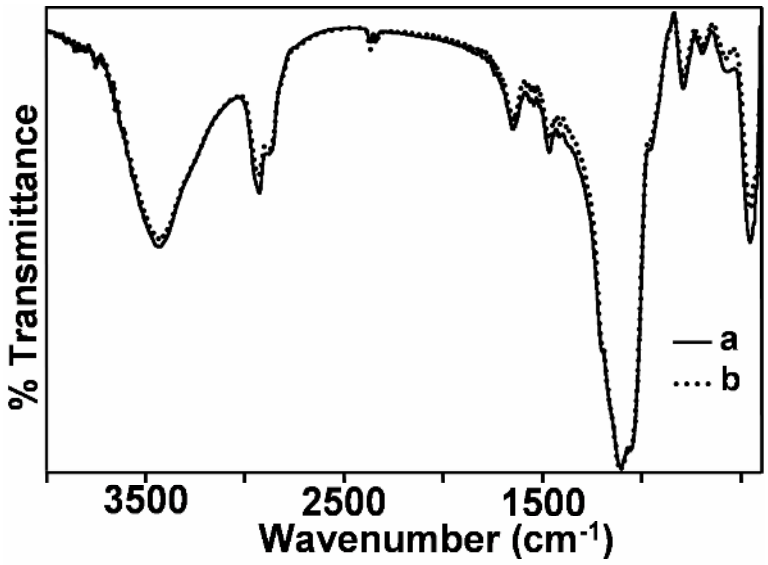

Figure 3.5.: FTIR spectra of samples prepared with a precursor ratio 0.5 and water ratio (a) 2 (b) 0.5

Adsorbed water is a major source of OH vibrations in porous materials. In the investigated systems, the DTA curves (discussed later) do not show the pronounced endotherm near 100 °C usually observed for adsorbed water. Moreover, it can be seen that the hybrid with precursor ratio 0.5 has the lowest surface area for all initial water content and have intensity of hydroxyl stretching frequency considerably higher compared to the 1 and 2 precursor ratio hybrids. This is evidence to the fact that adsorbed

water is not the major contributor to the observed hydroxyl stretching frequency. The epoxy polymerization is initiated by the nucleophilic attack of the catalyst on the epoxy carbon and the nucleophilic oxygen of the epoxide ring attack another epoxy carbon propagating the chain. A hydroxyl group will result when the epoxide ring cleaves and the oxygen takes up a proton instead of attacking another epoxy group leading to the termination of the chain. In presence of proton donors this is a highly probable mechanism of chain termination. This is presented in scheme 3.2. But the increase in hydroxyl absorption is not proportional to the GPTMS concentration. This would mean that the 0.5 molar ratio hybrids are characterized by organic network with shorter chains, more terminated ends. The COH bending vibration at 687 cm^{-1} also show considerable increase in intensity when the precursor ratio changes from 1 to 0.5. The hybrids with precursor ratio 2 and 1 have almost the same intensity for these vibrations supplementing the above discussion.

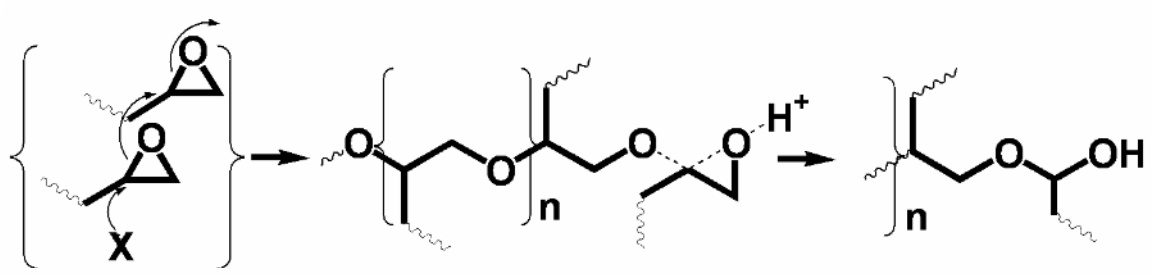

Scheme 3.2.: Termination of epoxy polymerization

Increasing the GPTMS molar ratio to 1, results in the incorporation of the glycidoxypropyl groups into the organic network without much termination or rather linear chains of higher molecular weight are formed. The epoxy ring opening is expected to continue beyond 24 h and this would mean that the epoxy polymerization will continue even after gelation in this case.[47] Hence a TEOS/GPTMS molar ratio of 1 seems to form a gel structure where the glycidoxypropyl groups are ideally placed for the epoxy polymerization to proceed unhindered. Further increase in the concentration of GPTMS

results in a crowding of glycidoxy groups in the pores and together with the constraints imposed by the rigid gel network results in shorter chains.

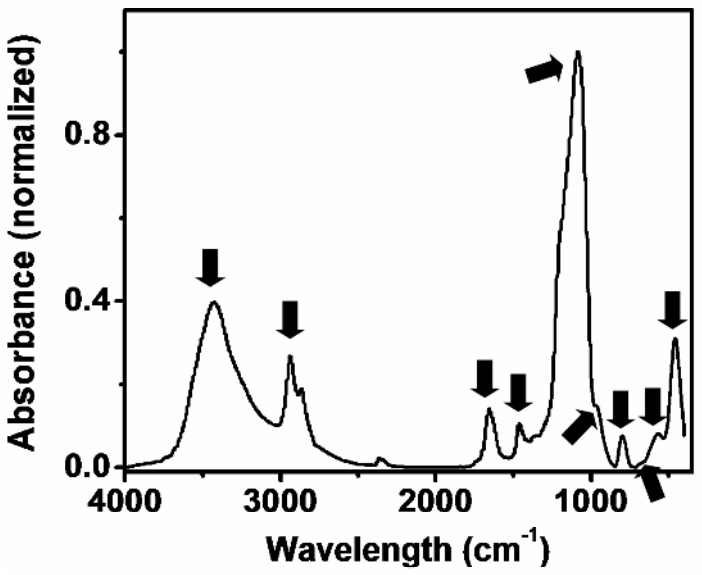

Figure 3.6.: FTIR of sample with precursor ratio 2, water ratio 0.5 and crosslinker ratio 1.5

In order to perform the Fourier Self Deconvolution, the FTIR spectra of the crosslinked samples were taken in the absorbance mode and all FTIR spectra of crosslinked samples are presented in the absorbance scale. The Si-O-Si asymmetric stretch is the most intense of the bands and always has the highest intensity. So all bands were normalized against this band for better comparison. The FTIR spectrum of sample with cross linker ratio 1.5 is shown in the figure 3.6. The spectrum contains peak due to both silica network and alkyl group from cross linker and glycidoxypropyl group. The broad peak observed around 3500 cm^{-1} is due to the stretching vibration of hydroxyl group. The peak around 2850 cm^{-1} corresponds to alkyl (C-H) stretching vibration of GPTMS and DEO. A sharp peak observed at about 1660 cm^{-1} is accounted for the bending vibration of adsorbed water. The alkyl hydrogen bending bands can be observed around 1460 cm^{-1}. The broad and intense band observed around 1090 cm^{-1} contains the fundamental Si-O-Si stretching vibration of the silica network. The C-O-C vibration due

to the ether linkage in the glycidoxypropyl group is also expected in this region. Due to its very low intensity compared to the absorption due to the silica network this peak cannot be identified. The shoulder peak at 962 cm^{-1} is due to the Si-OH stretching vibrations. Another fundamental vibration of the Si-O-Si network is found at 796 cm^{-1}. Absorption at 457 cm^{-1} and 569 cm^{-1} is due to the O-Si-O bonds. The peak at 687 cm^{-1} out of plane bending of the C-O-H group is rather weak to observe in the absorbance scale. From the 4000-3000 cm^{-1} region of the spectra, figure 3.7. we can observe that when the crosslinker ratio increases there is a corresponding increase in the alkyl stretching frequency. Again, this type of behaviour is not observed in the case of hydroxyl stretching frequency. Like in the case of non cross linked samples, the analysis of the OH stretching frequency can provide valuable insights to the nature of the organic network formed at various crosslinker concentrations. In order to give more evidence to the arguments in the case of non crosslinked samples we performed Fourier Self Deconvolution (FSD) on the FTIR spectra of crosslinked samples. The samples were degassed for 4 hours at 150 °C in flowing N_2 atmosphere prior to performing the FTIR measurements. The results are shown in figure 3.8.

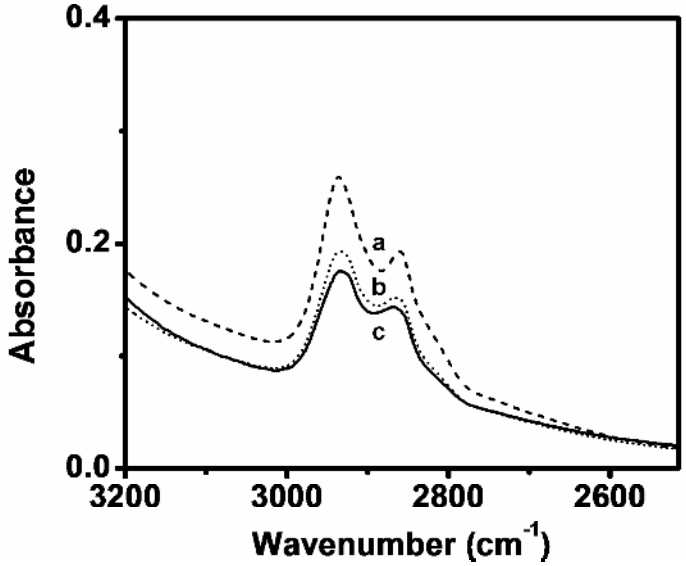

Figure 3.7.: Alkyl hydrogen stretching absorptions of samples with precursor ratio 2, water ratio 0.5 and crosslinker ratio (a) 1.5 (b) 0.5 (c) 0.25

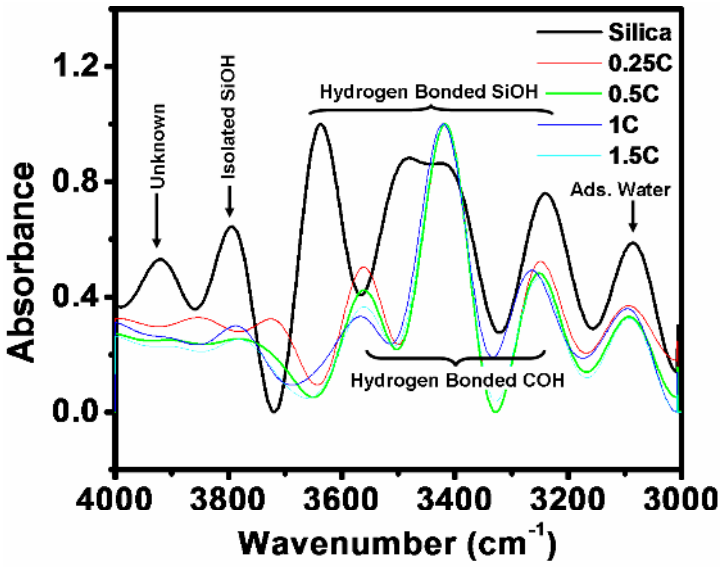

Figure 3.8.: Fourier Self Deconvolution Trace analysis on the 4000-3000 cm^{-1} region of the FTIR spectra of crosslinked samples and silica gel

The most significant contributions to the broad peak corresponding to the OH stretching in the silica sample come from six different peaks. This is in accordance with reported literature and a comprehensive discussion of various silanol groups responsible for these peaks can be seen in the review by Nawrocki.[48] The peak around 3790 cm^{-1} is due to the isolated silanol groups. Three hydrogen bonded silanol species are identified and they appear at 3630, 3450 and 3250 cm^{-1}. The adsorbed water gives rise to the peak at 3080 cm^{-1}. The peak at 3900 cm^{-1} is also due to surface silanols but the exact nature of the silanol groups is still under debate. In the hybrid samples it is evident that the silanol groups have disappeared and new peaks have formed. The silanol peak at 3900 and 3790 cm^{-1} are fingerprints for silanols and appear in the same region for all silica. The absence of these peaks is used as confirmation for the absence of silanol group. Hydrogen bonded COH groups are reported to appear in the 3600-3220 cm^{-1} region as observed in our spectra. So we can conclusively say that the hydroxyl absorption arise from the COH groups formed during the polymerization of the epoxy group in these hybrids. The adsorbed water must have arisen from the KBr used for the preparation of the pellets

since the samples were heat treatment prior to measurements. Even then its contribution is very low to the total hydroxyl peak.

Figure 3.9. shows the spectra of hybrids with different crosslinker ratios in the 4000-3000 cm^{-1} region. From the figure we can see that the intensity of hydroxyl stretching frequency is maximum for the crosslinker ratio 0.25. When the ratio increases to 0.5 the intensity of the hydroxyl stretching decreases, which indicates that the added DEO is incorporated into the organic network and the organic chains become more networked by the addition of DEO. This continues with the addition of DEO up to the molar ratio of 1. But, when the crosslinker ratio increases to 1.5, the intensity of hydroxyl stretching increases. So further increase in DEO no longer results in linear networking and rather a fragmentation of the network occurs. Localized network of polymer chains with lower molecular weight is formed.

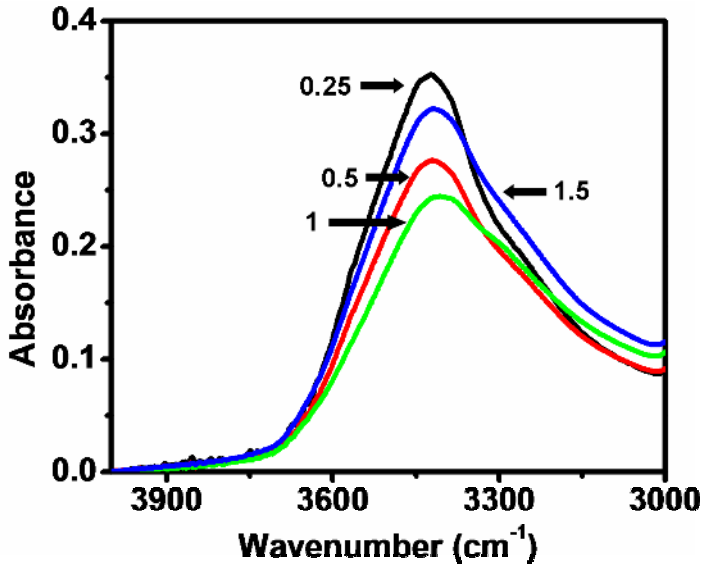

Figure 3.9.: The FTIR spectra of crosslinked samples in the region 4000-3000 cm^{-1}

The differential thermal analysis curves for various samples are provided in figure 3.10. The DTA patterns for the samples are similar and the decomposition of the organic network, observed as an exothermic peak occurs in a broad range from 210 °C to 480 °C. Markedly the endothermic peak usually observed for porous silica close to 100 °C is very

weak for all samples indicating that the amount of adsorbed water in the samples are very small.

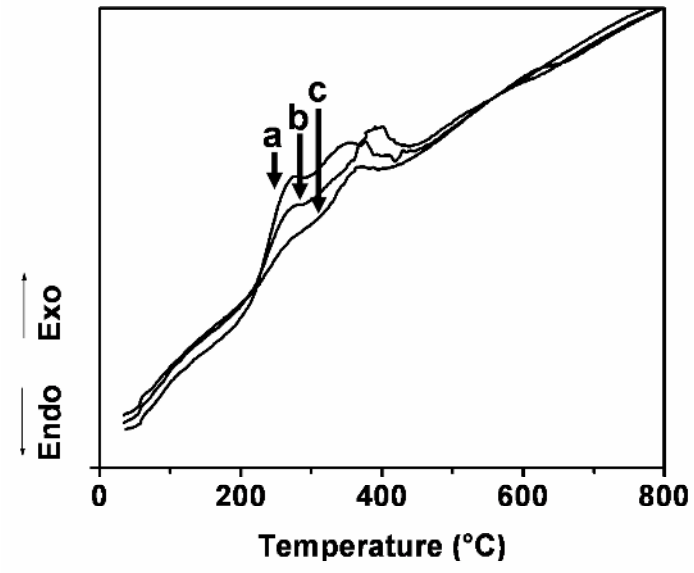

Figure 3.10.: DTA curves of samples prepared with precursor ratio (a) 0.5 (b) 1 and (c) 2 and water ratio of 1

The thermogravimetric analysis of the samples is provided in figure 3.11. The weight loss pattern is similar for all the gels. Initial water content has no influence on the weight loss. TG curve of the hybrids contains a two step weight loss. The smaller first step extending up to 150 °C indicate the removal of volatilities like drying solvent and corresponds to a weight loss of about 6% in all the samples. The extensive organic networking in the samples imparts hydrophobic nature to the gel surface which must have resulted in the gel surface retaining some amount of the drying solvent. The total weight loss depends on the amount of organically modified precursor in the gel. There is no weight loss above 600 °C for all samples.

Based on the following assumptions the weight loss due to the decomposition of the organic network in different hybrids can be calculated.

1) Only SiO_2 is present above 700 °C.
2) The organic network dissociates from the inorganic network by the cleavage of the Si-C bond.

3) The weight loss due to the removal of the organic network occurs only in the second step i.e. above 150 °C.

4) DETA is removed during the thermal decomposition.

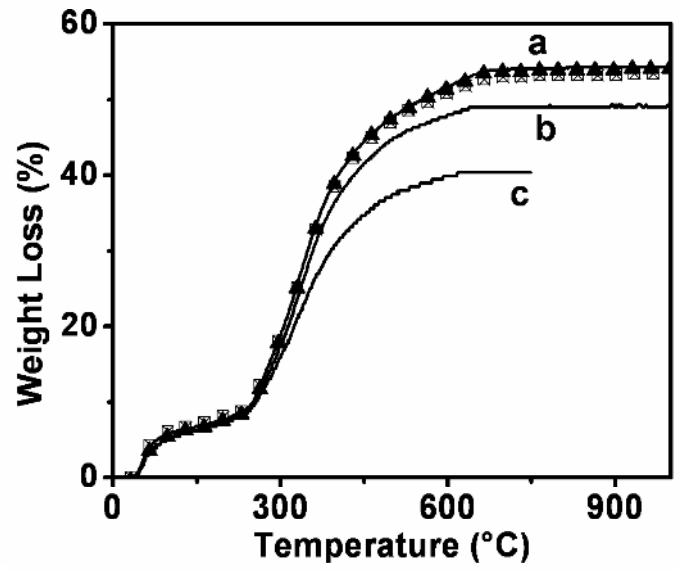

Figure 3.11.: TG curves of samples with precursor ratio (a) 0.5 (b) 1 and (c) 2, water ratio (▲) 0.5,(▁) 1 and (☒) 2

The results obtained are compiled in table 3.1. The calculated weight loss values are higher than the observed weight loss indicating that a part of the organic precursor is excluded from the gel. The difference between the calculated weight loss and the observed weight loss increases as the concentration of GPTMS increases in the hybrid. During aging of the gels in water, the formation of a jelly mass around the gels was observed, which was washed clean before the solvent exchange step. This was observed for all gels prepared. Assuming that the difference in weight loss corresponds to washing off of GPTMS and the corresponding amount of DETA, this would mean that for an initial precursor molar ratio (TEOS/GPTMS) of 2 approximately 75 % and for the ratio of 1, 70 % and for the ratio of 0.5, 65 % of GPTMS gets incorporated in to the gel network.

The DTA patterns of the gels containing the crosslinker are provided as figure 3.12. and contain strong exothermic peak spanning a wide region of 220 – 420 °C, similar to that observed for the gels without the crosslinker. The exotherm becomes more

resolved in higher molar ratio hybrids. Maxima at 260 °C and 400 °C can be distinguished. The endotherm observed for the weight loss around 150 °C is very weak. This clearly indicates that the volatiles contain only low vapour pressure solvents, since they have small heat of vaporisation.

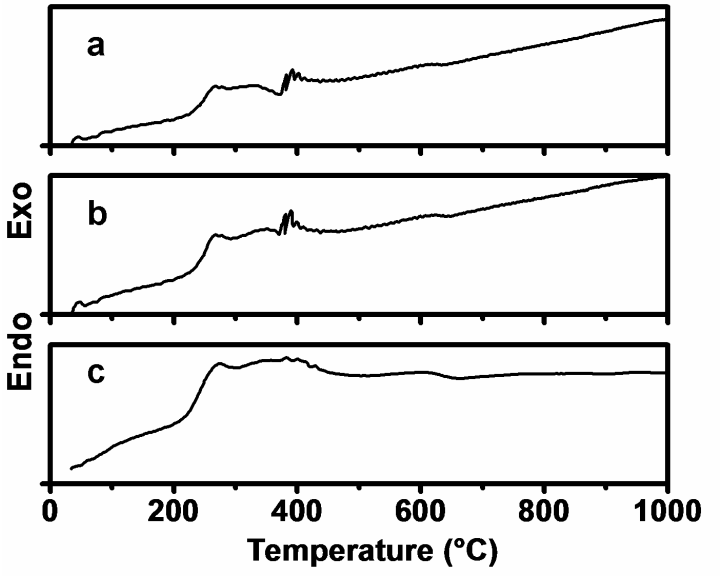

Figure 3.12.: DTA of sample with precursor ratio 2, water ratio 0.5 and crosslinker ratio (a) 1.5 (b) 1 (c) 0.25

Sample	Calculated Weight loss (%)	Observed Weight loss (%)
	Corresponding to removal of Organic network	
2P1W	46.5	34.1
1P1W	59.7	42.9
0.5P1W	72.3	46.4
0.5P2W	73.2	46.9
0.5P0.5W	71.8	46.1

Table 3.1.: Weight loss corresponding to the removal of organic network, observed and calculated from thermo gravimetric curves

Thermal analysis curves obtained for the crosslinked hybrids are given in figure 3.13. The TG patterns are similar to that observed for the samples without crosslinker and has a continuous weight loss up to around 620 °C. There are two distinct regions for the weight loss pattern. A small weight loss up to around 10% can be observed in the temperature regime 50-150°C due to the removal of volatiles like drying solvent. The weight loss from 150 °C to 620 °C is due to the removal of the organic network in the gel. A change in slope can be observed along this weight loss region. This happens above 400 °C and can be an indication of the organic networking being removed in two separate stages.

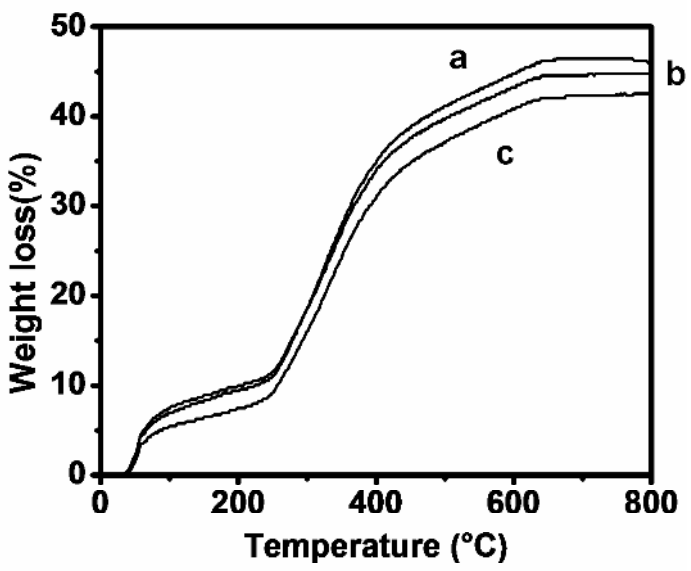

Figure 3.13.: TGA of sample with precursor ratio 2, water ratio 0.5 and crosslinker ratio (a) 1.5 (b) 1 (c) 0.25

The standard bond energy for Si-C bond is 76 $kcalmol^{-1}$, C-C is 83 $kcalmol^{-1}$ and C-O-C is 85.5 $kcalmol^{-1}$.[49] The evidence point to the fact that during thermal decomposition, the organic network breaks off from the inorganic network followed by the decomposition of the organic chains. The smaller fragments of the organic chain containing the ether linkages will decompose at higher temperatures. So during thermal decomposition, initially the organic network separates from the inorganic network and organic network decomposes through the temperature interval.

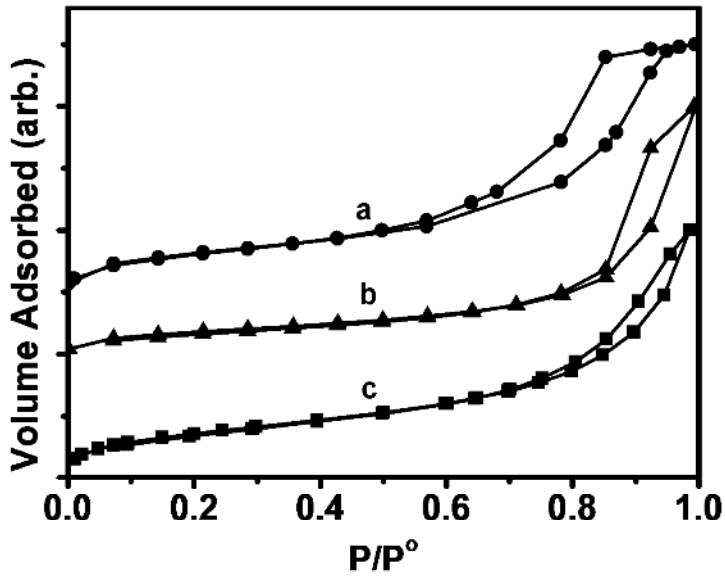

Figure 3.14.: Adsorption isotherms of gels with precursor ratio (a) 0.5 (b) 1 (c) 2 and water ratio 0.5

The adsorption isotherms of the gels prepared with varying precursor ratio at the same water ratio is provided as figure 3.14. The gels are all mesoporous as evident from the hysteresis loop. There is a gradual change in shape of the loop as the precursor ratio decreases. So there is a gradual change in shape of the pores from smooth pores, to necked pores as precursor ratio decreases. The change in water ratio does not change the pore structure of a particular precursor ratio hybrid as can be seen from figure 3.15. So the pore structure, particularly towards the larger radius end of the pore size distribution is strongly influenced by the precursor ratio.

The BET surface area analysis of the samples is provided in table 3.2. The lower surface area values indicate the presence of the organic network on the pore walls of the hybrids. The presence of organic groups on the surface prevents N_2 adsorption, lowering the surface area. The influence of initial water content on surface area is more pronounced for the precursor ratio 2. Similar influence is observed for the pore volume and pore radius. Total pore volume does not differ significantly when the precursor ratios are less than 2. The average pore radii are also close for these hybrids. The hybrids with precursor ratio 2 have C parameter in the range of 60 while other hybrids have the value

close to 50, suggesting that the former has a higher hydrophilic nature due to the lower organic content. The hybrids prepared with the precursor ratio 2 have the larger pore volumes. Higher surface area is obtained when the contribution to pore volume is higher from pores with smaller pore radius. The BJH pore size distribution obtained for the hybrids are given as figure 3.16. The BJH pore size distribution curves show that the distribution stretches to a larger interval when the precursor ratio is 2. The distribution shifts to lower pore sizes when the water content increases. The pore size distribution curves are narrow for the precursor ratio 0.5 and 1 compared to that of 2.

Sample	Specific Surface Area (m^2g^{-1})	C parameter	Total Pore Volume (cm^3g^{-1})	Average pore radius (nm)
2P0.5W	179	63.59	0.7876	8.8
2P1W	251	61.72	0.7154	5.7
2P2W	331	59.78	0.4965	3.0
1P0.5W	268	46.07	0.4288	3.2
1P1W	273	51.74	0.4368	3.2
1P2W	303	47.80	0.4998	3.3
0.5P0.5W	151	50.9	0.2492	3.3
0.5P1W	153	51.91	0.2907	3.8
0.5P2W	169	50.77	0.2788	3.3

Table 3.2.: BET analysis of the hybrid samples

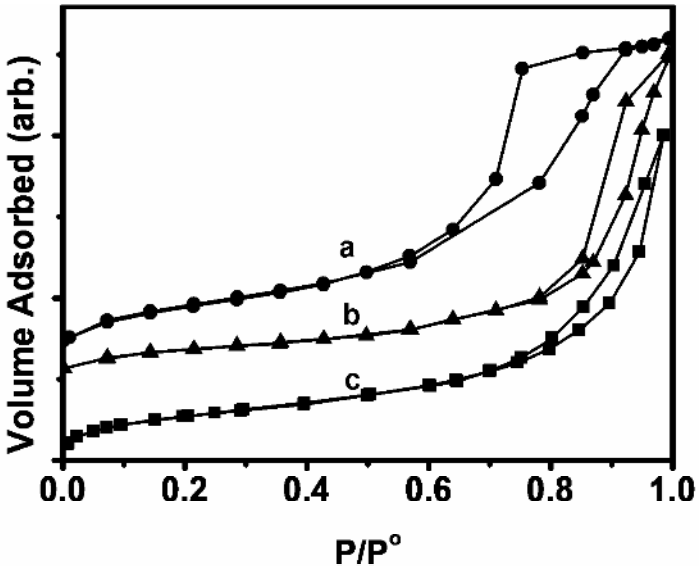

Figure 3.15.: Adsorption isotherms of gels with precursor ratio (a) 0.5 (b) 1 (c) 2 and water ratio 2

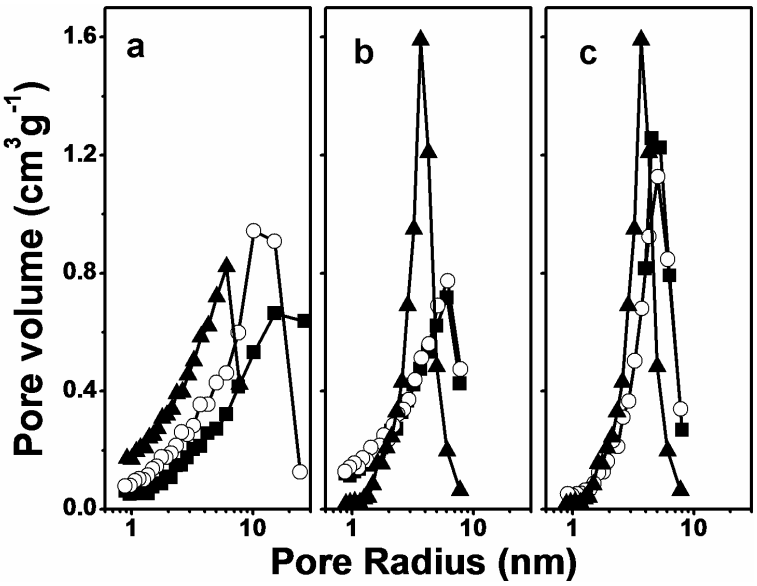

Figure 3.16.: BJH pore size distribution curves (dV/dlogR) of samples with precursor ratio (a) 2 (b) 1 and (c) 0.5 and initial water ratio (■) 0.5 (○) 1 and (▲) 2

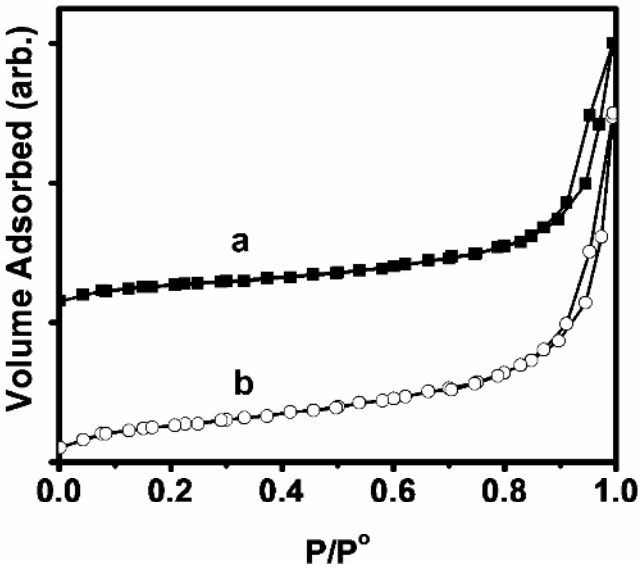

Figure 3.17.: Adsorption isotherms of samples with precursor ratio 2, water ratio 0.5 and crosslinker ratio (a) 1.5 and (b) 0.25

The adsorption isotherms of samples prepared with highest and lowest crosslinker ratio is provided as figure 3.17. The adsorption isotherms are similar to that obtained for the samples prepared at the same precursor ratio (2) and water ratio (0.5), but without crosslinker. So the pores are smooth for the samples with the crosslinker. The pore structure is governed by the organic part which is directly linked to the inorganic network. Further crosslinking of the network does not influence the pore structure. The BET analysis and the total pore volume data obtained for the hybrids are provided as table 3.3. Adding to the above discussion it can be seen that the average pore radius is almost same as the one obtained for the sample with the same precursor ratio and water ratio, but without the crosslinker. The average surface area decreases as the organic content increases in the sample. Total pore volume can also be seen to decrease with the increase in organic content. This is similar to the trend observed for the samples without the crosslinker. But smaller pore volumes are obtained for the hybrid samples without the crosslinker, but with similar organic content, for example (sample with crosslinker ratio 1 and hybrid sample with precursor ratio 1). This would also mean that the organic network in the hybrid without crosslinker is formed close to the inorganic surface, while using a

crosslinker provides a network that is flexible or is rather a loose cover for the inorganic network.

Meador et al, working with supercritically dried epoxy crosslinked aerogels, found that the epoxy crosslinker with a tri-epoxy functionality gives the aerogels with better mechanical strength compared to di-epoxy functionality.[14] From the present results it can be seen that as the organic network becomes closely linked to the inorganic network, then the best results in terms of mechanical strength is achieved. Meador used an amine modified silica surface to crosslink using the epoxy crosslinker. So a trifunctional crosslinker allows three linkages to the inorganic network compared to two in the case of the diepoxy. In the present case, the organic network is intimately bound to the inorganic network, in the absence of crosslinker since every organic chain is anchored to the inorganic network.

Sample	Specific Surface Area (m^2g^{-1})	C parameter	Total Pore Volume (cm^3g^{-1})	Average pore radius (nm)
0.25C	171	57	0.7267	8.5
0.5C	161	51	0.6698	8.3
1.0C	147	46	0.6057	8.2
1.5C	135	43	0.5570	8.2

Table 3.2.: BET analysis of crosslinked samples

Desorption pore size distribution curves obtained for the crosslinked samples are provided as figure 3.18. The identical nature of the distribution to that obtained for the samples with the same precursor ratio and water ratio is evident. The distributions span similar regions. There is a slight decrease in distribution towards larger pore radii compared to their non crosslinked counterparts. The distribution is similar for all crosslinker ratios and the difference is in the volume. The volume decreases with the increasing crosslinker.

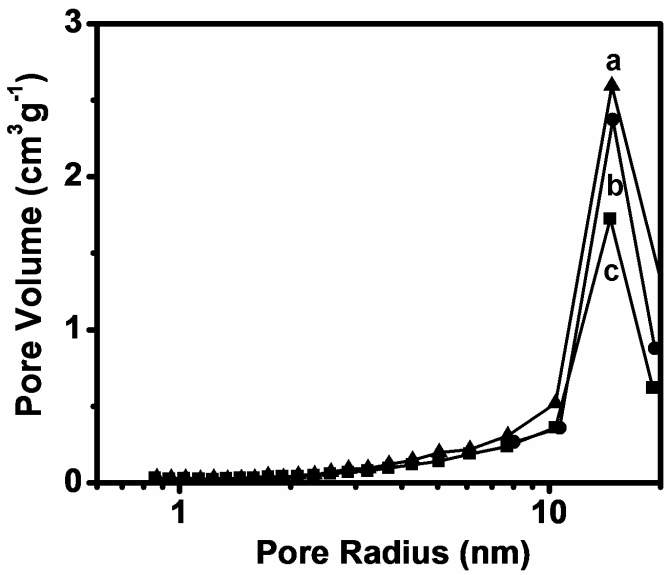

Figure 3.16.: BJH pore size distribution curves (dV/dlogR)of samples with precursor ratio 2, water ratio 0.5 and crosslinker ratio (a) 0.5 (b) 1 and (c)1.5

Bulk density of the samples without crosslinker is plotted against the initial water content in figure 3.17. The bulk density of the samples relies heavily on the proportion of the organic content. When the molar ratio of GPTMS increases in the sample there is a corresponding increase in the bulk density. While the samples prepared with a TEOS:GPTMS molar ratio of 2:1 have density in the range 0.3 to 0.4, it is between 0.5 to 0.6 when the ratio is 1:1 and the density is between 0.7 and 0.8 when the ratio becomes 1:2. On the other hand when the initial water content increases, density of the dry gel also increases. But the effect of water content on the density is very less compared to the precursor ratio. The density calculated for the gels prepared without crosslinker and that actually measured from the dimensions of the dry gel is provided as table 3.3. Two immediate observations can be made. When the precursor content increases the calculated density increases. But when water content increases the calculated density decreases. The increase in density with water content can then be due to an increased shrinkage arising from the low density of the network.

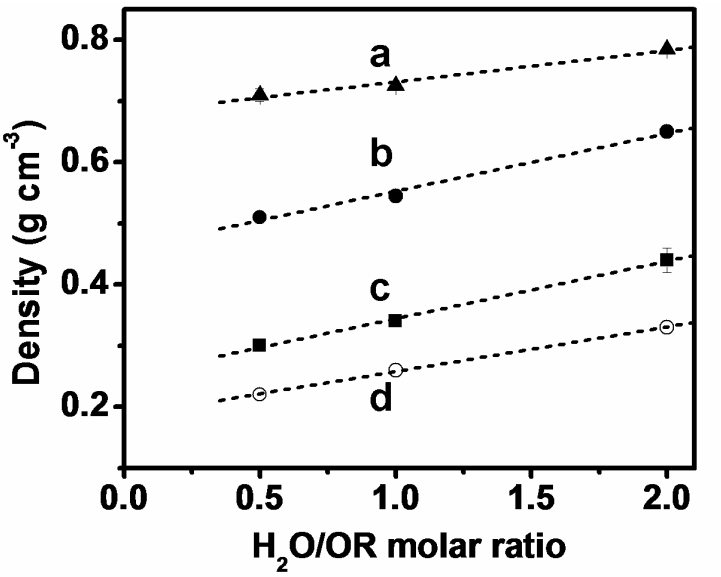

Figure 3.17.: Bulk density of samples with precursor ratio (a) 0.5 (b) 1 (c) 2 and (d) 3 plotted against initial water ratio

Sample	ρ (Calc.)	ρ (Obs.)
p3r.5c0	0.168	0.22
p2r.5c0	0.188	0.3
p1r.5c0	0.227	0.52
p3r1c0	0.158	0.22
p2r1c0	0.177	0.34
p1r1c0	0.215	0.56
p3r2c0	0.142	0.33
p2r2c0	0.16	0.49
p1r2c0	0.195	0.6

Table 3.3.: Density of samples without crosslinking agent

In order to verify this, a series of gels were prepared with varying calculated density keeping the water ratio and precursor ratio constant.[38] The values are provided in table 3.4.

Sample	ρ (calc.)	ρ (Obs.)
p2r.5c0d.16	0.16	0.29
p2r.5c0d.18	0.188	0.3
p2r.5c0d.2	0.2	0.31
p2r.5c0d.25	0.25	0.39

Table 3.4.: Density of samples by varying the target density without crosslinking agent

The observed density of the gels increases with the target density. So, increasing the target density cannot make a difference in ambient pressure drying. The effect of increasing wet gel density on shrinkage during drying is too small compared to the increased weight acquired due to the added solid content. So the dry gel density is rather determined by the chemical nature of the gel structure. So the increase in density in the case of increasing water content must then be due to some other factor that has been over looked.

Similar tabulation has been done for samples with the crosslinker and is provided as table 3.5.

Sample	ρ (calc.)	ρ (Obs.)
p2r.5c.25	0.188	0.33
p2r.5c.5	0.188	0.36
p2r.5c1	0.188	0.41
p2r.5c1.5	0.188	0.47
p2r1c.25	0.188	0.38
p2r1c.5	0.188	0.4

Table 3.5.: Density of samples prepared with varying crosslinker ratio and water content

The target density of all gels prepared with varying crosslinker ratio was fixed to the same value. The effect is obvious; increasing organic networking increases the density. Increasing the organic network need not improve the response of the gels to drying shrinkage. Meador et al has observed a similar surface saturation effect, where

they found that the maximum strength of the network was not obtained at the maximum density or at the maximum concentration of amine groups, used to anchor the organic network to the inorganic network.[14]

The acid catalyzed hydrolysis of silicon alkoxides has a first order dependence on the concentration of water. So increase in concentration of water increases the rate of hydrolysis. Under acidic conditions the hydrolysis of silicon alkoxides proceeds through the protonation of the alkoxide group in a fast step followed by an S_N2 attack of water opposite to the leaving group. This leaves the Si atom in a pentacoordinated configuration in the transition state. The bulky glycidoxypropylgroup will destabilize the penta coordinated transition state due to steric repulsion, reducing the hydrolysis rate of GPTMS compared to that of TEOS. The condensation mechanism operative at pH above the isoelectric point involves the attack of an anionic silanolate species on a neutral silanol species. The acidity of the silanol species depends on the groups attached to the Si atom. Electron donating groups like GPTMS, decrease the acidity of the silanol while electron withdrawing groups like O-Si increase the acidity. So the more condensed species will be more acidic and condensation will proceed through the addition of less condensed or monomeric species to the more condensed clusters. More over the intermediate formed during the condensation reaction is a penta or hexa coordinated species and steric factors can limit the condensation rates of silane molecules.[50] Hence GPTMS should undergo condensation at a slower rate than TEOS. This would mean that the siloxane network will be mostly contributed by the TEOS derived particles and GPTMS will condense on to the network at a much slower rate. Husing arrived at similar conclusions for base catalysed hydrolysis-condensation of mixed precursor systems containing TEOS and various monoalkyl substituted silanes including GPTMS, for a water ratio of 1.[38]

The addition of DETA for the polymerization of epoxy group also catalyzes the inorganic condensation by increasing the pH of the solution. The faster gelation observed, even for hybrids with high GPTMS content is due to the dual role played by DETA. The relative concentrations of Q3/Q4 Si species would have given conclusive evidence to the

variation in networking with the varying precursor ratio, but we were not able to perform Si CP-MAS NMR spectroscopy for this work.

The influence of the organic networking on the gel structure is reflected on the variation of density with the organic precursor content; where as the influence of the inorganic networking on the structure is reflected on the variation of density with initial water content. Increasing the amount of initial water increases the hydrolysis rates facilitating the concentration of silanol groups as soon as the reaction commence. This in turn will increase the condensation rate and considerable condensation would have occurred by the time DETA is added. This will result in a precursor gel with a highly condensed inorganic network. When the precursor ratio is 2 the organic networking strengthens the gel network to withstand the drying stress, decreasing shrinkage and density of the dried gel.

The organic precursor has three alkoxy groups compared to four in the inorganic precursor. Hence the inorganic networking ability has to be sacrificed for the organic networking when the proportion of the organic precursor increases. The inorganic network ends in the direction in which the organic group is oriented when the organic precursor becomes part of the inorganic network. As the ratio of the organic precursor increases, this results in the weakening of the inorganic network, due to the frequent terminations of the network at the organic precursor. When the GPTMS content increases, the inorganic networking decreases due to its lower networking ability compared to TEOS, increasing shrinkage and the density of the dried gel.

The BET analysis provides information on the influence of the processing parameters on the pore structure of the gels. The average pore diameter obtained for the various hybrids shifts to lower values when the GPTMS content increases. Porosity in aerogel like porous materials resides in two places. The smaller pores are formed between primary particles and larger ones between secondary particles. Primary particles are the result of the initial condensation reactions where by clusters are formed. Due to the lower hydrolysis condensation rates of the GPTMS precursor there is only a very small probability for the presence of the glycidoxypropyl group within the initially formed

clusters. The contribution to the smaller pore sizes come from within these clusters. This is represented in scheme 3.3.

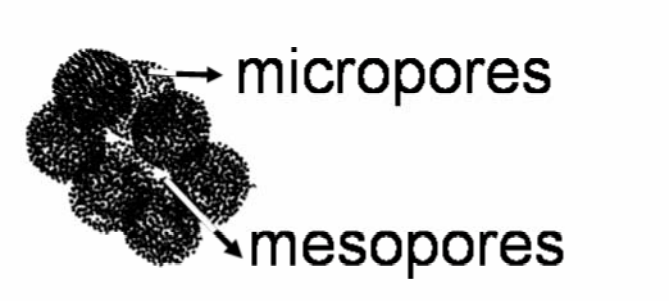

Scheme 3.3.: Porosity in aerogels

The glycidoxypropyl groups condense on to these initially formed clusters and strongly influence the secondary structure. As the proportion of GPTMS increases, the inorganic network between secondary particles reduces and the structure easily shrinks, reducing porosity between them. This in turn decreases the volume of the larger pores and primarily results in the shifting of the average pore radius to the lower region. The initial water content has a much larger influence on the pore structure for the precursor ratio 2 due to the larger proportion of the TEOS precursor. The higher water content results in a more condensed gel network resulting in lower pore volume. Since the hydrolysis rates of GPTMS are low compared to that of TEOS, the TEOS molecules will have a much higher ratio of water available for their hydrolysis than what the H_2O/OR ratio indicates. So, for a lower precursor ratio, a water content of 0.5 represents an excess of water for the hydrolysis of TEOS and this is also the reason for the insensitivity of the average pore radii towards the variation in water ratio for these hybrids. The narrow pore size distribution curves obtained for the precursor ratio 0.5 and 1 are indicative of the effects of the reducing contribution from larger pores mainly formed between secondary particles. On the other hand the added crosslinker seem to have an effect comparable to increasing precursor ratio but at a much lower magnitude.

The skeletal densities of the samples prepared, measured using He pycnometry is provided in table 3.6. The skeletal density data of samples varies in the range of 1.6 to 2.2 g cm^{-3} and is in the range observed for aerogels. The data shows that as organic precursor

content increases skeletal density decreases. As water ratio for hydrolysis increases the skeletal density also increases.

samples	$\rho_{skel.}$	sample	$\rho_{skel.}$
p3r.5c0	1.8	p2r.5c.25	2.2
p2r.5c0	1.8	p2r.5c.5	1.9
p1r.5c0	1.6	p2r.5c1	2.1
p3r1c0	1.8	p2r.5c1.5	1.9
p2r1c0	1.7	p2r1c.25	1.8
p1r1c0	1.6	p2r1c.5	1.7
p3r2c0	2.2		
p2r2c0	2.1		
p1r2c0	1.9		

Table 3.6.: Skeletal density of samples

It has been observed that the presence of lower density chemical species like methoxy groups lower the skeletal density of aerogel than that of dense silica.[51,52] So the increasing precursor ratio increases the organic groups which in turn decrease the skeletal density. Increase in water content increases the degree of condensation of the inorganic network. Consequently the skeletal density also increases.

The TEM images of hybrids prepared with the precursor ratio 2 and water ratios 0.5 and 2 are provided as figure 3.18. The largely condensed nature of the hybrid with higher water content is visible. TEM micrograph of the hybrid with lower water content, at a higher magnification is provided as figure 3.19. The aerogel like networked structure can be seen in this image.[53] Hybrids with higher organic content were unstable under the operating voltage.

The TEM images of samples with crosslinker ratio 0.5 and 1.5 are presented as figure 3.20. On the right is the corresponding high resolution image. The SAED pattern shows that the material is highly amorphous. The high resolution image shows the

networked structure of the material. The denser nature of the sample with increase in concentration of the organic crosslinker can be seen in the image.

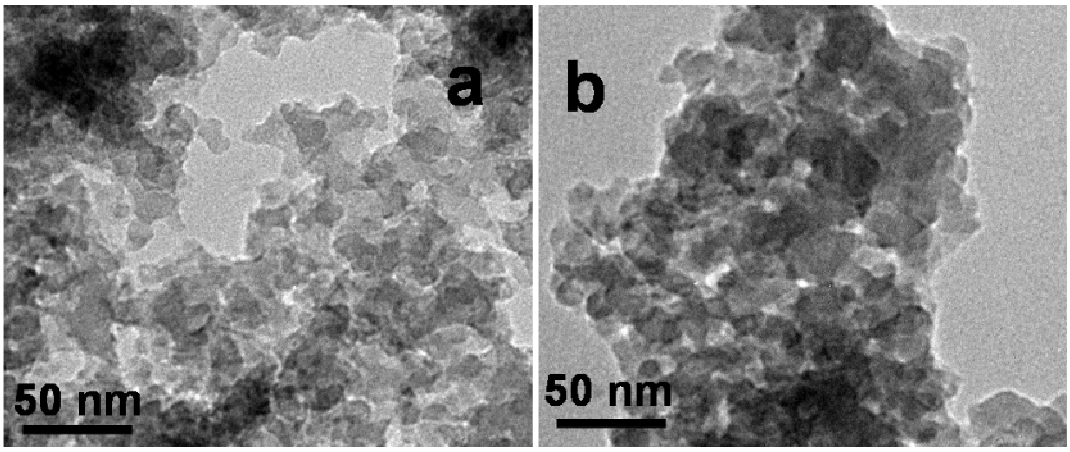

Figure 3.18.: TEM of samples with precursor ratio 2 and water ratio (a) 0.5 and (b) 1

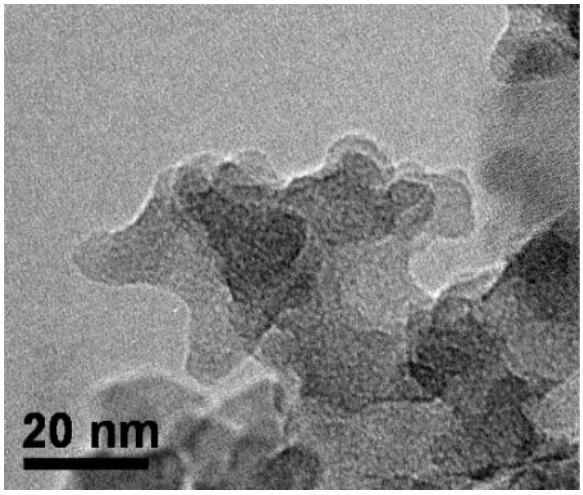

Figure 3.19.: TEM of sample with precursor ratio 2 and water ratio 0.5 at a higher magnification

The dielectric properties of the hybrid networks were investigated for two main reasons. Even though dielectric response of aerogels has been reported, there are only a few reports on the dielectric response of subcritically dried aerogels. The dielectric property, unlike thermal conductivity is dependent on the nature of the solid network forming the porous network. So the dielectric response of subcritically dried aerogels

needs to be recorded to establish the nature of the gels formed at ambient pressure. On the other hand this will also be a test to the hybrids prepared, to stand up to the performance of supercritially dried aerogels.

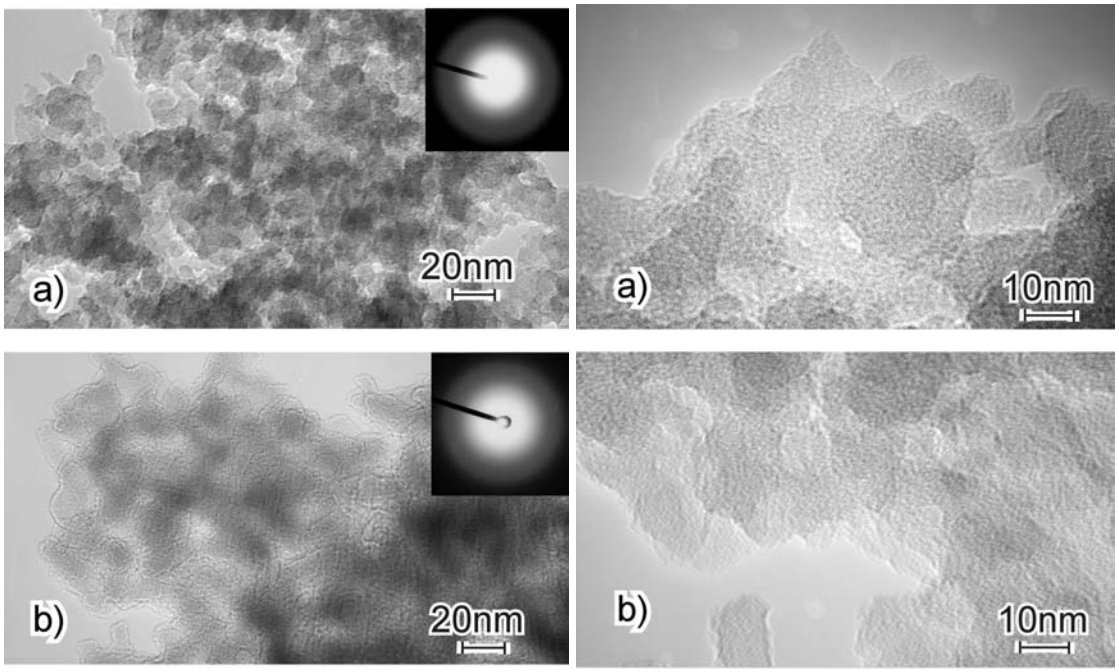

Figure 3.20: TEM image of samples with crosslinker ratio a) 0.5 b) 1.5

The dielectric properties of aerogels are mostly determined by the gases present inside the pores. The dielectric constants observed for aerogels are lower than that of amorphous fused silica (~3.8) and higher than that of air (1).[54] Initial attempts to measure the dielectric constant of silica aerogels were made by da Silva et al and they treated the aerogel as a bicomponent system with air as one component and silica as the other.[55] They calculated the dielectric constant of the bi component system from the Looyenga's equation given as $\varepsilon'_{Gel} = [\varepsilon_2^{1/3} + (1-P)(\varepsilon_1^{1/3} - \varepsilon_2^{1/3})]^3$. ε_1 and ε_2 are the dielectric constants of silica and air respectively and P the porosity. The dielectric response was measured in the lower frequency region from 50-10^5 Hz and they obtained dielectric constants less than 2. They could correlate the observed response to the bi component

system where the dielectric constant of silica had a higher value of 7. This value was reported by Chandrashekar et al and was attributed to the presence of carbon.[56]

A more comprehensive approach was made by Hrubesh and he measured the dielectric response of aerogels in the GHz region which was more required for the microelectronics industry.[54] In this approach the dielectric property of aerogels is considered from the perspective that since the gas inside the pores is largely responsible for the low dielectric property of aerogels, their dielectric properties should also be gas like rather than solid like. The dielectric constant of a gas is linearly dependent on the density and is given by the Clausius- Mosotti equation. $\varepsilon = 1 + (N_0\alpha / M\varepsilon_0)\rho$ Where ε is the dielectric constant, N_0 is the Avogadro number, α is the polarizability of the gas, M is the molecular mass, ε_0 is the permittivity of free space and ρ is the density.

In the case of aerogels the density refers to the bulk density of the aerogel. On a physical sense, the slope $(N_0\alpha/M\varepsilon_0)$ can be considered as the dielectric constant per bulk density. When the bulk density is zero i.e. in the absence of the solid network we will get the dielectric constant of air. Hrubesh could obtained slopes for various aerogels and found that it varied with the composition of the aerogel. For silica aerogel the value obtained was 1.6×10^{-3} and for organic aerogel, 1.75×10^{-3} (for resorcinol-formaldehyde) and 1.83×10^{-3} (for melamine formaldehyde) when dielectric constant was plotted against density in kgm^{-3}. He found that the contribution to the dielectric constant from adsorbed water correspond to about 7%.

The dielectric constants obtained for hybrid gels at 2MHz is plotted against density of the gels, in Kgm^{-3} in figure 3.21. The dielectric loss factors obtained for the gels were in the range 0.02-0.08. Three distinct dielectric responses can be seen. In the initial region at low densities the dielectric response increases with temperature. In the second region the dielectric constant is rather less dependent on density. Final region is distinguished by high sensitivity of dielectric constant on density.

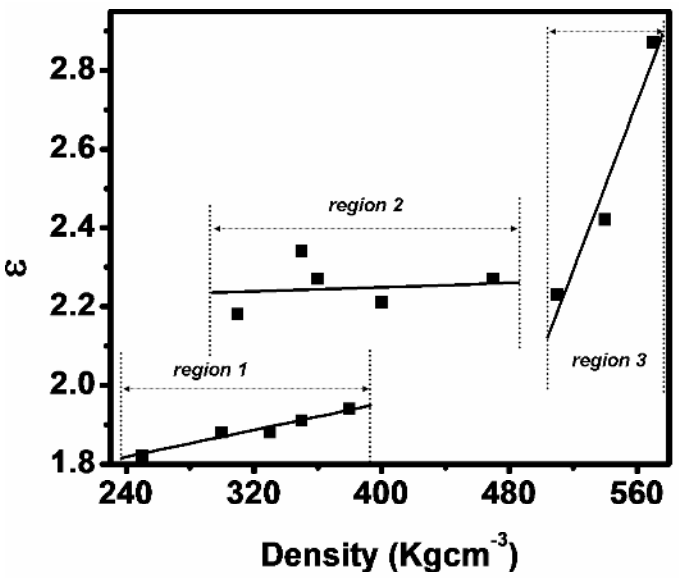

Figure 3.21: Dielectric response of hybrids

In the first region it can be seen that the density is linearly dependent on the density and a straight line fit is given by the equation, $\varepsilon = 1.6+0.0009\ \rho$. The values are close to the values obtained by Hrubesh for silica aerogels. But we have a value of 1.6 for the dielectric constant of air which is rather high. But if we look at the processing sequence of our gels we can very well see that the dielectric constant of the drying solvent, hexane has a dielectric constant of 1.8. Hence this unexpected value of dielectric constant of air must be due to the contribution of hexane. As we had seen in the thermogravimetric curve there is some presence of hexane in the gels due to its retention by the organic network. Then the lower value of 1.6 must be due to the fact that the adsorbed hexane can no longer be considered as a liquid and is in dynamic equilibrium with its vapour phase in the pores. In order to test this hypothesis, the gels were calcined at a temperature of 200 °C. In presence of air the calcinations led to shrinkage and charring of the gels. So a gel was calcined in flowing Ar atmosphere at 200 °C for 2 hours. The dielectric constant was then measured and we obtained a value of 1.43 for the gel with density 0.22 gcm^{-3}. It can be seen that this value is related to the density as $\varepsilon = 1+0.00195\rho$. We did not have the set up to calcine all the gels in Ar atmosphere and in

the absence of the inert atmosphere the gels showed large shrinkage. So we could not perform the measurements on all gels.

We tried to calculate the value of the dielectric constant of our gels from the Looyenga's equation. Dielectric constant of silica was chosen as 3.8 and that of air was taken as 1.6. Porosity of the hybrids was calculated as $P = \frac{\rho_{Skel.} - \rho_{Bulk}}{\rho_{Skel.}}$, skeletal densities were obtained from pycnometry and bulk densities were measured. The obtained results are provided in figure 3.22. It can be seen that the obtained dielectric constants are close to the values obtained from the Looyenga's equation. The dielectric constants obtained, if the dielectric constant of air was taken as 1, is also provided in the figure. Hence the modification of the dielectric constant of the hybrid aerogels is due to the hexane adsorbed on to the pore walls.

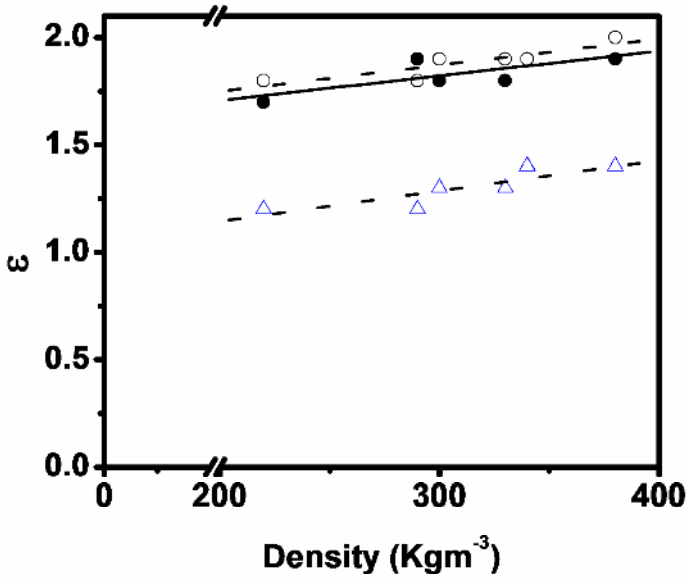

Figure 3.22: Plot of dielectric constant against density where the dashed line indicates fit to theoretical (Looyenga's equation) data (open circle) using the dielectric constant 1.6 for air, continuous line indicate fit to observed data(solid circles) and triangle indicates fit to theoretical data with dielectric constant of air =1.

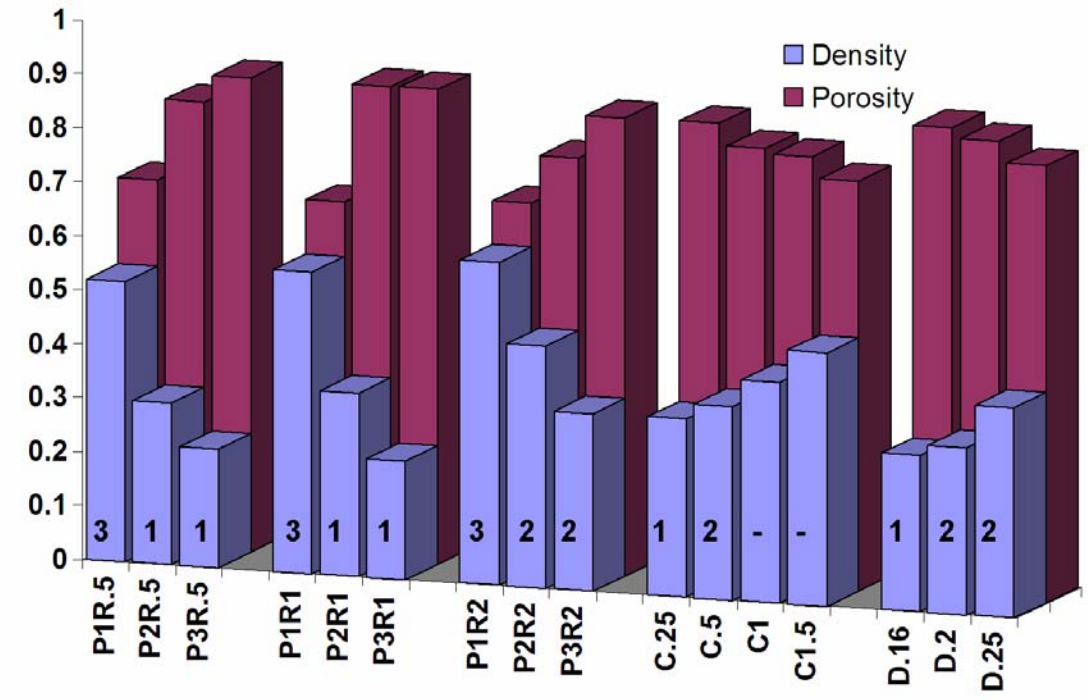

Figure 3.22: The density (cm^3g^{-1}) and porosity plot of various precursors. The numbers on the plot indicate the region (1, 2 or 3) where the dielectric constant of the sample is observed.

It can be seen that many samples falling in the second region have densities same as that observed for samples in region 1. The porosity and density are plotted for different samples in figure 3.22. Here it can be seen that the porosity of most of the samples, which show dielectric response in the region 2 have porosities close to 80% which is expected for aerogels. So the observed values were tried to fit using the Looyenga's equation. The closest values were obtained when the value of ε_1 was 1.8 and ε_2 was 3.8. The value of 1.8 is the dielectric constant of liquid hexane. So the values may be shifted due to the higher hexane content in the samples. But the probability of such a situation is perplexing since all pellets were heated at 100 °C for 24 hours prior to electroding the samples. So the probability of excess concentration of hexane is doubtful. Also it can be seen that the sample with precursor ratio 2 prepared with the water ratio 2 lies in the second region that prepared with a water ratio 1 falls in the region 1. One would have expected that the excess water used in the preparation must have reduced the adsorption of hexane even

when aging treatments are performed. Also, in the case of samples prepared with same precursor ratio but different target densities, as the target density increases the dielectric response move into the region 2. More studies are required to clearly identify the reason for this difference in behaviour. In the region 3 the dielectric constant increases steeply with increase in bulk density. Here the dielectric response has more xerogel character and can be assumed from the lower porosity obtained for these samples. Samples prepared from precursor ratio 1 fall in this region.

The variation of dielectric constant of different gels prepared with temperature is given in figure 3.23. There is little effect on increasing temperature on the dielectric constant till 90 °C. Aerogels have also been seen to show such invariant behaviour to temperature.[54]

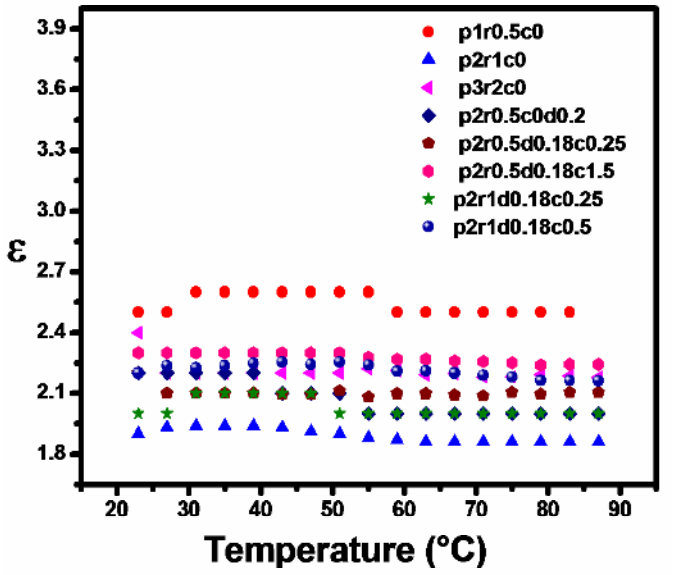

Figure 3.23: The variation of dielectric constant with temperature for various samples (given in the legend). P is the precursor ratio, C the crosslinker ratio, R the water ratio and d the target density)

Conclusion

This study has shown that organic inorganic hybrid networks can be successfully dried by the ambient pressure drying technique involving aging and solvent exchange to

produce aerogels. The technique provides highly porous gels >70% porosity in almost all compositions studied. But aerogels are obtained when gels are prepared with a precursor (TEOS/GPTMS) ratio >1. Higher precursor ratios give xerogels. Ratio of organic network to the inorganic network is the predominant factor that affects the density of the final gel and hence the aerogel properties. Water ratio used for condensation has only a secondary effect.

The porosity features are also largely dependent on the extent and nature of the organic network. As the ratio of organic networking decreases there is a larger influence of water ratio on the nature of porosity formed. The organic networking influences the secondary structure of the aerogel network, and increasing the precursor ratio decreases the volume of the pores between secondary particles.

The nature of the organic network formed from the crosslinking is also strongly dependent on the concentration of the organic precursor, be it modified silane or the crosslinker. As the concentration of the organic precursor increases the length of the organic network increases initially, i.e. longer polymer chains are formed and beyond a certain point 1 for the precursor and crosslinker ratio the polymer network is composed of shorter chains or has more terminated ends.

The organic network anchored to the inorganic network is more efficient in reinforcing the inorganic network compared to the loosely bound organic network formed from the use of crosslinker.

The dielectric response of the ambient pressure dried aerogels are similar to superciritically dried ones. But there are gels with high porosity ~80% which shows dielectric response higher than that expected for aerogels even when the porosity features are similar to that of aerogels.

Finally, a subtle balance between the organic part and inorganic part of the network is required to obtain aerogels through ambient pressure drying. The organic network cannot be a substitute for inorganic network and only at symbiotic proportions will the networks resist drying shrinkage.

References

1. Haereid, S.; Dahle, M.; Lima, S.; Einarsrud, M.-A., *Journal of Non-Crystalline Solids*, 186 (1995) 96.

2. Smitha, S.; Shajesh, P.; Aravind, P. R.; Kumar, S. R.; Pillai, P. K.; Warrier, K. G. K., *Microporous and Mesoporous Materials*, 91 (2006) 286.

3. Smitha, S.; Shajesh, P.; Kumar, S. R.; Krishna Pillai, P.; Warrier, K. G. K., *Journal of Porous Materials*, 14 (2007) 1.

4. Prakash, S. S.; Brinker, C. J.; Hurd, A. J.; Rao, S. M., *Nature*, 374 (1995) 439.

5. Hwang, S.-W.; Jung, H.-H.; Hyun, S.-H.; Ahn, Y.-S., *Journal of Sol-Gel Science and Technology*, 41 (2007) 139.

6. Kanamori, K.; Aizawa, M.; Nakanishi, K.; Hanada, T., *Advanced Materials*, 19 (2007) 1589.

7. Kanamori, K.; Aizawa, M.; Nakanishi, K.; Hanada, T., *Journal of Sol Gel Science and Technology*, 48 (2008) 172.

8. Rao, V. A.; Bhagat, S. D.; Hirashima, H.; Pajonk, G. M., *Journal of Colloid and Interface Science*, 300 (2006) 279.

9. Novak, B. M.; Auerbach, D.; Verrier, C., *Chemistry of Materials*, 6 (1994) 282.

10. Leventis, N.; Sotiriou-Leventis, C.; Zhang, G.; Rawashdeh, A.-M. M., *Nano Letters*, 2 (2002) 957.

11. Zhang, G.; Dass, A.; Rawashdeh, A.-M. M.; Thomas, J.; Counsil, J. A.; Sotiriou-Leventis, C.; Fabrizio, E. F.; Ilhan, F.; Vassilaras, P.; Scheiman, D. A.; McCorkle, L.; Palczer, A.; Johnston, J. C.; Meador, M. A.; Leventis, N., *Journal of Non-Crystalline Solids*, 350 (2004) 152.

12. Katti, A.; Shimpi, N.; Roy, S.; Lu, H.; Fabrizio, E. F.; Dass, A.; Capadona, L. A.; Leventis, N., *Chemistry of Materials*, 18 (2006) 285.

13. Meador, M. A. B.; Capadona, L. A.; McCorkle, L.; Papadopoulos, D. S.; Leventis, N., *Chemistry of Materials*, 19 (2007) 2247.

14. Meador, M. A. B.; Fabrizio, E. F.; Ilhan, F.; Dass, A.; Zhang, G.; Vassilaras, P.; Johnston, J. C.; Leventis, N., *Chemistry of Materials*, 17 (2005) 1085.

15. Leventis, N.; Palczer, A.; McCorkle, L.; Zhang, G.; Sotiriou-Leventis, C., *Journal of Sol-Gel Science and Technology*, 35 (2005) 99–105.

16. Nguyen, B. N.; Meador, M. A. B.; Tousley, M. E.; Shonkwiler, B.; McCorkle, L.; Scheiman, D. A.; Palczer, A., *Applied Materials and Interfaces*, 1 (2009) 621.

17. de Buyl, F.; Kretschmer, A., *Journal of Adhesion*, 84 (2008) 125.

18. Sforça, M. L.; Yoshida, I. V. P.; Nunes, S. P., *Journal of Membrane Science*, 159 (1999) 197.

19. Popall, M.; Durand, H., *Electrochimica Acta*, 37 (1992) 1593.

20. Sorek, Y.; Zevin, M.; Reisfeld, R.; Hurvits, T.; Ruschin, S., *Chemistry of Materials*, 9 (1997) 670.

21. Sorek, Y.; Reisfeld, R.; Finkelstein, I.; Ruschin, S., *Applied Physics Letters*, 63 (1993) 3256.

22. Sorek, Y.; Reisfeld, R.; Tenne, R., *Chemical Physics Letters*, 227 (1994) 235.

23. Signorini, R.; Meneghetti, M.; Bozio, R.; Maggini, M.; Scorrano, G.; Prato, M.; Brusatin, G.; Innocenzi, P.; Guglielmi, M., *Carbon*, 38 (2000) 1653.

24. Abbotto, A.; Bozio, R.; Brusatin, G.; Facchetti, A.; Guglielmi, M.; Innocenzi, P.; Meneghetti, M.; Pagani, G. A.; Signorini, R., *SPIE*, 3803 (1999) 18.

25. Casalboni, M.; De Matteis, F.; Prosposito, P.; Pizzoferrato, R., *Applied Physics Letters*, 75 (1999) 2172.

26. Tadanaga, K.; Yoshida, H.; Matsuda, A.; Minami, T.; Tatsumisago, M., *Electrochemistry*, 70 (2002) 998.

27. Tadanaga, K.; Yoshida, H.; Matsuda, A.; Minami, T.; Tatsumisago, M., *Chemistry of Materials*, 15 (2003) 1910.

28. Kasemann, R.; Bruck, S.; Schmidt, H., *SPIE*, 2288 (1994) 321.

29. Popall, M.; Durand, H., *Electrochimica Acta*, 37 (1992) 1593.

30. Schmidt, H., *Journal of Non-Crystalline Solids*, 178 (1994) 302.

31. Riegel, B.; Blittersdorf, S.; Kiefer, W.; Hofacker, S.; Muller, M.; Schottner, G., *Journal of Non-Crystalline Solids*, 226 (1998) 76.

32. Hoebbel, D.; Nacken, M.; Schmidt, H., *Journal of Sol Gel Science and Technology*, 12 (1998) 169.

33. Templin, M.; Wiesner, U.; Spiess, H. W., *Advanced Materials*, 9 (1997) 814.

34. Brusatin, G.; Innocenzi, P.; Guglielmi, M.; Bozio, R.; Meneghetti, M.; Signorini, R.; Maggini, M.; Scorrano, G.; Prato, M., *SPIE*, 3803 (1999) 90.

35. Innocenzi, P.; Brusatin, G.; Guglielmi, M.; Bertani, R., *Chemistry of Materials*, 11 (1999) 1672.

36. Innocenzi, P.; Brusatin, G.; Babonneau, F., *Chemistry of Materials*, 12 (2000) 3726.

37. Davis, S. R.; Brough, A. R.; Atkinson, A., *Journal of Non-Crystalline Solids*, 315 (2003) 197.

38. Husing, N.; Schubert, U.; Misof, K.; Fratzl, P., *Chemistry of Materials*, 10 (1998) 3024.

39. El Rassy, H.; Pierre, A. C., *Journal of Non-Crystalline Solids*, 351 (2005) 1603.

40. Silverstein, R. M.; Webster, F. X., *Spectrometric Identification of Organic Compounds*, ed. 6th; John Wiley & Sons, Inc.: Singapore, 2004.

41. Ou, D. L.; Seddon, A. B., *Journal of Non-Crystalline Solids*, 210 (1997) 187.

42. Yoda, S.; Ohshima, S., *Journal of Non-Crystalline Solids*, 248 (1999) 224.

43. Jabbour, J.; Calas, S.; Gatti, S.; Kribich, R. K.; Myara, M.; Pille, G.; Etienne, P.; Moreau, Y., *Journal of Non-Crystalline Solids*, 354 (2008) 651.

44. Wu, C.; Wu, Y.; Xu, T.; Yang, W., *Journal of Non-Crystalline Solids*, 352 (2006) 5642.

45. Olejniczak, Z.; Leczka, M.; Cholewa-Kowalska, K.; Wojtach, K.; Rokita, M.; Mozgawa, W., *Journal of Molecular Structure*, 744-747 (2005) 465.

46. Smith, B. C., *Infrared Spectral Interpretation: A Systematic Approach*, ed. CRC Press LLC: Boca Raton, Florida, 1999.

47. Chu, L.; Daniels, M. W.; Francis, L. F., *Chemistry of Materials*, 9 (1997) 2577.

48. Nawrocki, J., *Journal of Chromatography A*, 779 (1997) 29.

49. Sanderson, R. T., *Polar Covalence*, ed. Academic Press: New York, 1983.

50. Brinker, C. J.; Scherer, G. W., *Sol-Gel Science:The physics and Chemistry of sol-gel processing*, ed. Academic Press: London, 1990.

51. Ayral, A.; Phalippou, J.; Woignier, T., *Journal of Materials Science*, 27 (1992) 1166.

52. Woignier, T.; Phalippou, J., *Journal of Non-Crystalline Solids*, 93 (1987) 17.

53. Stroud, R. M.; Long, J. W.; Pietron, J. J.; Rolison, D. R., *Journal of Non-Crystalline Solids*, 350 (2004) 277.

54. Hrubesh, L. W.; Keene, L. E.; Latorre, V. R., *Journal of Materials Research*, 8 (1993) 1736.

55. Silva, A. A. d.; Santos, D. I. d.; Aegerter, M. A., *Journal of Non-Crystalline Solids*, 95-96 (1987) 1159.

56. Chandrashekhar, G. V.; Shafer, M. W., *Better Ceramics Through Chemistry II, Materials Research Society Symposium Proceedings*, 33 (1980) 705.

Chapter 4

Highly Porous, Photoactive Organic Inorganic Hybrid Coatings

In the preceding chapters a methodology for the preparation of aerogel like highly porous organic inorganic networks at ambient pressure was described. The properties of these networks have been shown to resemble that of supercritically dried aerogels from the dielectric response of these networks. Such high performance networks can prove advantageous in a variety of fields. In this chapter a possible application of these networks is tested.

Photoactive coatings have acquired immense interest in recent years and they find application in areas of increasing relevance like environmental clean up. Si-doped TiO_2 layers was fabricated for the purpose of realizing filtration and photocatalysis in a single device in water purification process.[1] Composite titanium dioxide films on woven glass fabric were prepared and photoactivity tested for oxidation of nitric oxide.[2] Photocatalytic degradation of both inorganic and organic compounds in wastewaters is well reported.[3] Photocatalytic purification, decontamination, and deodorization of waste gases and indoor air and photocatalytic destruction of bacteria and viruses, are relatively new outlooks but have developed relatively fast.[4-6] Volatile organic compounds (VOC) contribute to major environmental problems such as photochemical ozone formation, global warming, and stratospheric ozone depletion. Heterogeneous photocatalytic degradation is by far the most promising approach for the removal of these hazardous materials.[7]

Semiconductor photocatalysts based on metal oxides (e.g., TiO_2 and ZnO) and chalcogenides (e.g., CdS, ZnS, CdSe, ZnSe and CdTe) have been reported for photo degradation.[8-20] TiO_2 is by far the most widely investigated, mainly because of its chemical stability, nontoxicity, and suitable positioned valence band and conduction band edges.[21] The VB redox potentials of both types of TiO_2 are more positive than that of the (•OH/−OH) redox couple.[22] Consequently, adsorbed water and hydroxyl groups can be

oxidized to highly reactive hydroxyl radicals on both irradiated rutile and anatase surfaces.[23] Of the two phases the anatase phase has been found to be more active due to a more open structure and lower recombinant rates of electron hole pair in it.[21]

Silica and titania-silica prepared by sol-gel method find use as either catalyst or support in reactions including isomerization, esterification, epoxidation, hydroxylation, CO oxidation, photo-oxidation, and reductions.[24] An inherent problem for the preparation of mixed oxides by sol–gel processing of a mixture of different metal alkoxides is that phase separation may occur because of different hydrolysis and condensation rates. For example, addition of water to a solution of $Si(OR)_4$ and $Ti(OR)_4$ results in the precipitation of titania.[25] Common solutions to this problem which allow the preparation of homogeneous (well mixed on the nanometer scale) silica–titania gels involve pre-hydrolyzing $Si(OR)_4$ or lowering the reactivity of the faster reacting precursor, $Ti(OR)_4$, by chemical modification, e.g. by replacing part of the alkoxide groups by chelating or bridging ligands.[26-28] Homogeneous silica–titania gels were also obtained by non-hydrolytic sol–gel processes, in which one component is an alkoxide and the other a chloride or acetate.[29]

Interest in silica titania aerogels stems from their enormous surface area and easy accessibility, which are ideal for catalytic applications. The preparation of free standing titania-silica aerogels is more difficult due to the weaker Si–O–Ti network. Impregnation of silica alcogels with a titanium precursor is an alternative method to obtain aerogels of good mechanical strength.[30] Modifying the precursors by chelation for slowing down the hydrolysis rates of titania precursor has also been attempted.[31] Gas permeable, mesoporous titania-silica aerogels of uniform titanium distribution and excellent activity for photocatalytic oxidation of airborne organics have been prepared by Cao.[32,33] Free standing and crack-free titania-silica aerogels with high titanium content (Ti/Si = 1) were successfully prepared by adjusting the hydrolysis of the two alkoxide precursors to a comparable rate during the sol-gel processing. Photoactive anatase TiO_2 nanocrystals with a large surface area (up to 300 m^2g^{-1}) crystallized from the gel network by the high-temperature ethanol supercritical drying. The crystalline domains were solidly anchored

to the aerogel network by Ti-O-Si bonds.[32] To improve the visible light activity of silica titania aerogels metal ion doping has been found to be successful. Interestingly these doped aerogel mixtures were only active when SiO_2 was present.[34] On the other hand an about to gel silica sol can glue chemically and physically diverse particles added into it to the three dimensional gel network.[35] The volume fraction of the second solid can be varied above or below a percolation threshold to tune the transport properties of the composite aerogel. This approach has been used to prepare silica titania aerogels.[35]

Titania containing silica based organic inorganic hybrid systems are well known in optical applications. Hybrid silica titania coatings for planar wave guides were prepared from Methyltriethoxysilane, tetraethoxysilane and tetrabutoxytitanate.[36,37] SiO_2/TiO_2/poly(vinylpyrrolidone) composite materials processed by the sol gel technique were also studied for optical waveguide applications.[38] Modifications of the organic groups on silicon is also a subject of interest. Polydimethylsiloxane with oxides of silicon, titanium and germanium have yielded new hybrid planar waveguides.[39] GPTMS is a frequent component for the fabrication of wave guides.[40] GPTMS-TiO_2 sol-gel derived materials were explored for optical limiting applications because of their possibility to obtain thick films by a single layer and to entrap organic molecules with suitable non-linear optical properties for optical limiting.[41]

GPTMS and titanium alkoxides are frequently employed for the preparation of dense heterometal hybrid polymers which are used, e.g., for hard coatings of organic polymers and contact lens materials.[42] GPTMS-water-titaniumtetraethoxide presents a picture with myriad number of chemical reactions which include hydrolysis, homo- and hetero-condensation of the metal alkoxides and ring-opening reactions of the epoxide group. The catalytic effect of titanium alkoxide on the silanol condensation is known.[43] It is also known to cause the epoxide ring opening of the glycidoxy group.[44] In the mixed titaniumtetraethoxide-GPTMS system Hoebbel observed the formation of Si-O-Ti bonds and the bonds accounted for about 50% of the Si-O bonds at low water concentration.[45] But at high water concentration these bonds we found to hydrolyze in favour of Si-O-Si bonds and only 20% bonds remained in highly hydrolysed sols. The condensation degree

was largely influenced and a high degree of condensation was observed in titanium containing sols. The epoxide ring opening was found to be influenced by the concentration of Ti-OH groups rather than the alkoxide itself. Innocenzi tried a non hydrolytic route to synthesize the hybrids from GPTMS and $TiCl_4$. In the first step $TiCl_4$ was added to GPTMS in CH_2Cl_2 and efficient promotion of epoxide ring opening of GPTMS was reached at room temperature in short reaction times. On addition of water, in the last step, hydrolysis-condensation reactions gave an inorganic network.[46]

So, the organic inorganic hybrid materials incorporating titania particles can be achieved in a TEOS-GPTMS system if the processing variables are carefully controlled. A pre hydrolysis of the silicon alkoxide will be necessary to reduce phase segregation. Hydrolysis of titanium alkoxide in the pre hydrolyzed silica sol should give a titania incorporated network. The ambient pressure drying technique will ensure the porosity of the final gel or coating. In case of coatings, the addition of an amine to the silica sol (procedure used in chapter 3), can reduce the time available to coat the slides since the gelation time of the system is considerably lowered once the amine is added. But the addition of titanium alkoxide can effectively induce the polymerization of the epoxy group. Soaking of the coatings in the amine solution can confirm the completion of organic polymerization. Baiju et al has studied the effect of processing variables on the photoactivity of sol-gel derived tiania.[47] A major conclusion arising from the study was the increase in the activity with the increasing molar ratio of water. Very high water ratios in the mixed oxide systems is ruled out due to the possibility of precipitation of titania at higher water content. So a rather high value of 10 was used for the hydrolysis of the titania precursor. The hydrolysis was performed in silica sol so that the formed titania particles will be attached to the silica network through the Si-O-Ti bonds.

Experimental

(3-glycidoxypropyl)trimethoxysilane (GPTMS), tetraethylorthosilicate (TEOS) titaniumisopropoxide (TIP), acetylacetone (AcAc) and diethylenetriamine (DETA) were

procured from Aldrich (Steinheim, Germany) and used as obtained. Isopropylalcohol (IPA) and hydrochloric acid were obtained from S.D. Fine chemicals (Mumbai, India). Water used for the preparation was doubly distilled. In a typical preparation, weighed amounts of GPTMS and TEOS were mixed with weighed quantity of isopropanol by stirring on a magnetic stirrer. To this solution weighed amount of 10^{-3} N HCl was added. Water was taken in the molar ratio (water/OR) = 0.5, where OR is the alkoxide group on the silane precursor. The precursors were in the ratio (TEOS/GPTMS) = 2. The alcohol was taken in the ratio (IPA/Si) = 4. The solution was stirred for 2 hours. To this, a solution made up of weighed amounts of TIP, AcAc, such that the molar ratio was 1, taken in isopropanol, was added. Different compositions of titania was calculated as weight percentage of SiO_2 and compositions corresponding to 20, 30, 50 and 60% were prepared. The amount of isopropanol was calculated such that the final gel will have the same density for all titania compositions. The calculation detailed in chapter 3 was slightly modified to calculate the target density of the gels. Titania and acetyl acetone were considered to become part of the network for the calculations. Finally a calculated amount of acid such that the molar ratio (water/TIP) = 10, was added drop wise to the stirring solution. After stirring for 5 minutes the sols were used for coating. The coatings were deposited on cleaned glass slides using a dipcoater (KSV, KSV instruments, Finland) operating at a withdrawal speed of 80 mmmin^{-1}. The glass slides were cleaned by ultrasonication in Extran solution and then with ultrasonication in distilled water. A dwell time of 1 min was given for all samples in the coating solution. The coating was performed in a dust free room under a controlled uniform atmospheric temperature of 25 °C. All samples were coated once and then allowed to remain in air for 30 s. The glass slides were then transferred to a beaker containing 10 % DETA in alcohol. After five minutes the slides were moved to 20% isopropanol solution and aged for 6 hours. The slides are then solvent exchanged with isopropanol for 3 hours. The isopropanol was replaced with fresh alcohol every 15 min. The slides were then aged in a 50% TEOS solution for 3 hours. Finally the slides were washed with hexane for 3 hours using the same procedure used for solvent exchange. The slides were then dried at 70 °C in a

hexane saturated atmosphere initially and then in air. The preparation scheme is provided as scheme 4.1. The slides were then separated into two batches. One batch was heat treated at 300 °C in flowing Ar atmosphere for 2 hours at a heating rate of 2 °Cmin^{-1}. Another batch was heat treated for 4 hours.

To prepare solid gels, the sols used for coating were poured into polypropelene vials after adding DETA and kept at 50 °C for gelation. GPTMS/DETA molar ratio was 3 for all compositions. Gelation occurred within 30 minutes for all samples. The gels then underwent the same aging and washing process detailed for the slides, except that the duration of the washing steps and initial aging was 24 hours and that for the silane aging was 48 hours. The gels were also heat treated at 300 °C for 2 hours and 4 hours in flowing N_2 atmosphere.

The use of lower aging and washing times for the coatings are well justified considering the lower solid content in the coatings.

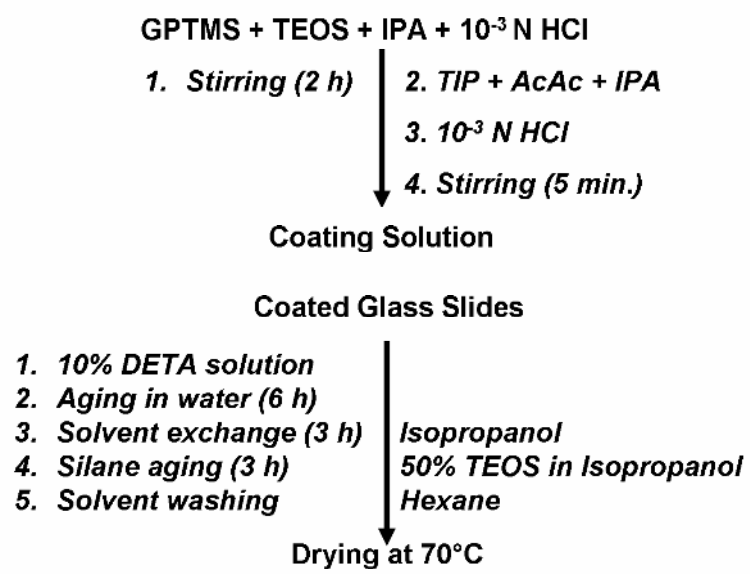

Scheme 4.1.: Preparation procedure adopted

Viscosity of the sols was measured using a Rheoviscometer (Anton Paar GmbH, Graz, Austria). The measurements were done at 25 °C.

Coatings were characterized by Raman spectroscopy, IFS-66 Bruker spectrometer

connected with a Raman module (Bruker, FRA-106, USA) with radiation from an Nd:YAG laser of about 200 mW, Ellipsometry (Jobin Yuvon, France), Scanning Electron Microscopy, Atomic Force microscopy (Nanoscope, Digital Instruments, USA) and Tunnelling Electron microscopy. The gels were characterized using X-ray diffraction, Surface area and FTIR spectroscopy (Magna 560, Nicolet, Madison, Wisconsin).

The bulk density of the dried gels was calculated from the measured dimensions and weight. TEM observations were made on a FEI high-resolution transmission electron microscope (Technai 30 G2 S-TWIN, Eindhoven, Netherlands). Nitrogen adsorption data were obtained using a BET surface area analyzer (Gemini 2375, Micromeritics, Norcross, U.S.A) at 77 K. All analyses were conducted after degassing the samples at 200 °C for 3 hours. The pore size distributions were calculated using the Barrett Joiner-Halenda (BJH) method from the desorption curve of the isotherm. The calculations were performed by the software StarDriver V2.03 supplied by the manufacturer. The BJH average pore radius was calculated using the equation (2V/A), where V is the BJH adsorption total pore volume and A is the specific surface area. XRD patterns of the gels were taken using a Philips X' pert X-ray diffractometer in the diffraction angle 2θ range 20–40° using Cu Kα radiation.

The photocatalytic activity of the titania hybrid coatings were measured by following the methylene blue dye degradation. Methylene blue was adsorbed on to the coatings and then exposed to UV radiation. The radiation was provided by fifteen 15W tubes (Philips G15 T8) arranged in circular fashion, emitting radiation in the region 200–400 nm in a Rayonet Photoreactor (Netherlands). The amount of dye degraded at different time intervals were noted. The concentration of the dye was measured as the absorbance of the dye in the region 500 to 700 nm using a UV–Vis spectrometer (UV-2401 PC, Shimadzu, Japan).

Results and Discussion

Bulk density of gels prepared with varying titania content is provided in table 4.1. It can be seen that the bulk density decreases with titania content initially and then slightly increases. In order to verify the trend samples with titania content 15% and 10% were also prepared and their density was 2.92 and 2.95 gcm^{-3} respectively. So increasing the titania content initially decreases the gel density, but above 30% the density increases.

TiO_2 Content (%)	Density (gcm^{-3})
60	0.39
50	0.34
30	0.25
20	0.27

Table 4.1.: Bulk density of dried gels

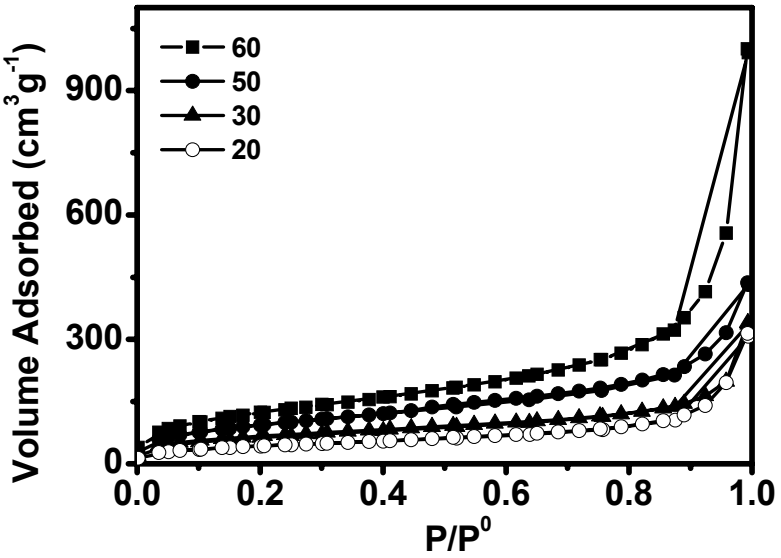

Figure 4.1.: Adsorption isotherms of dried gels with various titania weight percentages as given in the legend

Figure 4.1. presents the adsorption isotherm of the gels dried at 70 °C, but degassed at 200 °C. The isotherms contain the hysteresis loop confirming that the prepared gels are mesoporous. The loops have the H3 nature and points to smoother pores. The gels prepared with 60 wt% titania have the largest pore volume as indicated by the increased adsorption at high pressures. It can be seen that the nature of the adsorption isotherm and hysteresis is similar to that obtained for the hybrids with out titania (chapter 3). So the nature of porosity is not disturbed by the presence of titania.

TiO_2 Content (%)	BET Surface Area (m^2g^{-1})	C Parameter	Total Pore Volume cm^3g^{-1}	Average Pore Radius (nm)
60	455	67	1.53326	6.7
50	342	66	0.66844	3.9
30	228	81	0.51987	4.5
20	155	68	0.47636	6.1

Table 4.2.: BET analysis of dried gels

BET analysis along with the pore volume of the dried gels is provided in table 4.2. It can be seen that the surface area increases progressively with the increase in titania content. Similar increase in pore volume is also observed in the case of total pore volume except for the 60% sample, where there is a sharp increase in total pore volume. On the other hand the average pore radius can be seen to decrease progressively till the 50% composition and then increases sharply. The C parameter on the other hand peaks for the 30% titania composition. The rest of the samples have almost the same value for the C parameter. So there is a definite change in the nature of the surface for the 30 % tiania gel.

The pore size distribution curves obtained for various hybrids are provided as figure 4.2. It can be seen that the distribution stretches along the same region for all samples. But there is a small peak in the distribution towards the lower radius region.

Except for this peak, the distribution resembles the one obtained for hybrids without any titania, discussed in chapter 3.

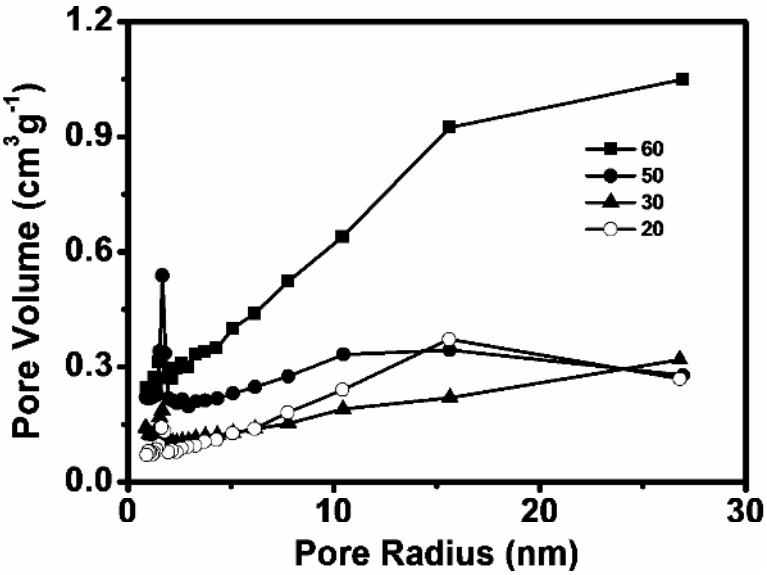

Figure 4.2.: Pore size distribution curves obtained for dried gels with varying titania concentration as provided in the legend

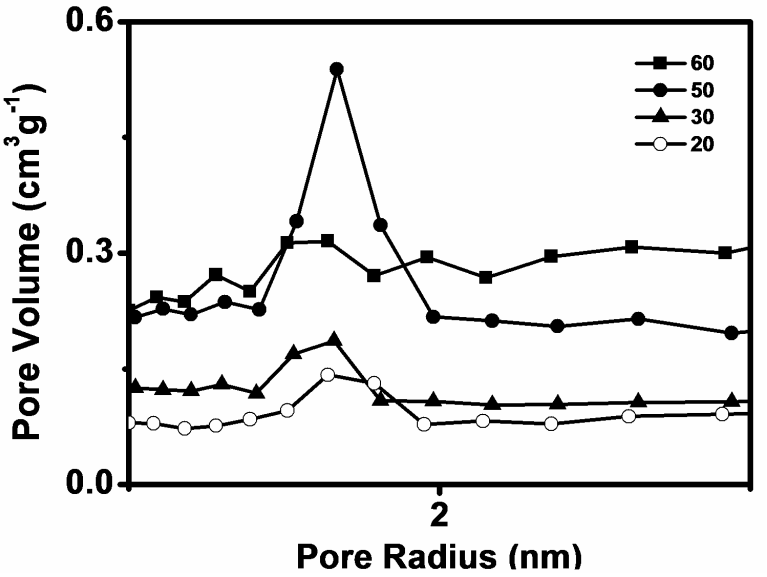

Figure 4.3.: Pore size distribution curves towards lower radius region obtained for dried gels with varying titania concentration as provided in the legend

The pore size distribution towards the lower pore radius region is magnified in the figure 4.3. Interestingly there is a peak in the distribution close to 2 nm and the pore volume increases with the titania content till 30%, which has a distinct peak in this region.

The adsorption isotherms of gels heated at 300 °C for 2 hours in flowing N_2 is provided as figure 4.4. Here, again the 60% titania composition seems to have the highest adsorption capacity and the nature of the isotherm and the hysteresis loop are unchanged by the calcination. The corresponding pore size distribution obtained is provided as figure 4.5.

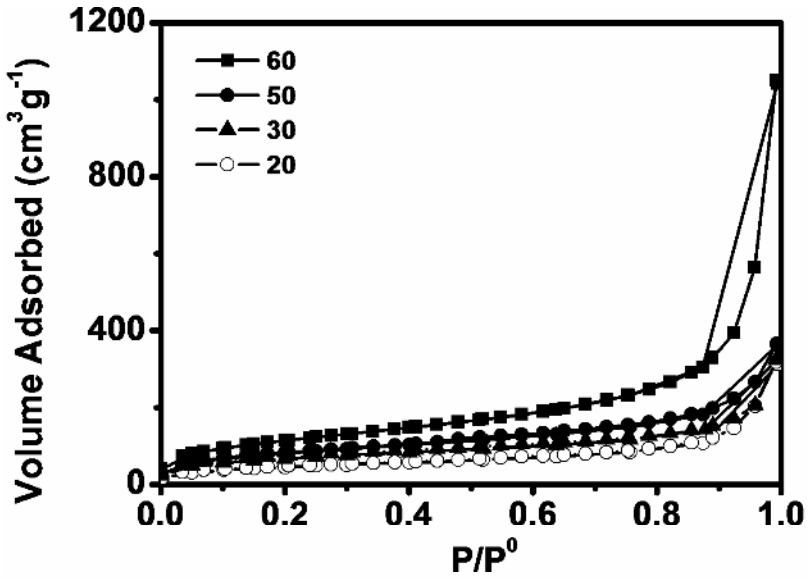

Figure 4.4.: Adsorption isotherms of gels, calcined at 300 ℃ for 2 H, containing various titania weight percentages as given in the legend

It can be seen that there is no considerable change in the distribution upon calcination for 3 hours. Again there is a peak in the distribution towards the lower radius region. Figure 4.6. presents the distribution towards the lower radius region. Again the 50% hybrid has the most prominent peak in this region.

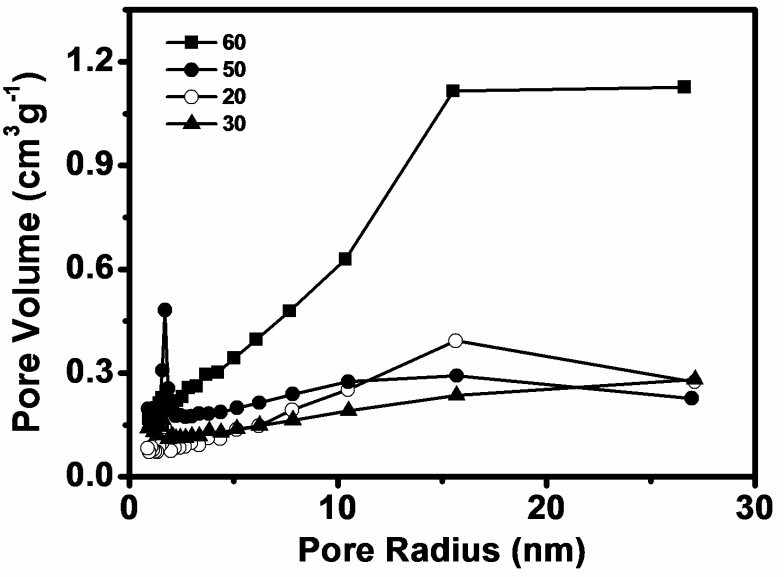

Figure 4.5.: Pore size distribution curve of gels, calcined at 300 ℃ for 2 H, containing various titania weight percentages as given in the legend

TiO_2 Content (%)	BET Surface Area (m^2g^{-1})	C Parameter	Total Pore Volume (cm^3g^{-1})	Average Pore Radius (nm)
60	416	75	1.61214	7.8
50	291	88	0.55979	3.9
30	238	120	0.50091	4.2
20	160	96	0.48311	6.0

Table 4.3.: BET analysis of gels calcined at 300 ℃ for 2 H

The BET analysis of the gels heated at 300 °C for 2 hours is provided as table 4.3. The trends are similar to that observed for the dried sample. There is only slight variations in the observed values but the trends are maintained. The C parameter distinctly shows that the 30% hybrid has the higher hydrophilic character.

The adsorption isotherms of different gels calcined at 300 °C for 4 hours is provided as figure 4.7. It can be seen that the shapes of the isotherms are not considerably

affected by the heat treatment. The trend observed for the other sets are followed well, here. The 60% incorporated gel has the highest adsorption capacity.

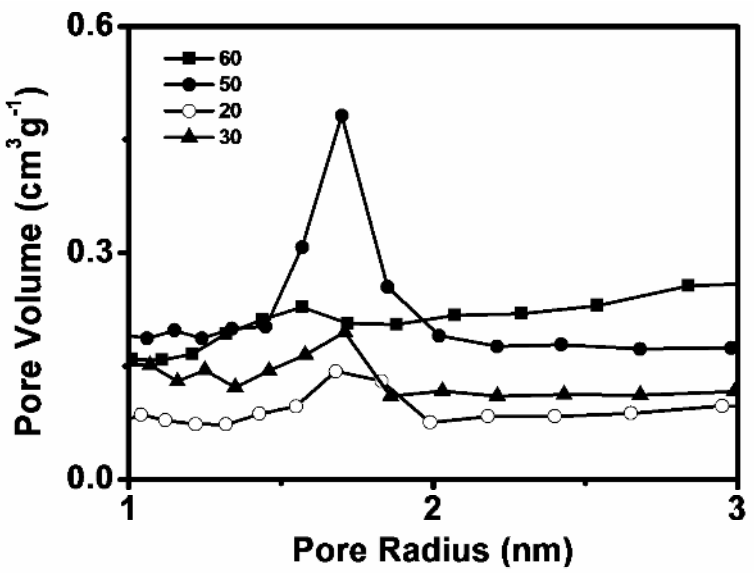

Figure 4.6.: Pore size distribution curves towards lower radius region obtained for gels, calcined at 300 ℃ for 2 H, with varying titania concentration as provided in the legend

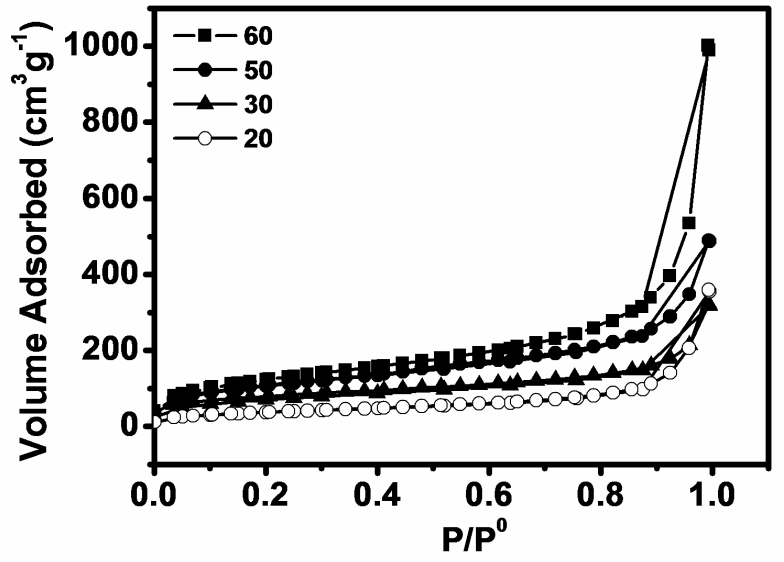

Figure 4.7.: Adsorption isotherms of gels, calcined at 300 ℃ for 4 H, containing various titania weight percentages as given in the legend

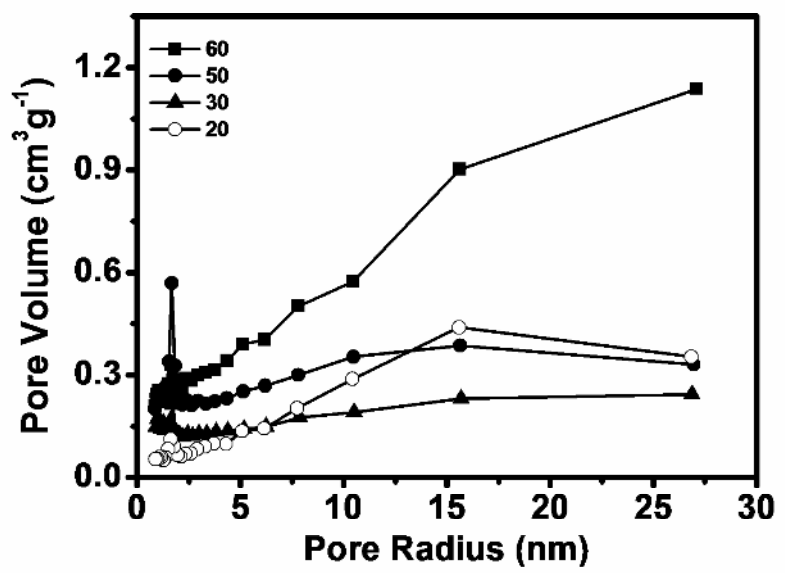

Figure 4.8.: Pore size distribution curves of gels, calcined at 300 ℃ for 4 H, containing various titania weight percentages as given in the legend

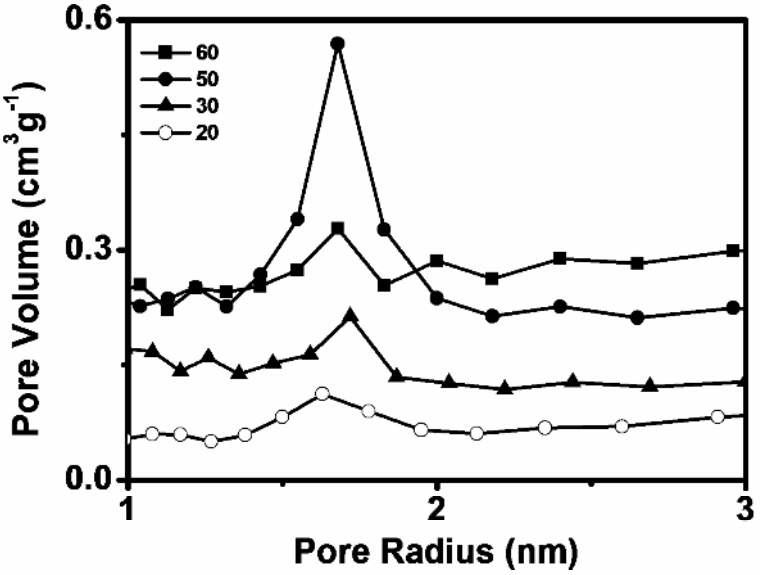

Figure 4.8a.: Pore size distribution curves towards lower radius region obtained for gels, calcined at 300 ℃ for 4 H, containing various titania weight percentages as given in the legend

The adsorption pore size distribution curve obtained for the gels calcined at 300 °C for 4 hours is provided as figure 4.8., 4.8a. The distribution also follows the same

trend observed before. The small peak to the distribution at lower pore radius is also observed again. The BET analysis data for the gels is provided as table 4.4.

TiO_2 Content (%)	BET Surface Area (m^2g^{-1})	C Parameter	Total Pore Volume (cm^3g^{-1})	Average Pore Radius (nm)
60	444	83	1.52982	6.9
50	382	93	0.75425	3.9
30	249	118	0.48986	3.9
20	134	77	0.54884	8.2

Table 4.4.: BET analysis of gels calcined at 300 ℃ for 4 H

The increase in density with a corresponding increase in total pore volume seems contradictory but can be understood when one considers the fact that N_2 adsorption do not give information on pore sizes above mesoporous range.[48] So even when the pore volume from nitrogen adsorption is lower, the material can contain porosity in the higher porosity range. So there seems to be an indication of hierarchical porosity or porosity in different length scales for the prepared materials. Addition of titania to the gel network seems to increase the stiffness of the gel network and they resist shrinkage, from the low density values obtained for all hybrids. Highly homogeneous silica titania aerogels were prepared by Kim et al and according to those results the increase in titania content increased the shrinkage and induced cracks in the monoliths.[31] The lower densities achieved without any cracking at ambient pressure, here, would mean that colloidal sized titania particles are participating in the network formation rather than a homogenous distribution of titanium atoms in the network. The larger weight concentrations prepared and also the way of processing must have ensured this. This is a situation more helpful in harvesting the photo activity of the titania particles.

On the other hand the surface area of the compositions increases with the titania content. This has to be expected since the silica surface is more or less modified by the crosslinked alkyl chains and titania provides added adsorption sites in the network. The

most interesting is the variation of C parameter. The high value observed for the C parameter for the 30% composition is really baffling. One reason may be that the titania particles formed in this composition represents an optimum in particle size and their distribution in the network, increasing the surface nature of the total surface of the gel. The idea is presented as scheme 4.2.

The presence of a peak at the lower end of the pore size distribution suggests the presence of a different set of network and the most obvious presence is in the titania particles. So the titania particles formed are not dense and are in itself porous and the concentration of 50% gives the ideal concentration for the formation of micro porous titania particles.

Thermal treatment is expected to cause the removal of organic groups, but is largely prevented by the calcinations in inert atmosphere. But some removal may have occurred due to, either the inadequacy in the inert atmosphere or due to the low thermal stability of certain organics. Gels with lower titania concentrations may have suffered some shrinkage during the removal due to the lower mechanical stability of the network.

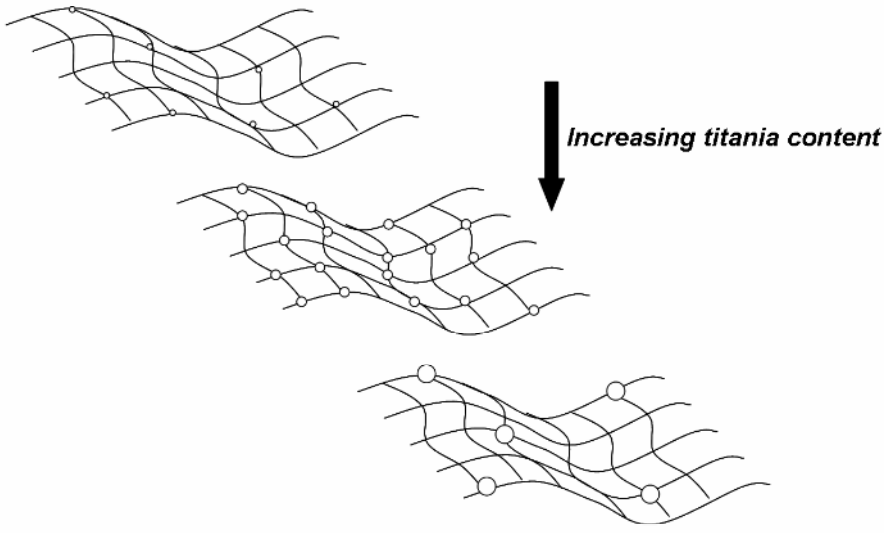

Scheme 4.2.: A schematic representation of the distribution of titania particles as the titania content increases in the gel. The grids are merely guides for eyes and have no resemblance with the physical nature of the gel.

In order to confirm the formation of titania particles, viscosity measurements were performed on the sols prepared with a titania content of 60%. Viscosity measurements were first made on the sol without adding titania. Then TIP, AcAc solution in isopropanol was added to the same sol, then water is added dropwise, stirred for a minute and viscosity was measured. The plots of shear rate versus viscosity is provided as figure 4.9. It can be seen that the nature of the viscosity changes markedly upon addition of tiania. The shear thickening behaviour observed for the silica sol is replaced with a shear thinning behaviour at low shear rates. The viscosity also increases sharply. The increase in viscosity on increasing the solid content is obvious. The shear thickening behaviour of silica sols have been observed and is due to the expenditure of shear in breaking the networked structure at low shear rates instead of increasing the flow.[49,50] But once the network has been broken the smaller clusters formed provide little resistance to flow and the applied shear increases the flow, decreasing viscosity at high shear rates. On the other hand, in solutions containing discrete colloidal particles, initial resistance to flow is large due to the higher energy required to set the particles in motion. But once the particles are set in motion the flow increases with shear and a shear thinning behaviour can be observed.[51,52] This is ample proof to the formation of discreet titania colloidal particles.

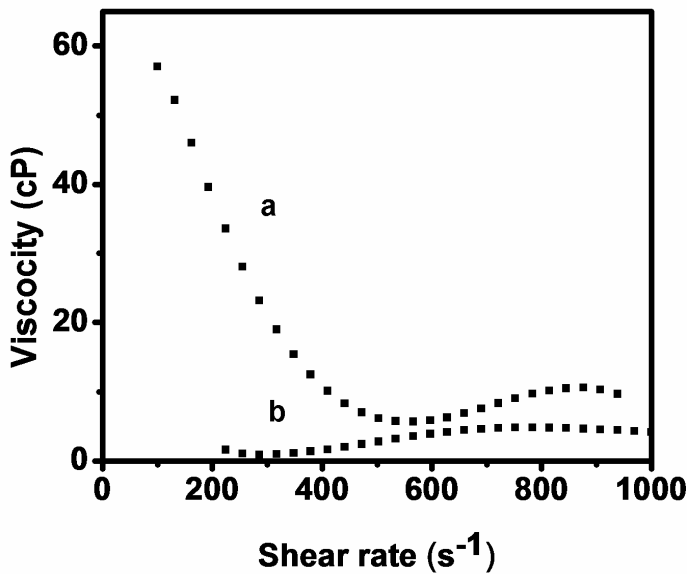

Figure 4.9.: Viscosity curves of sols (a) with titania (60%) (b) without titania

FTIR spectra of the prepared gels were analysed to understand the chemical structure of the network. The FTIR spectra obtained for various dry gels is provided as figure 4.10 and that of the gels calcined at 300 °C for 2 hours and 4 hours are provided as figure 4.11. and 4.12. respectively. The FTIR spectra show peaks corresponding to hydroxyl stretching (3500 cm^{-1}), alkyl hydrogen stretching (2940, 2875 cm^{-1}), stretching due to adsorbed water (1623 cm^{-1}), alkyl C-C bending vibrations (1454 cm^{-1}), Si-O-Si stretching (1100 cm^{-1}, 800 cm^{-1}), and O-Si-O bands (574, 453 cm^{-1}). The Si-OH stretching is observed at 946 cm^{-1}). The Si-O-Ti bonds are also known to stretch at 940 cm^{-1} making the identification of the peak dufficult.[32,53] But on comparing the peaks it could be found that the intensity and the broadness of the bonds increases with the increase in titania concentration indicating the formation of Si-O-Ti bonds. So the titania particles are anchored to the silica network through the Si-O-Ti bonds. Calcination at 300 °C seems to decrease the alky bands indicating the removal of some organic groups.

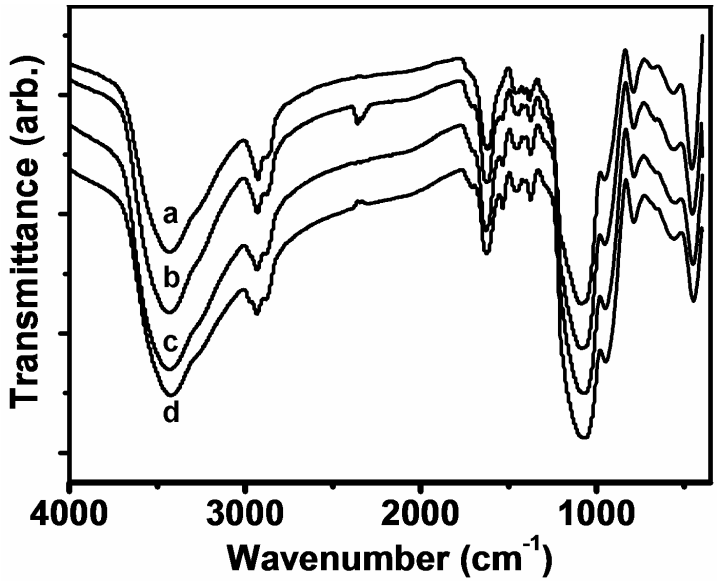

Figure 4.10.: FTIR spectra of gels with varying titania content (a) 20 (b) 30 (c) 50 (d) 60 wt.%, dried at 70 °C

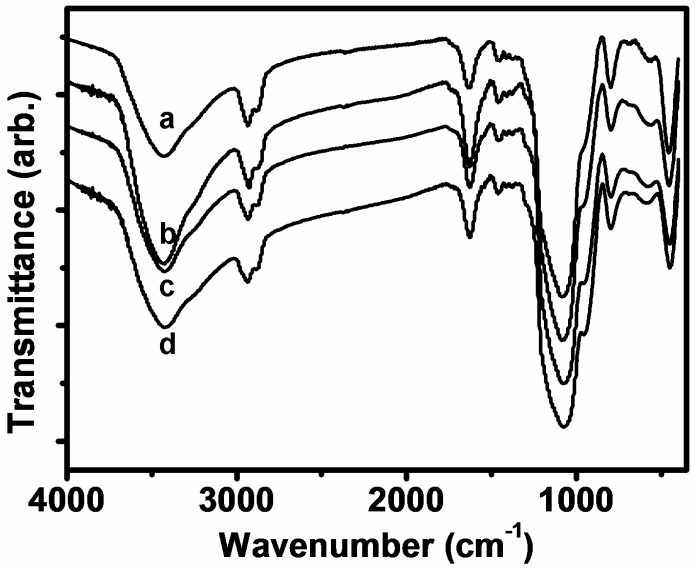

Figure 4.11.: FTIR spectra of gels with varying titania content (a) 20 (b) 30 (c) 50 (d) 60 wt.%, heated at 300 ℃ for 2H

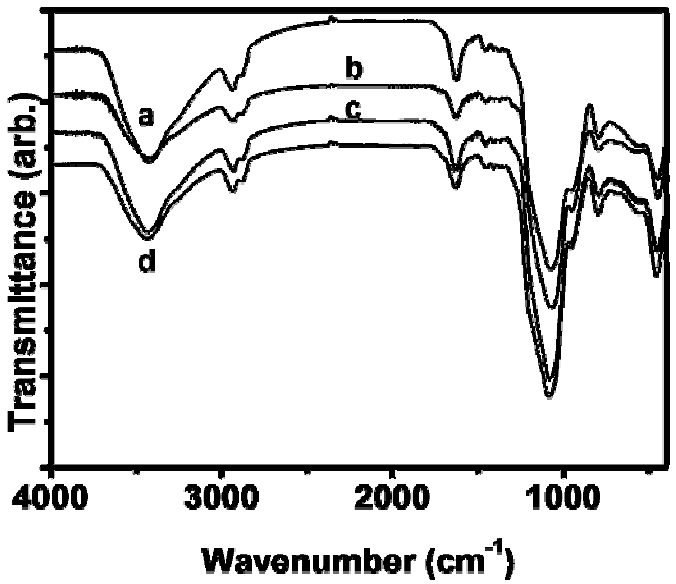

Figure 4.12.: FTIR spectra of gels with varying titania content (a) 60 (b) 50 (c) 30 (d) 20 wt.%, heated at 300 ℃ for 4H

The XRD patterns of the gels were taken to see if the crystallinity of titania has improved due to the thermal treatment. The calcination temperatures are low to induce

crystallisation, but processing in organic media has been reported to yield anatase titania at low temperature.[54]

The XRD patterns of gels prepared with higher titania content is provided as figure 4.13. The XRD patterns indicate a rather amorphous nature and there is no evidence to any crystalline phases of titania in these gels. Hence Raman spectroscopy was used to identify the phases in the coatings.

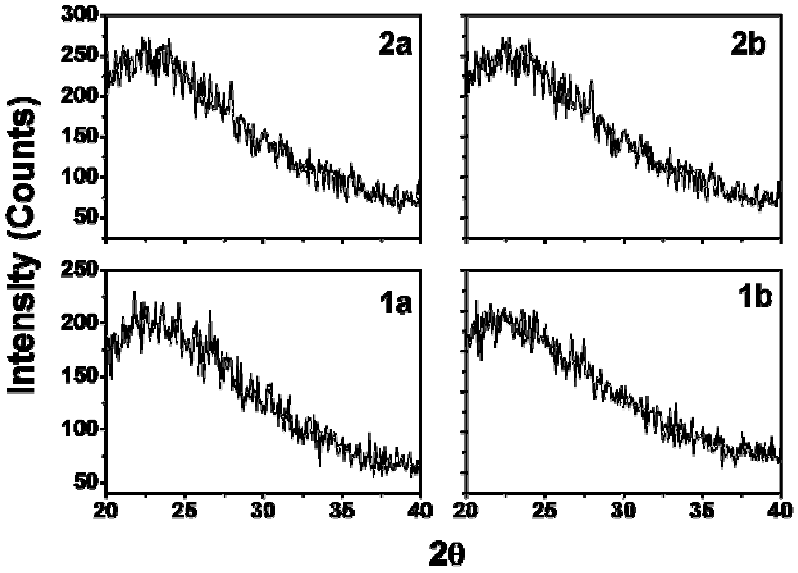

Figure 4.13.: XRD patterns observed for gels calcined at 300 °C for 2H with varying titania content (1a) 60 (2a) 50 % heated at 300 °C for 2 H and the corresponding gels heated for 3 H on the right

The coating thickness was evaluated using spectrometric ellipsometry. The acquired data was fitted to a coating model based on the composition of the coating as represented in scheme 4.3. Here the coating is considered as silica, titania mixed layer with voids, representing porosity. The χ^2 values obtained for all fits were between 0.2 and 0.4. A typical fit obtained is presented as figure 4.14.

Titania + Silica + Void
Substrate

Scheme 4.3.: Model used for fitting experimental data

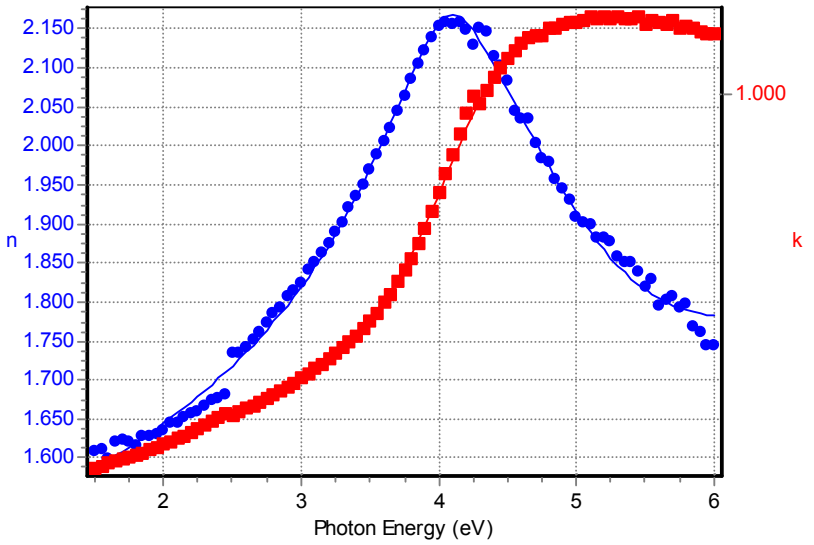

Figure 4.14.: A typical fit (continuous line) obtained for the experimental data (solid shapes). Refractive index on the left axis and extinction coefficient on the right. The typical absorption of titania can be seen above 3.2 eV

All compositions had a coating thickness between 730 and 750 nm and a light shrinkage can be observed for the composition with low titania content. The thickness obtained is provided as table 4.5.

TiO_2 Content (%)	Dried	300 °C 2H	300 ° C 4H
	Thickness (nm)		
20	730	700	400
30	778	795	796
50	544	560	557
60	652	636	643

Table 4.5.: Thickness values obtained for different coatings

The coatings prepared with high titania content were further analysed by SEM. The SEM images obtained are provided as figure 4.15.-4.20.

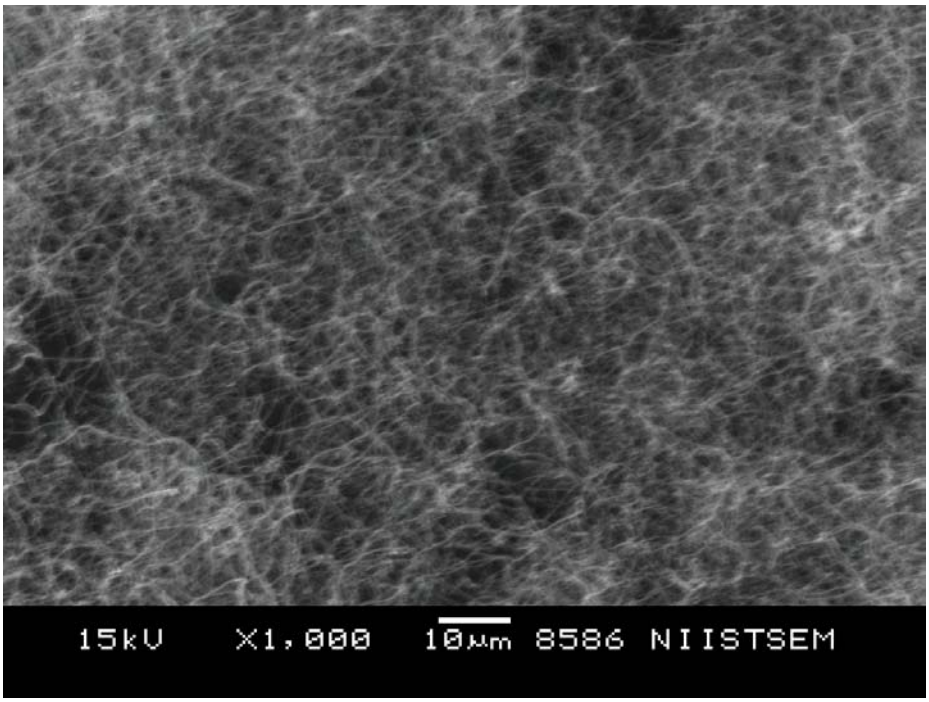

Figure 4.15.:SEM image of dried 60% titania coating

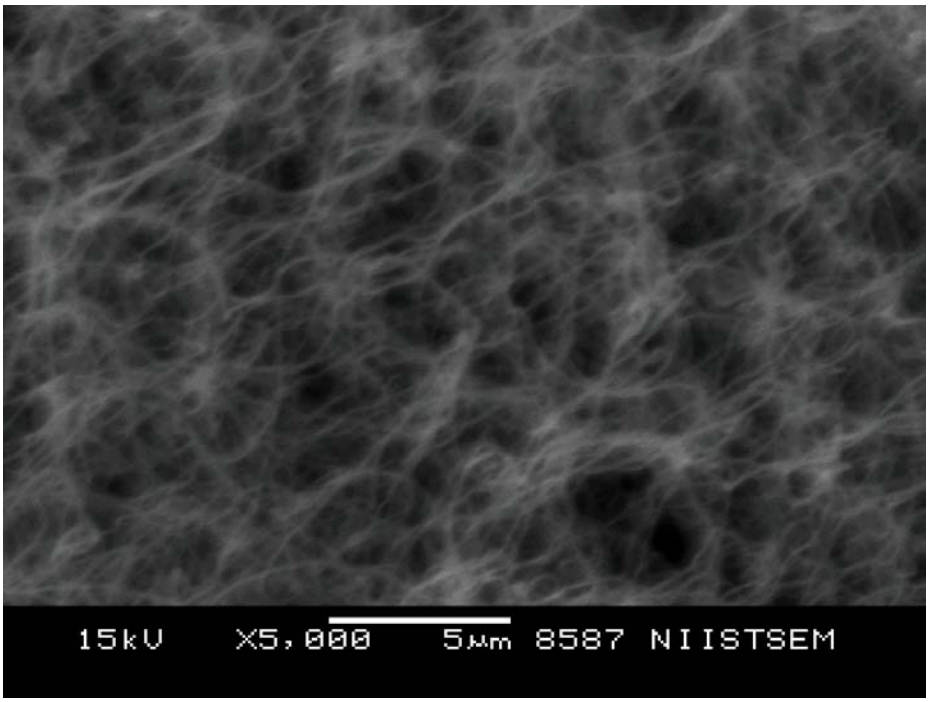

Figure 4.16.:SEM image of dried 60% titania coating at a higher magnification

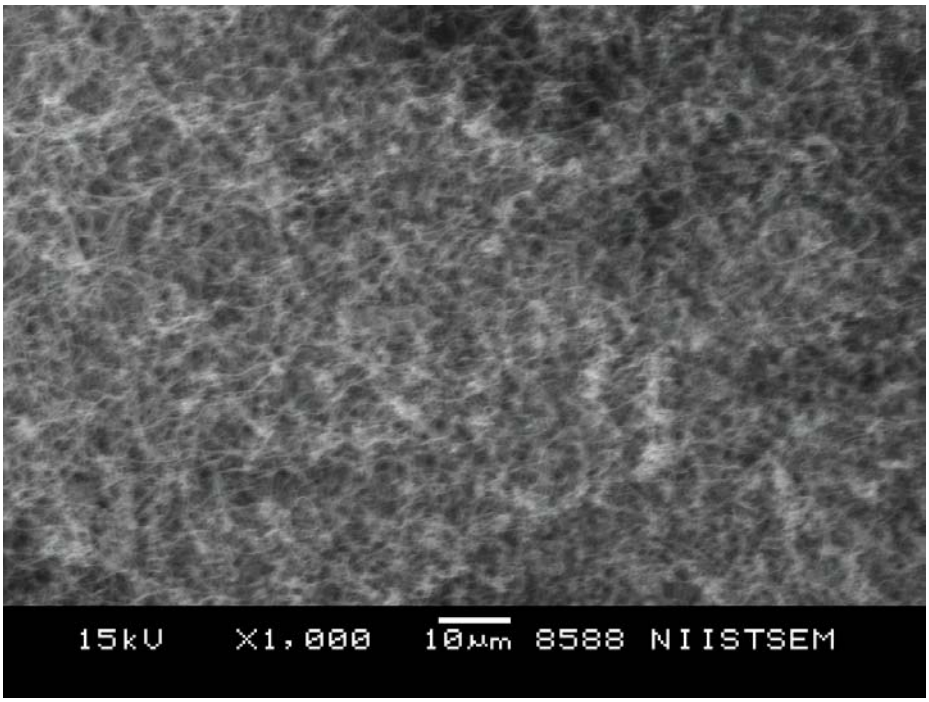

Figure 4.17.:SEM image of 60% titania coating calcined at 300 ℃ for 2 H

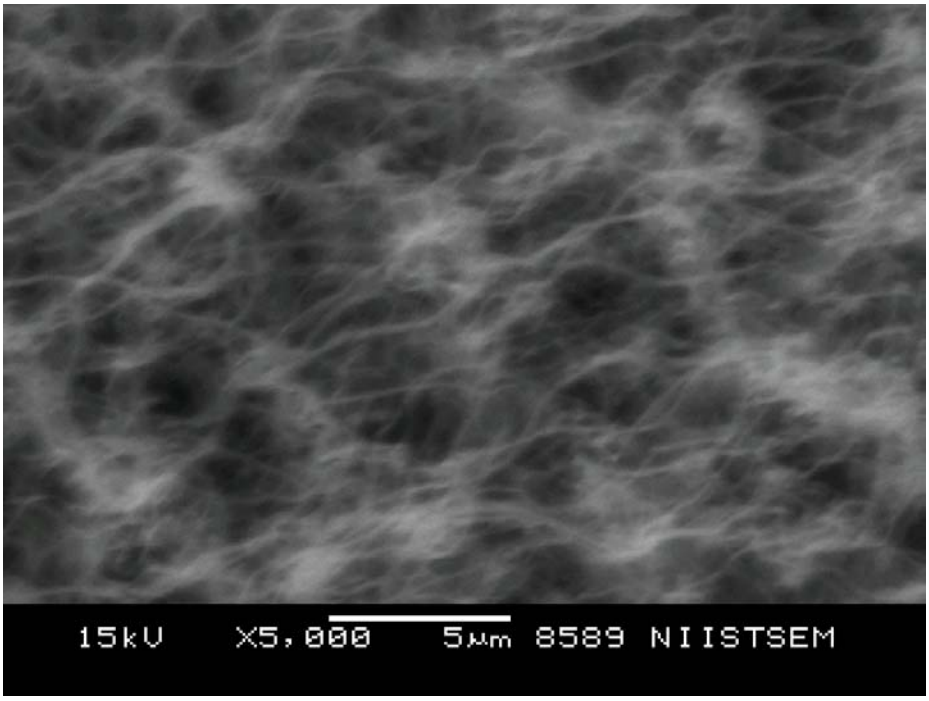

Figure 4.18.:SEM image of 60% titania coating calcined at 300 ℃ for 2 H at a higher magnification

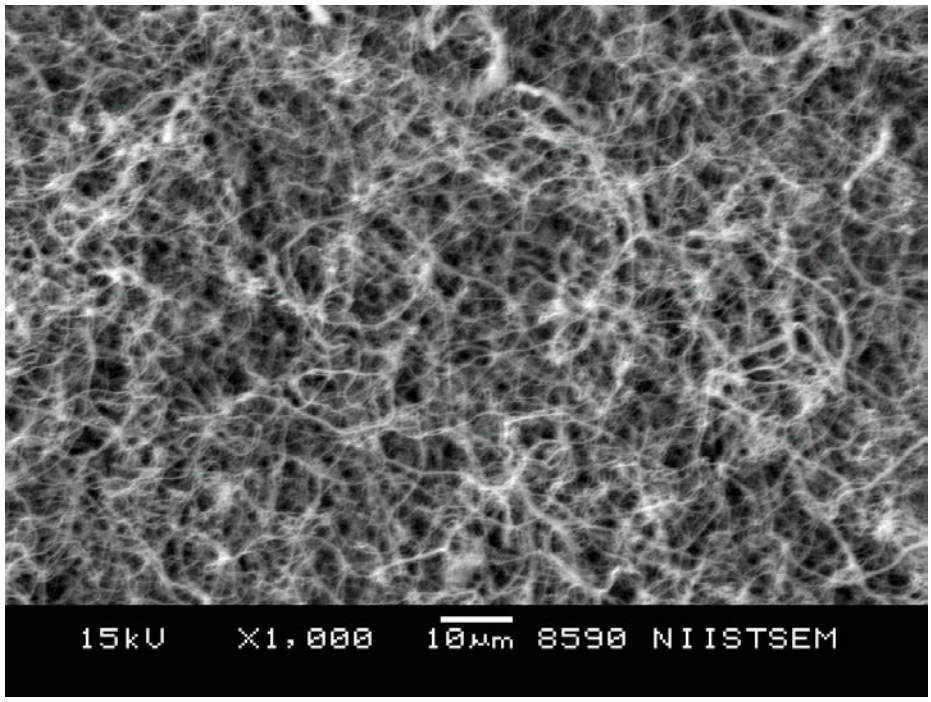

Figure 4.19.:SEM image of 60% titania coating calcined at 300 ℃ for 4 H

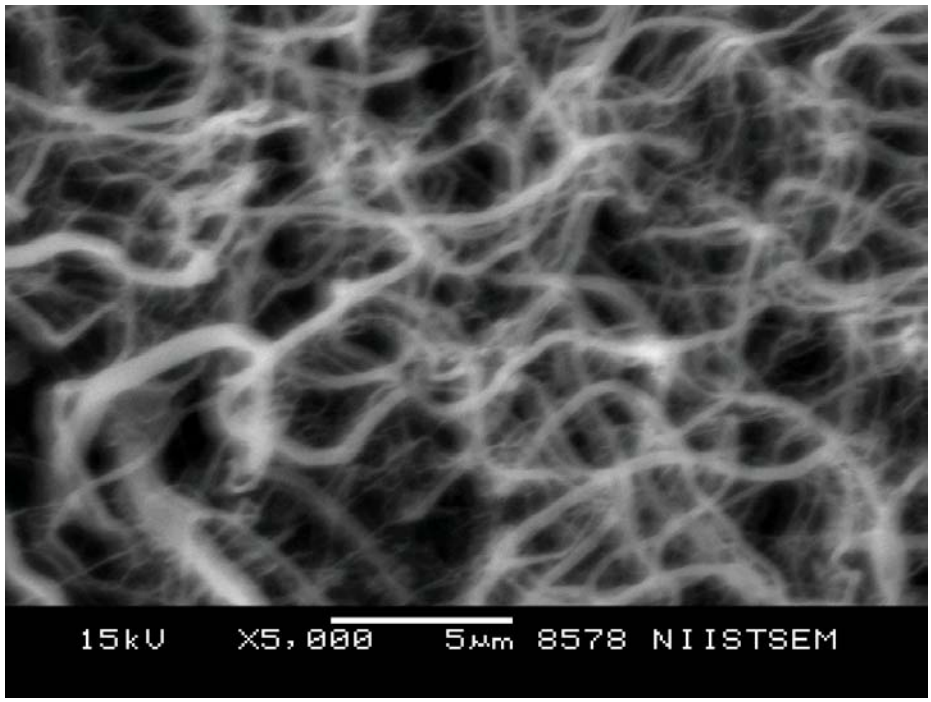

Figure 4.20.:SEM image of 30% titania coating calcined at 300 ℃ for 4 H

The SEM images provide evidence to a highly porous fibrous network in which titania particles are dispersed. It can be seen that the titania particles are present as distinct islands on the network (highly scattering titania particles appear bright on the network) in 60% compositions, where as the 30% composition has a continuous distribution of titania on the network. Hence the networking fibres appear thicker in the 30 % composition. This corroborates the observations from the surface area measurements. Aerogel like materials, having fractal geometries will have different associated structures are various length scales. We assume that below these networked structures there will be a more uniform and smooth structure with porosity only in the nano dimensions. The AFM images of these coatings are provided as figure 4.21-4.27.

The AFM images of the coatings indicate the uniform nature of the fibrous network. As the magnification increases it can be seen that the rough nature reappears. The fractal nature of the coatings is obvious.

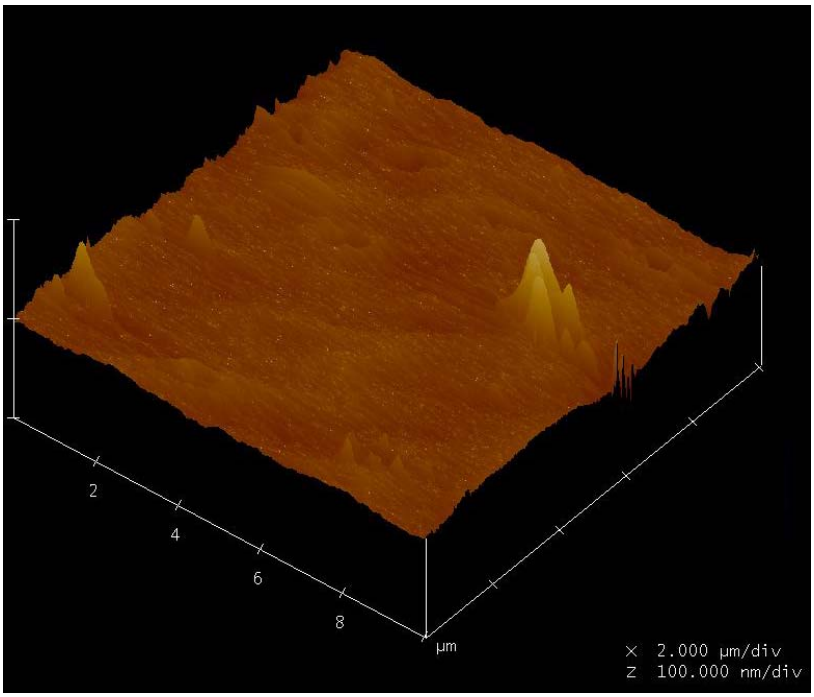

Figure 4.21.:AFM image of dried 60% titania coating

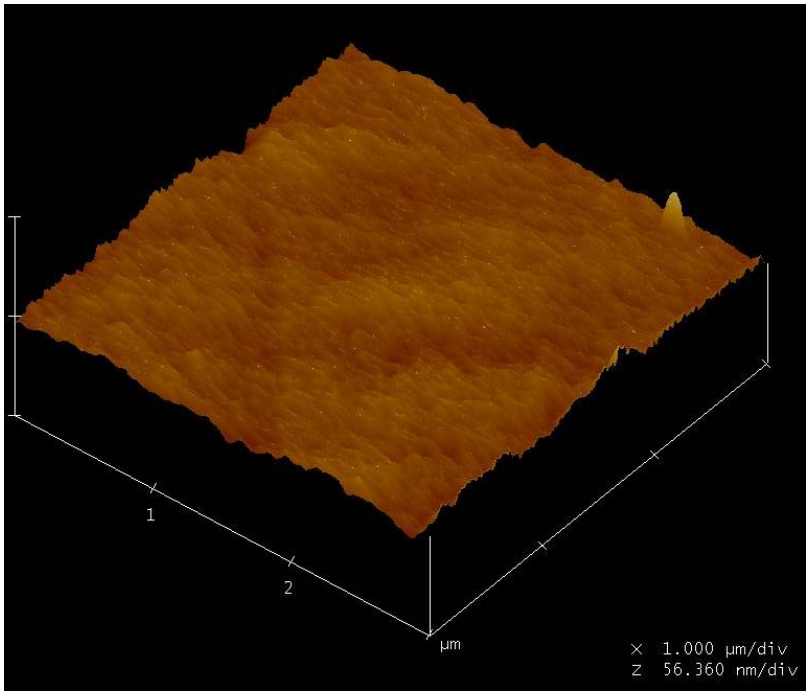

Figure 4.22.:AFM image of dried 60% titania coating (smaller area)

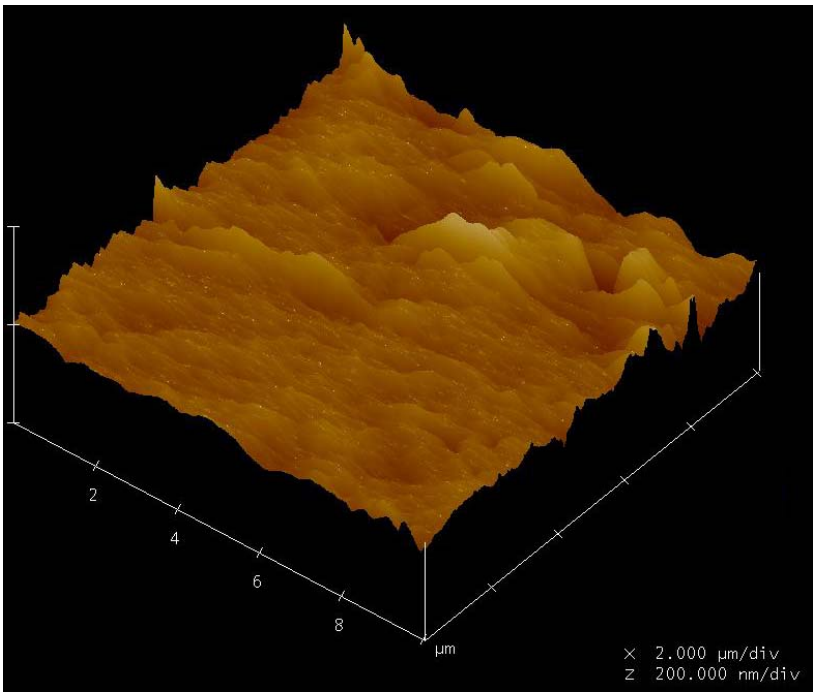

Figure 4.23.:AFM image of 60% titania coating calcined at 300 ℃ for 2 H

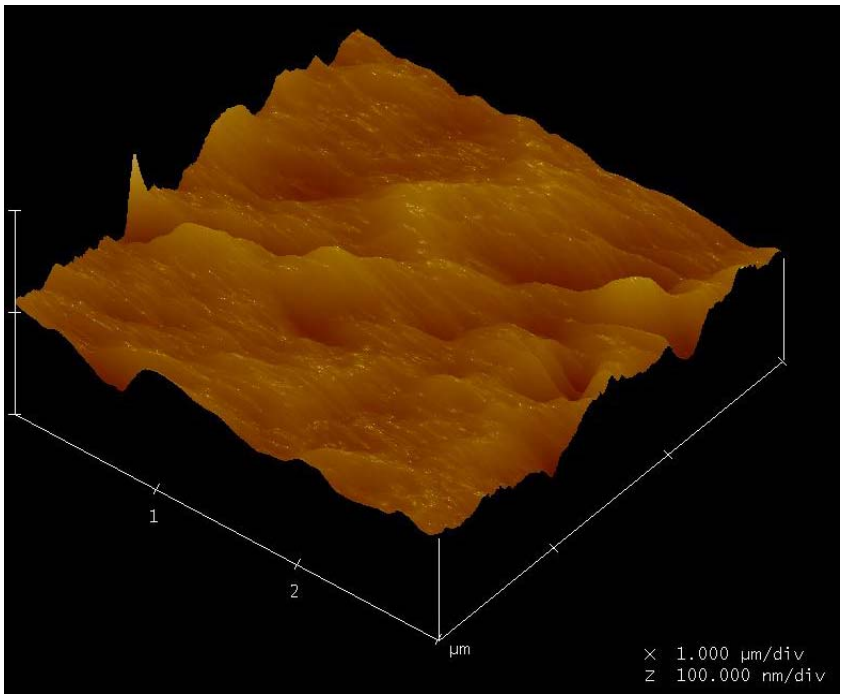

Figure 4.24.:AFM image of 60% titania coating calcined at 300 ℃ for 2 H (smaller area)

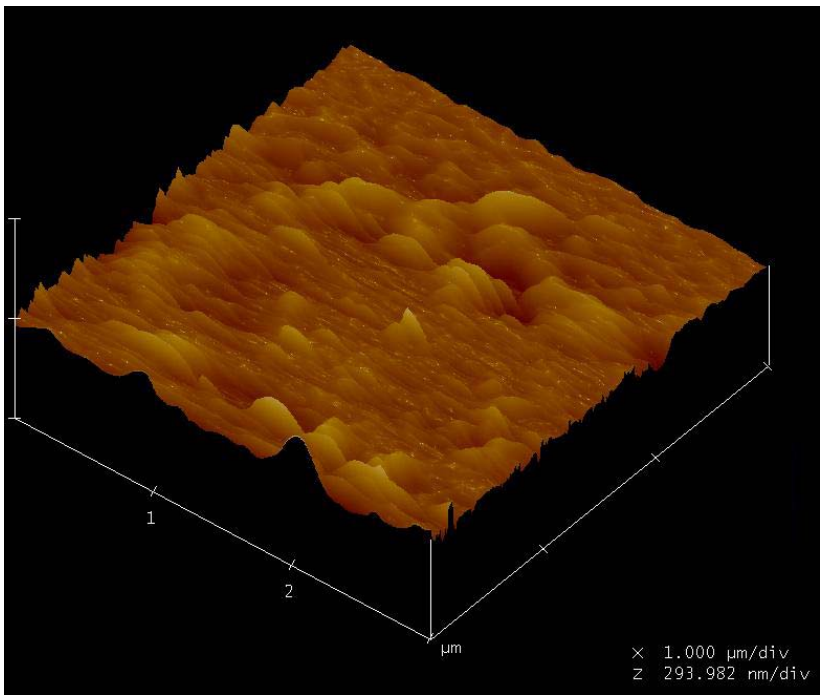

Figure 4.25.:AFM image of 60% titania coating calcined at 300 ℃ for 4 H (smaller area)

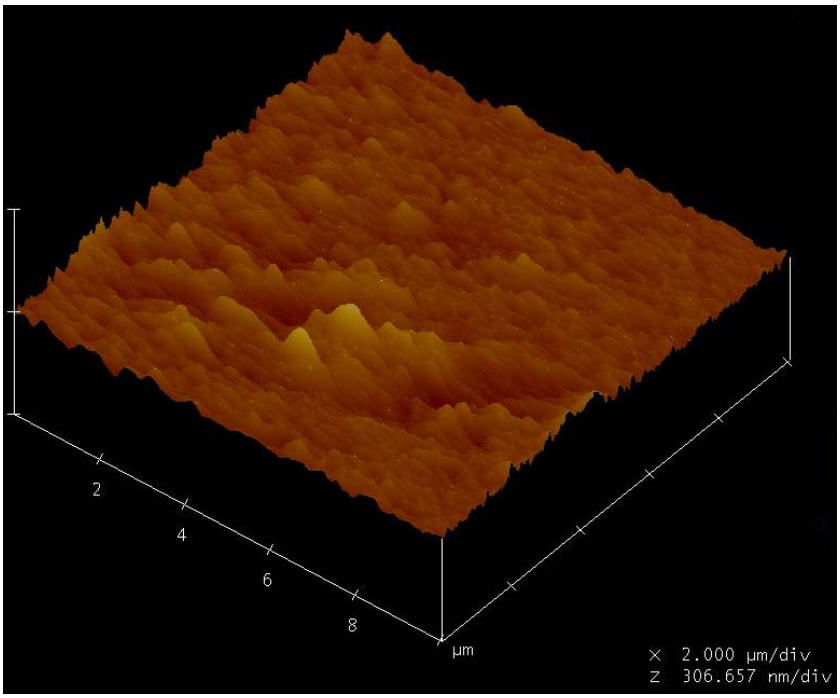

Figure 4.26.:AFM image of 30% titania coating calcined at 300 ℃ for 4 H

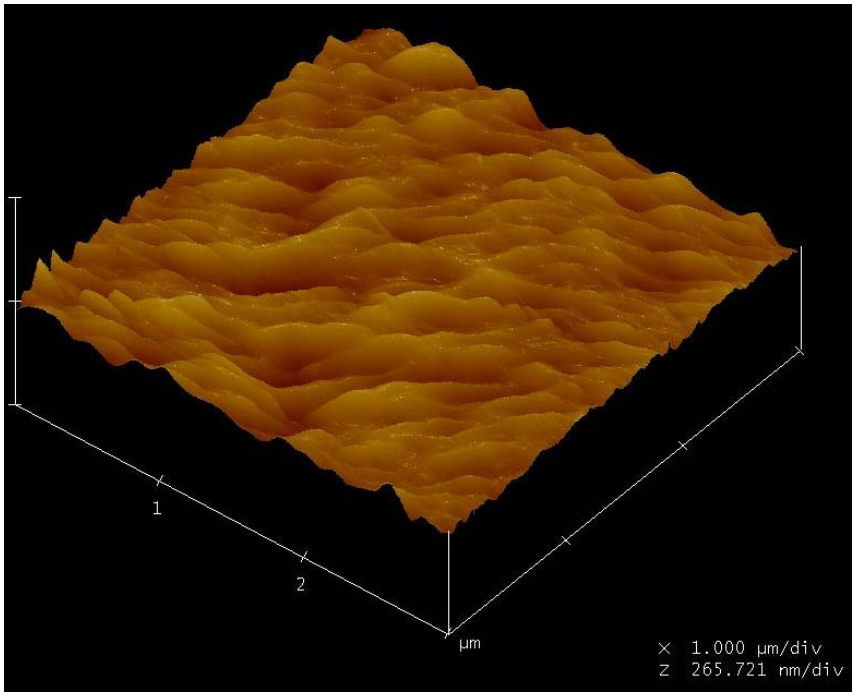

Figure 4.27.:AFM image of 30% titania coating calcined at 300 ℃ for 4 H (smaller area)

The particles appear dense and suggest the presence of titania in these dimensions also. The more rough nature of the samples with 30% titania indicates the larger distribution of titania discussed previously. From the AFM image of silica 60% titania dried at 70°C, the area appears smooth and small "bumps" <10 nm can be observed. Large pores of the order of <1μm can also be observed. Presence of titania is less in these samples. In a lower area scan, figure 4.22, surface roughness appears to be about 10 nm and pores of the order of 100 nm could be observed but not much evidence of titania can be seen. Roughness increases on calcination of the coating for 2 hours. Titania aggregates of height about 100 nm can be seen along with porosity of about 300 nm in figure 4.23. In the lower area scan provided in figure 4.24., roughness can be clearly identified and the titania particles are of the order 50-70 nm and porosity appears in the order 300-500 nm. The increased roughness may be due to the removal of organics and the baring of titania particles. In figure 4.26., 4 hour calcined 30 % sample is rougher and the "bumps" are of the order of 45 nm and pores of about 300 nm can be seen. In the low area scan, the "bumps" appear to be about 40-50 nm and pores of size 500 nm can be seen. So the average titania particles may have size about 75 nm in the 60% sample and about 40 nm in the 30 %.

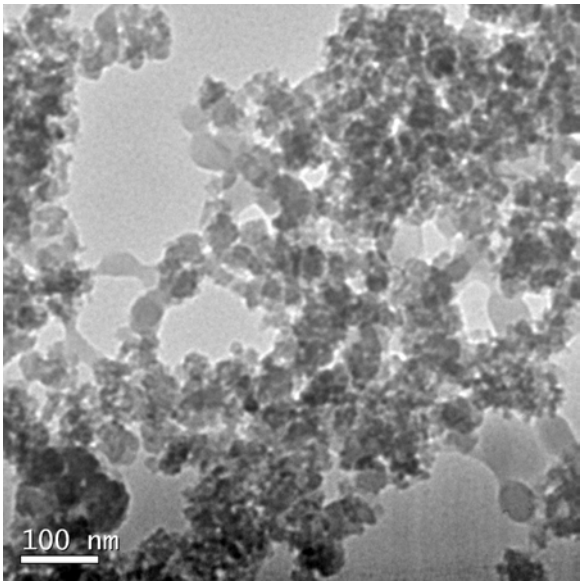

Figure 4.28.:TEM image of 60% titania gels calcined at 300 ℃ for 4 H

The TEM images of the 60% titania monolith, calcined for 4 hours is provided as figure 2.28. The TEM image of the 60 % titania gel, calcined for 4 hours has a networked structure observed in the case of organic inorganic hybrids (chapter 3). The structure of the gels are highly networked and porous in these length scales. But the marked difference is the appearance of denser particles on the basic network and imparts a rough appearance to the network. When the corresponding coating was peeled on to the grid and analysed, discrete titania particles with length range ~100 nm could be observed (figure 4.29.).

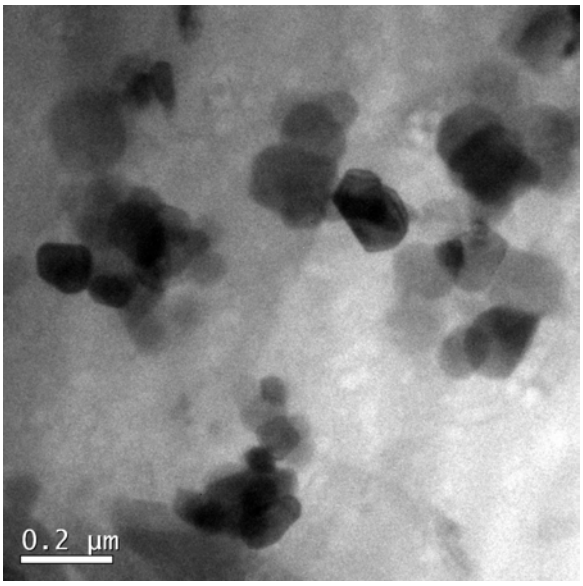

Figure 4.29.:TEM image of 60% titania coating calcined at 300 ℃ for 4 H

In order to find out whether any crystalline form of titania is present in the coatings, which can be crucial to its photoactivity, Raman spectra of the coatings were recorded. The obtained spectra are provided as figure 4.30. There are interfering peaks from the substrate which could not be avoided since the substrate is glass. The spectra in the region 1500 to 50 cm^{-1} were taken since the prominent peaks due to anatase and rutile titania are expected here.[55] The network vibrational modes of SiO_2 are observed at 436, 796, 1052 and 1178 cm^{-1}.[56] The absorptions are 639 and 603 cm^{-1} corresponds to SiO_3 stretching vibrations of GPTMS.[57] The Si-O-Ti vibrational modes are observed at 431,

1100 and 950 cm^{-1}.[58] The octahedral TiO stretching is observed at 667 and small bands in the region 600 to 650 cm^{-1}.[59] The bands are marked in the figure 4.30. for easy identification.

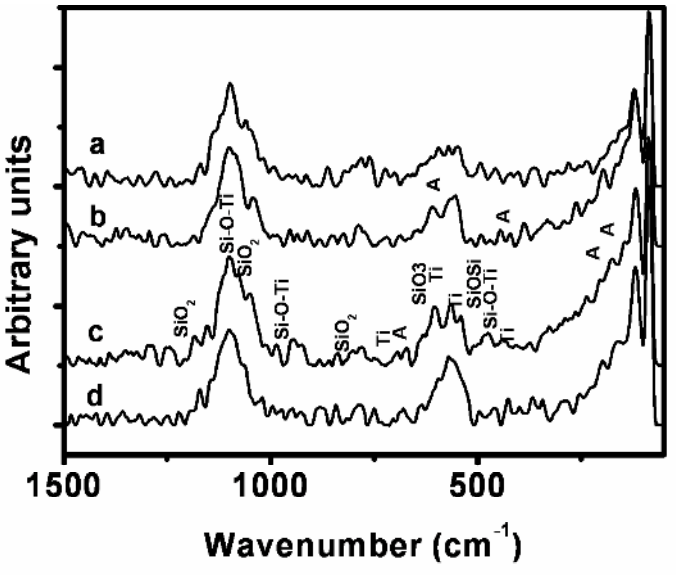

Figure 4.30.: Raman spectra of coated glass slides (a) 60 % dried (b) 60 % calcined at 300 °C for 4 H (c) 60 % for 2 H (d) 30% calcined at 300 °C for 2 H

There are five Raman bands for anatase and are observed at 144, 198, 398, 580 and 639 cm^{-1}.[60] In the figure 4.28., the spectra corresponding to 60 % titania sample calcined at 300 °C for 4 hours has bands at 145, 198, 398, 580 and 634 cm^{-1}. The peaks are rather weak but can be identified in the spectra. The corresponding bands are still weak in the 2 hour calcined sample and the 2 hour calcined 30% sample, but completely absent in the 60 % dried sample. So from the Raman spectra, there is evidence to the formation of anatase titania, but uncertainty exists regarding the extent of crystallinity and percentage of the anatase phase. But photoactivity in the prepared coatings may be a real possibility.

The photocatalytic activity of the coatings was evaluated using the methylene blue degradation study which is a generally followed procedure.[22] The coated slides were dipped in a methylene blue solution (0.01 M in isopropanol) for about a minute and the

absorbance in the region 500 – 700 nm measured. The methylene blue dye absorbs in this region and has absorption maxima at 660 and 610 nm. These corresponds to the aggregates of the dye and depending of the conditions the maximum intensity peak will vary.[61] The slides were then exposed to UV radiation in a photoreactor. The slides were taken out at intervals of 1 min and absorbance measured. The absorbance plots used for further calculation for the 50 % titania incorporated coating is provided figure 4.31. for reference.

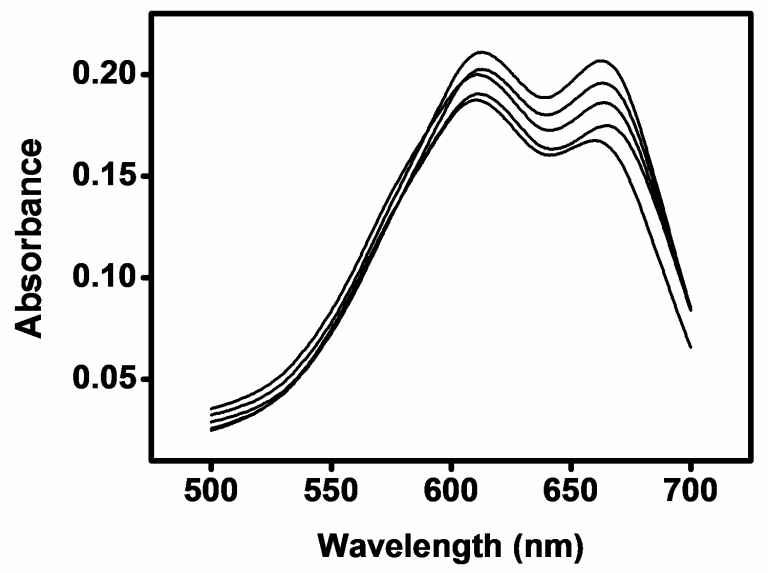

Figure 4.31.: Absorbance plot of methylene blue adsorbed on 50% titania coating irradiated for various time intervals

The absorbance of methylene blue is proportional to the concentration of the dye and the degradation of the dye is found to follow a first order rate.[62] For a first order reaction the plot of $\ln(C_0/C)$ against time will be a straight line with the slope equal to the rate constant. So $\ln(A_0/A)$, where A is the absorbance at any particular time and A_0, the absorbance at zero time, was plotted against time for each composition and a straight line fit was used to determine the slope. The graph obtained for the coatings calcined at 300 °C for 4 hour is provided as figure 4.32. The rate constants obtained for the various coatings are plotted against their titania compositions in figure 4.33.

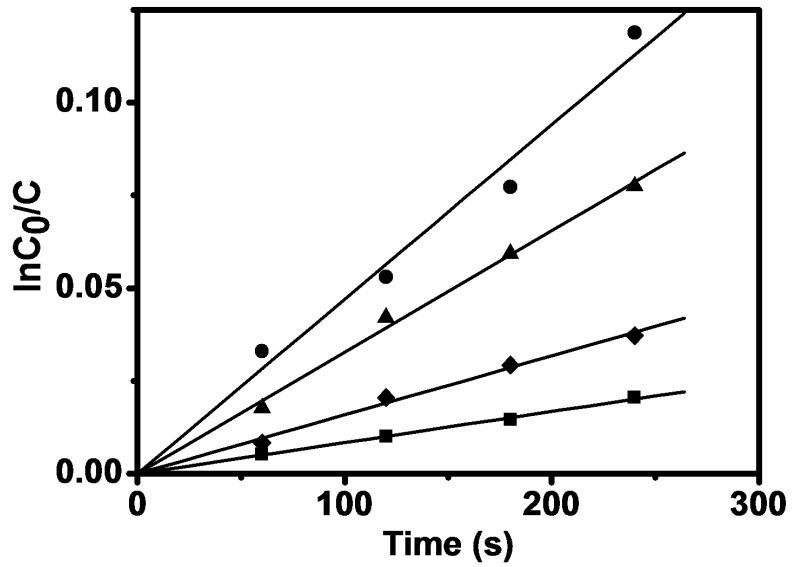

Figure 4.32.: ln C_0/C against time plot for methylene blue degradation on coatings, calcined at 300 ℃ for 4 H, with titania content from bottom 20%, 30%, 50% and 60%

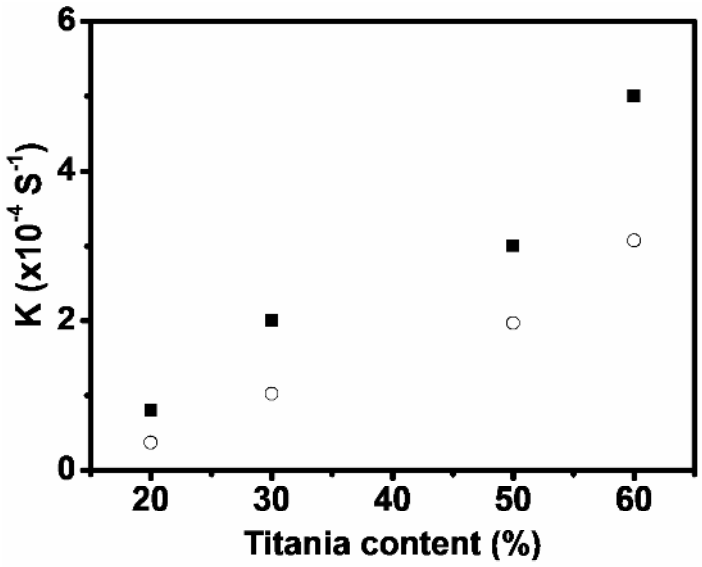

Figure 4.33.: Rate constants calculated for different coatings calcined at 300 ℃ for 2 H (open circles) and 4 H (solid squares) plotted against titania concentration.

It can be seen that the photocatalytic activity increases with increasing titania concentration and increasing calcination temperature. So the structural aspects of the coatings do not have a direct bearing on the photoactivity. The added advantage may be

the increased crystallinity observed in the higher compositions. Also the increasing thermal treatment has significant effect on the photoactivity. There may be an optimum treatment time which may give still higher activity. But the fact that the titania incorporated hybrid coatings can be made photoactive without disturbing the highly porous network and also the fact that this can be achieved at atmospheric pressure is a significant achievement.

Conclusions

In this chapter, a potential use of the ambient pressure dried aerogel like organic inorganic hybrid networks as photoactive porous coatings has been proposed and demonstrated. Unlike other synthesis techniques available in literature for silica titania aerogels, the present technique provides a way to obtain organic inorganic hybrid networks decorated with titania particles. Titania colloidal particles were found to form in the solution, from viscosity measurements and occupy the network from μm to nm length scales from AFM TEM and SEM studies.

The incorporation of titania increases the strength of the network and it resists shrinkage at low titania concentrations. Increasing titania concentration results in denser networks. Even then the density easily falls in the range of aerogels.

The coatings have been found to posses hierarchical porosity with a highly fibrous, networked structure at μm length scales. The pore size at this range is macroporous and the mesoporosity has been observed from N_2 adsorption measurements. Mesoporosity resides within the networked, fibrous structure and can be observed in TEM.

Anatase titania has been detected from Raman spectra of the coatings. The presence of anatase phase is more pronounced in the hybrid coatings with higher concentration of titania. The anatase particles are formed by thermal treatment but the optimum thermal treatment to maximise photoactivity could not be achieved in this study.

The coatings have been found be photoactive and the activity increases with the titania content. The activity was also increased by extending the thermal treatment.

The high porosity of the coatings and the considerable activity achieved, with room for improving the activity by increasing the thermal treatment, all points to a method for obtaining high performance coatings with possible application in degradation of noxious gases.

References

1. Ma, N.; Quan, X.; Zhang, Y.; Chen, S.; Zhao, H., *Journal of Membrane Science*, 335 (2009) 58.

2. Wang, H.; Wu, Z.; Liu, Y., *Journal of Hazardous Materials*, 164 (2009) 600.

3. Bhatkhande, D. S.; Pangarkar, V. G.; Beenackers, A. A. C. M., *Journal of Chemical Technology Biotechnology*, 77 (2001) 102.

4. Peral, J.; Domenech, X.; Ollis, D. F., *Journal of Chemical Technology Biotechnology*, 70 (1997) 117.

5. Zhao, J.; X., Y., *Building and Enviornment*, 38 (2003) 645.

6. Wolfrum, E. J.; Huang, J.; Blake, D. M.; Maness, P.; Huang, Z.; Fiest, J.; Jacoby, W. A., *Environmental Science and Technology*, 36 (2002) 3412.

7. Demeestere, K.; Dewulf, J.; Langenhove, H. V., *Critical Reviews in Enviornmental Science and Technology*, 37 (2007) 489.

8. Muthu, K.; Selvam, K.; Krishnakumar, B.; Swaminathan, M., *Applied Catalysis A: General*, 358 (2009) 259.

9. Liu, B.; Wen, L.; Zhao, X., *Progress in Organic Coatings*, 64 (2009) 120.

10. Li, Y.; He, X.; Cao, M., *Materials Research Bulletin*, 43 (2008) 3100.

11. Feng, S.-A.; Zhao, J.-H.; Zhu, Z.-P., *Xinxing Tan Cailiao/ New Carbon Materials*, 23 (2008) 228.

12. Bai, X.; Fan, H.; Wang, P., *Taiyangneng Xuebao/Acta Energiae Solaris Sinica*, 29 (2008) 1117.

13. Andrew Frame, F.; Carroll, E. C.; Larsen, D. S.; Sarahan, M.; Browning, N. D.; Osterloh, F. E., *Chemical Communications*, (2008) 2206.

14. Yao, W.-T.; Yu, S.-H.; Liu, S.-J.; Chen, J.-P.; Liu, X.-M.; Li, F.-Q., *Journal of Physical Chemistry B*, 110 (2006) 11704.

15. Cao, F.; Shi, W.; Zhao, L.; Song, S.; Yang, J.; Lei, Y.; Zhang, H., *Journal of Physical Chemistry C*, 112 (2008) 17095.

16. Ni, Y.; Zhang, L.; Zhang, L.; Wei, X., *Crystal Research and Technology*, 43 (2008) 1030.

17. Lee, M.-K.; Shih, T.-H., *Journal of the Electrochemical Society*, 155 (2008).

18. Avachat, U. S.; Dhere, N. G., *Journal of Vacuum Science and Technology A: Vacuum, Surfaces and Films*, 24 (2006) 1664.

19. Chen, X.; Lou, Y.; Dayal, S.; Qiu, X.; Krolicki, R.; Burda, C.; Zhao, C.; Becker, J., *Journal of Nanoscience and Nanotechnology*, 5 (2005) 1408.

20. Murase, K.; Watanabe, H.; Uchida, H.; Hirato, T.; Awakura, Y., *Electrochemistry*, 67 (1999) 331.

21. Tracy, L. T.; John Jr., T. Y., *Chemical Reviews*, 106 (2006) 4428.

22. Baiju, K. V., *Aqueous Sol-Gel Process For Nano Crystalline Photocatalytic Titania, Transparent Functional Coatings and Ceramic Membrane*, PhD. thesis, (2007), Faculty of Science, Cochin University of Science and Technology.

23. Diebold, U., *Surface Science Reports*, 48 (2003) 53.

24. Davis, R. J.; Liu, Z., *Chemistry of Materials*, 9 (1997) 2311.

25. Aravind, P. R., *Mixed Oxide Silica Aerogels Synthesized Through Non Supercritical Route for Functional Applications*, PhD. Thesis, (2008), Faculty of Science, Cochin University of Science and Technology.

26. Holland, M. A.; Pickup, D. M.; Mountjoy, G.; Tsang, E. S. C.; Wallidge, G. W.; Newport, R. J.; Smith, M. E., *Journal of Materials Chemistry*, 10 (2000) 2495.

27. Yoldas, B. E., *Journal of Non-Crystalline Solids*, 38-39 (1980) 81.

28. Pickup, D. M.; Mountjoy, G.; Wallidge, G. W.; Anderson, R.; Cole, J. M.; Newport, R. J.; Smith, M. E., *Journal of Materials Chemistry*, 9 (1999) 1299.

29. Hay, J. N.; Raval, H. M., *Journal of Materials Chemistry*, 8 (1998) 1233.

30. Yoda, S.; Ohtake, K.; Takebayashi, Y.; Sugeta, T.; Sako, T.; Sato, T., *Journal of Materials Chemistry*, 10 (2000) 2151.

31. Kim, W.-I.; Hong, I.-K., *Journal of Industrial and Engineering Chemistry*, 9 (2003) 728.

32. Cao, S.; Yeung, K. L.; Yue, P.-L., *Applied Catalysis B: Environmental*, 68 (2006) 99.

33. Cao, S.; Yeung, K. L.; Yue, P.-L., *Applied Catalysis B: Environmental*, 76 (2007) 64.

34. Wang, J.; Uma, S.; Klabunde, K. J., *Applied Catalysis B: Environmental*, 48 (2004) 151.

35. Morris, C. A.; Anderson, M. L.; Stroud, R. M.; Merzbacher, C. I.; Rolison, D. R., *Science*, 284 (1999) 622.

36. Brusatin, G.; Guglielmi, M.; Innocenzi, P.; Martucci, A.; Battaglin, G.; Pelli, S.; Righini, G., *Journal of Non-Crystalline Solids*, 220 (1997) 202.

37. Yang, L.; Saavedra, S. S.; Armstrong, N. R.; Hayes, J., *Analytical Chemistry*, 66 (1994) 1254.

38. Yoshida, M.; Prasad, P. N., *Chemistry of Materials*, 8 (1996) 235.

39. Motakef, S.; Suratwala, T.; Roncome, R. L.; Boulton, J. M.; Teowee, G.; Uhlmann, D. R., *Journal of Non-Crystalline Solids*, 178 (1994) 37.

40. Sorek, Y.; Reisfeld, R.; Tenne, R., *Chemical Physics Letters*, 227 (1994) 235.

41. Innocenzi, P.; Brusatin, G.; Guglielmi, M.; Signorini, R.; Bozio, R.; Maggini, M., *Journal of Non-Crystalline Solids*, 265 (2000) 68.

42. Philipp, G.; Schmidt, H., *Journal of Non-Crystalline Solids*, 63 (1984) 283.

43. Hoebbel, D.; Reinert, T.; Schmidt, H., *Journal of Sol-Gel Science and Technology*, 7 (1996) 217.

44. Philipp, G.; Schmidt, H., *Journal of Non-Crystalline Solids*, 82 (1986) 31.

45. Hoebbel, D.; Nacken, M.; Schmidt, H., *Journal of Sol-Gel Science and Technology*, 12 (1998) 169.

46. Innocenzi, P.; Sassi, A.; Brusatin, G.; Guglielmi, M.; Favretto, D.; Bertani, R.; Venzo, A.; Babonneau, F., *Chemistry of Materials*, 13 (2001) 3635.

47. Baiju, K. V.; Shukla, S.; Sandhya, K. S.; James, J.; Warrier, K. G. K., *The Journal of Physical Chemistry C*, 111 (2007) 7612.

48. Gregg, S. J.; Sing, K. S. W. *Adsorption, Surface area and Porosity*, ed. Academic Press: San Diego, 1995.

49. Iler, R. K. *The chemistry of silica: solubility, polymerization, colloid and surface properties and biochemistry of silica*, ed. Wiley and Sons: New York, 1979.

50. Kyekyoon (Kevin) Kim, K. Y. J., Ravindra S. Upadhye,, *Journal of the American Ceramic Society*, 74 (1991) 1987.

51. Melrose, J. R.; Ball, R. C., *Journal of Rheology*, 48 (2004) 961.

52. Ahn, K. H.; Osaki, K., *Journal of Non-Newtonian Fluid Mechanics*, 56 (1995) 267.

53. Innocenzi, P.; Martucci, A.; Guglielmi, M.; Armelao, L.; Pelli, S.; Righini, G. C.; Battaglin, G. C., *Journal of Non-Crystalline Solids*, 259 (1999) 182.

54. Niederberger, M.; Bartl, M. H.; Stucky, G. D., *Chemistry of Materials*, 14 (2002) 4364.

55. Zhang, Y.; Ebbinghaus, S. G.; Weidenkaff, A.; Kurz, T.; Nidda, H.-A. K. v.; Klar, P. J.; Gungerich, M.; Reller, A., *Chemistry of Materials*, 15 (2003) 4018.

56. Bertoluzza, A.; Fagnano, C.; Antonietta Morelli, M.; Gottardi, V.; Guglielmi, M., *Journal of Non-Crystalline Solids*, 48 (1982) 117.

57. Riegel, B.; Kiefer, W.; Hofacker, S.; Schottner, G., *Journal of Sol-Gel Science and Technology*, 13 (1998) 385.

58. Best, M. F.; Condrate Sr., R. A., *Journal of Materials Science Letters*, 4 (1985) 994.

59. Brinker, C. J.; Scherer, G. W. *Sol-Gel Science:The physics and Chemistry of sol-gel processing*, ed. Academic Press: London, 1990.

60. Baddour-Hadjean, R.; Bach, S.; Smirnov, M.; Pereira-Ramos, J.-P., *Journal of Raman Spectroscopy*, 35 (2004) 577.

61. Ohline, S. M.; Lee, S.; Williams, S.; Chang, C., *Chemical Physics Letters*, 346 (2001) 9.

62. Houas, A.; Lachheb, H.; Ksibi, M.; Elaloui, E.; Guillard, C.; Herrmann, J.-M., *Applied Catalysis B: Environmental*, 31 (2001) 145.

Summary

Even though a large number of applications have been prescribed for aerogels only a few has found significant mileage due to the extreme brittleness arising from the high porosity. The supercritical drying technique required for the preparation of these materials also imposes severe restrictions on their large scale applicability. One of the most important developments to grace the materials world in recent years is the organic inorganic hybrid concept. The ability to combine the properties of organic and inorganic materials into a single material has paved way to significant achievements in materials science. New materials with tailored properties, improved properties in existing materials as well as properties to conventional materials have all been possible by virtue of the organic inorganic hybrid concepts. Aerogels are also not left behind. The hybrid aerogels have been prepared with added properties like luminescence and flexibility. The conformal polymer coated aerogels are organic inorganic hybrid networks intimately linked through covalent bonds and posses mechanical properties nearly 300 times that of the native silica aerogels. The improved mechanical properties also present an opportunity to obtain aerogel properties at ambient pressure.

In this thesis an attempt has been made to unite the concepts of organic inorganic hybrids and ambient pressure drying for aerogels. In the first chapter the use of an organically modified precursor in the ambient pressure process involving solvent exchange and silane aging for aerogels has been investigated. The organically modified silane precursors were used to incorporate the organic functionality into the inorganic network. Investigations using the 3-glycidoxypropyltrimethoxysilane precursor showed that the improved hydrolysis rates and decreasing concentration of the precursor can be balanced by an optimum amount of water to obtain low gelation times. Organic groups can be conveniently placed on the pore walls by the sol-gel processing of the mixed precursor system. The organic groups were found to improve on the ambient pressure drying possibly by preventing the condensation of silanol groups during drying

shrinkage. The studies using modified silanes with organic groups of varying chain lengths show that the nature of porosity is largely determined by the inorganic precursor and the organically modified precursor has its effect only in the drying stages. At low concentrations of the organic precursor the silanes bearing small organic groups have been found to be more effective, while at higher concentration the groups with longer chains are more effective in improving the drying technique.

The presence of organic groups in the pore walls of the gels allows the introduction of an organic network on to the inorganic network if the organic groups were to be polymerised. The 3-glycidoxypropyltrimethoxysilane precursor contain an epoxy group that can be polymerised to form a poly ethylene oxide like network and its polymerisation can lead to an intimately linked organic inorganic network. The added presence of the organic network can reinforce the inorganic network and the mechanically superior system can effectively cope with the drying stress. This is the philosophy of the work attempted in the third chapter. The study proved that organic inorganic hybrid networks can be dried at ambient pressure to produce aerogels. Highly porous gels, >70% porosity was achieved for all compositions. But in contrast to the expected behaviour, the porosity of the gels decreased with increasing organic networking and highly porous gels were obtained at precursor ratios (inorganic precursor/organic precursor) below 1. As the organic precursor ratio increased, the aerogel properties decreased and xerogel properties increased. The porosity features were also largely dependent on the extent and nature of the organic network. The organic networking influences the secondary structure of the aerogel network, and increasing the precursor ratio decreases the volume of the pores between secondary particles. The nature of the organic network was also found to depend on the organic precursor content. As the concentration of the organic precursor increases, the length of the organic network increases initially, i.e. longer polymer chains were formed and beyond a certain point, for the precursor and crosslinker ratio equal to one, the polymer network contained shorter chains or had more terminated ends. The organic network anchored to the inorganic network was more efficient in reinforcing the inorganic network compared to the loosely

bound organic network formed from the use of crosslinker. The dielectric response of the ambient pressure dried aerogels were similar to the supercritically dried ones. But there were gels with high porosity (~80%) which show dielectric response higher than that expected for aerogels. Finally, a subtle balance between the organic part and inorganic part of the network is required to obtain aerogels through ambient pressure drying. The organic network cannot be a substitute for inorganic network and only at symbiotic proportions will the networks resist drying shrinkage.

The high porosity achieved at ambient pressure prompted the investigation into the development of photoactive hybrid coatings based on titania. A highly porous photoactive coating can find application in photooxidation of noxious gases, since the porosity will increase the adsorption of the gas and the photoactive property will degrade the gas. This forms the basis of the third chapter where titania incorporated hybrid coatings have been developed. Titania colloidal particles were found to form in the processed sol, which were confirmed from viscosity measurements. Further the presence of nanoparticles in the network from μm to nm length scales was identified from AFM, TEM and SEM data. The incorporation of titania increases the strength of the network and effectively resists shrinkage at low titania concentrations. Increasing titania concentration results in more dense networks. Even then the density easily falls in the range of aerogels. The coatings possessed hierarchical porosity with a highly fibrous, networked structure at μm length scales. Anatase titania was detected in the Raman spectra of the coatings and was more pronounced in the hybrid coatings with higher concentration of titania. The anatase particles are formed by thermal treatment but the optimum thermal treatment to maximise photoactivity could not be achieved in this study. The coatings were all photoactive and the activity increased with the titania content. The activity was also increased by extending the thermal treatment.

This thesis has shown that the organic inorganic hybrid networks can be dried at ambient pressure to obtain aerogels. So the added functional properties can be inter woven into aerogel property at ambient pressure. This is the first attempt to record the dielectric response of ambient pressure dried aerogels and the properties show that even

ultra low dielectric constants (<1.6) can be achieved by ambient pressure processing. Similarly the photoactive titania coatings with high porosity promises applications in photo oxidation of hazardous gases.

Publications

1. ***P. Shajesh****, S. Smitha, P.R. Aravind and K.G.K. Warrier*, "Synthesis, structure, and properties of cross-linked $R(SiO_{1.5})/SiO_2$ (R = 3-glycidoxy propyl) porous organic inorganic hybrid networks dried at ambient pressure", ***Journal of Colloid and Interface Science***, (2009) accepted

2. ***P. Shajesh****, S. Smitha, P.R. Aravind and K.G.K. Warrier*, "Effect of 3-glycidoxypropyltrimethoxysilane precursor on the properties of ambient pressure dried silica aerogels", ***Journal of Sol-Gel Science and Technology***, (2009) *doi: 10.1007/s10971-009-1926-1*

3. *S.A. Moore, C.P. Sibu, W. Wünderlich,* ***P. Shajesh****, K.V. Baiju, F.J. Berry, and K.G.K. Warrier*, "Thermally Stable Nanophase Anatase Titania with Mesoporous Texture by Pseudo-Inorganic Templating", ***Microporous and Mesoporous Materials***, 120 (2009) 467

4. *S. Smitha,* ***P. Shajesh****, P. Mukundan and K.G.K Warrier*, "Synthesis of Mesoporous Hydrophobic Silica Microspheres Through a Modified Sol-Emulsion-Gel Process", ***Journal of Sol-Gel Science and Technology***, 48 (2008) 356

5. *K. Rajesh,* ***P. Shajesh****, Biji P. and K.G.K. Warrier*, "High Surface Area Mesoporous Nanocrystalline Lanthanum Phosphate Nanorod through a Sol Gel Process - Effect of Alcohol Washing on a Non-oxide Gel", ***Microporous and Mesoporous Materials***, 116 (2008) 69

6. *P.R. Aravind,* ***P. Shajesh****, P. Mukundan, P. Krishna Pillai and K.G.K. Warrier ,*"Non-supercritically dried silica–silica composite aerogel and its possible application for confining simulated nuclear wastes", ***Journal of Sol-Gel Science and Technology***, 46 (2008) 146

7. *S. Smitha,* ***P. Shajesh****, P. Mukundan and K.G.K. Warrier,* "Sol-Gel Synthesis of Biocompatible Silica-Chitosan Hybrids and Hydrophobic Coatings", ***Journal of Materials Research***, 23 (2008) 2053

8. *P.R. Aravind,* ***P. Shajesh****, S. Smitha, P. Mukundan and K.G.K. Warrier,* "Non- Supercritically Dried Silica-Alumina Aerogels-Effect of Gelation pH", ***Journal of the American Ceramic Society***, 91 (2008) 1326

9. *K. V. Baiju,* ***P. Shajesh****, W. Wunderlich, P. Mukundan, S. Rajesh Kumar and K. G. K. Warrier,* "Effect of Tantalum Addition on Anatase Phase Stability and Photo activity of Aqueous Sol gel Derived Mesoporous Titania", ***Journal of Molecular Catalysis A: Chemical***, 276 (2007) 41

10. *K. Rajesh****, P. Shajesh****, O. Seidel, P. Mukundan and K.G. K. Warrier*, "A Facile Sol- Gel Strategy for the Synthesis of Rod Shaped Nano Crystalline High Surface Area Lanthanum Phosphate Powders and Nano Coatings", ***Advanced Functional Materials***, 17 (2007) 1682

11. *S. Smitha,* ***P. Shajesh****, S. Rajesh Kumar, P. Krishna Pillai and K.G.K. Warrier*, **"**Effect of aging temperature on the porosity characteristics of subcritically dried silica aerogels**",** ***Journal of Porous Materials***, 14 (2007) 1

12. *S. Smitha,* ***P. Shajesh,*** *P. Mukundan and K.G.K. Warrier*, "Antiwetting Silica-Gelatin Nanohybrid And Transparent Nano Coatings Synthesised Through An Aqueous Sol- Gel Process", ***Journal of Sol-Gel Science and Technology***, 42 (2007) 157

13. *S. Smitha,* ***P. Shajesh****, P. Mukundan, T.D.R. Nair and K.G.K. Warrier*, "Synthesis of Biocompatible Hydrophobic Silica-Gelatin Nano Hybrid by Sol-Gel Process", ***Colloids and Surfaces B***, 55 (2007) 38

14. *S. Smitha,* ***P. Shajesh****, P.R. Aravind, S. Rajesh Kumar, P. Krishna Pillai and K.G.K. Warrier*, "Effect of aging time and concentration of aging solution on the porosity characteristics of subcritically dried silica aerogels", ***Microporous and Mesoporous Materials***, 91 (2006) 286

Contributory Talks:

1. *S. Smitha,* ***P. Shajesh****, P.R. Aravind, S. Rajesh Kumar, K.G.K. Warrier*, "Optimization of aging time and concentration of aging solution in a subcritical drying technique for preparation of silica aerogels", *'National Conference on Advanced Materials for Hostile Environments', IIM, Trivandrum Chapter*, Trivandrum, 1th-2nd March, 2007

2. ***P. Shajesh****, S. Smitha, P. R. Aravind, P. Krishna Pillai, K.G.K. Warrier*, "Exploration of Sol-Gel Chemistry and Subcritical Drying for the Preparation of Aerogels", National Seminar on Nanotechnology, *All Saints College,* Trivandrum, 17th – 18th August 2006

3. ***P. Shajesh****,* *S. Smitha, P.R. Aravind, K.G.K. Warrier* "Silica Aerogel Low Dielectric Substrates & Super Insulators For Possible Defence Related Applications", *'National Seminar & Group discussion meeting of DRDO sponsored research project PIs in Physics', Osmania University,* Hyderabad, Jan. 24 - 25, 2006

* *presenting author*